HIGH CYCLE COMPRESSIVE FATIGUE OF UNIDIRECTIONAL GLASS/POLYESTER PERFORMED AT HIGH FREQUENCY

by

Guangxu Wei

A thesis submitted in partial fulfillment
of the requirements for the degree

of

Master of Science

in

Chemical Engineering

MONTANA STATE UNIVERSITY
Bozeman, Montana

July 1995

APPROVAL

of a thesis submitted by

Guangxu Wei

This thesis has been read by each member of the committee and has been found to be satisfactory regarding content, English usage, format, citations, bibliographic style, and consistency, and is ready for submission to the College of Graduate Studies.

_____	_____
Date	Chairperson, Graduate Committee

Approved for the Major Department

_____	_____
Date	Head, Major Department

Approved for the College of Graduate Studies

_____	_____
Date	Graduate Dean

STATEMENT OF PERMISSION TO USE

In presenting this thesis in partial fulfillment of the requirements for a master's degree at Montana State University, I agree that the Library shall make it available to borrowers under rules of the library.

If I have indicated my intention to copyright this thesis by including a copyright notice page, copying is allowable only for scholarly purposes, consistent with "fair use" as prescribed in the U. S. Copyright Law. Requests for permission for extended quotation from or reproduction of this thesis in whole or in parts may be granted only by the copyright holder.

Signature ———————————

Date ———————————

TABLE OF CONTENTS

LIST OF TABLES

LIST OF FIGURES

ACKNOWLEDGMENTS

There are a few people to whom credit should be given for their help and assistance with this research. First of all, I would like to express my gratitude to my academic and research advisor Dr. John Mandell for his guidance, encouragement and support that enabled me to achieve my academic goal. I would also like to extend my thanks to the following people. To Dan Samborsky, his tireless effort to keep the test facility up and running. To Chuck Hedley and Andrew Belinky, who provide endless hours of conversation and idea to help me solve some research problems.

I especially acknowledge my parents and my wife with my love and gratitude for their endless support all the time.

Finally, I would like to thank Sandia National Laboratories for its support of this research and the wind turbine energy project.

CHAPTER 1

INTRODUCTION

Fatigue is the phenomenon of failure of a material under repeated or oscillatory loading. In a structure with high variable loading, such as a wind turbine blade, fatigue is very important because each time a blade passes the tower, it experiences a loading and unloading of applied wind load. Since a typical windmill usually operates at between one and three revolutions per second, a blade can experience between 10^8 and 10^9 fatigue cycles in its proposed 20 to 30 year lifetime [1]. Therefore, there is a clear need for fatigue data up to 10^8 cycles in industry for design purposes and lifetime prediction of windmill blade.

Fatigue testing of standard ASTM coupons of fiberglass, one to two inches wide and an eighth to a quarter inch thick, is limited to a frequency range of 10 to 20 cycles/second (Hz). This limitation is due to the internal hysteretic heating of polymer based materials, coupled with their poor heat transfer characteristics [2]. At 10 to 20 Hz, a test to 10^8 cycles would take 50 to 100 days. It is difficult or impossible to build a database for fatigue performance up to 10^8 cycles as required for wind turbine blade using standard coupons.

A special fatigue testing method have been developed by Mandell *et al*. [3,4] at MSU for tensile and compressive

fatigue of longitudinal unidirectional fiberglass which would allow testing be conducted at frequency's up to 100 Hz. The approach is to minimize test specimen thickness in order to improve heat transfer while maintaining the representative behavior of the materials.

This thesis is a continuation of previous work by Creed and Belinky [3,4]. The research extends the study to the reversed loading test of the longitudinal unidirectional fiberglass composite and various R-values (R=min.stress/max.stress) of the transverse unidirectional fiberglass composite tests.

CHAPTER 2

BACKGROUND

General Fatigue

It is well known that, when materials are subjected to repeated fluctuating or alternating loads, they may fail even though the maximum stress may never exceed the ultimate static strength of the material. In other words, cyclic loading reduces the strength of a material, or the fatigue strength of a material is lower than its ultimate static strength. This is true of almost all existing materials including: metals, plastics, and composite materials. However, the fatigue behavior of fiber composites varies greatly compared with that of homogeneous materials such as metals or plastics. This is due primarily to the high degree of heterogeneity and anisotropy in composites. Composite materials contain numerous internal boundaries which separate constituent materials that have different responses and different resistances to the long-term application of external influences. Therefore, fatigue as a phenomenon is much more complex in composites than it is for homogeneous materials.

In search for guidelines to a reasonable approach to the fatigue problem, there are basically two kinds of approaches: micro-approach and macro-approach [5]. In the micro-approach,

possible failure modes are examined based on detailed local failure development, such as fiber breakage or buckling, interface debonding and matrix cracking or yielding. For review of such investigations, the reader is directed to References [7,8]. In the macro-approach, it is assumed that failure can be described by a macroscopic criterion, mostly in terms of the average stresses to which the composite is subjected. The approach contains unknown parameters which must be determined using simple and experimentally realizable loadings. For more in-depth discussion see References [9,10]. The literature is focussed on research on the macro-approach, but based on micro-mechanics explanations and the identification of failure modes for specific loading conditions.

Failures of unidirectional composite materials, both static and fatigue, have been divided into two basic failure modes by Hashin and Rotem [6]: fiber-dominated failure modes and matrix-dominated modes. For θ (fiber orientation angles relative to the imposed load direction, see Figure 1) between 0 and a few

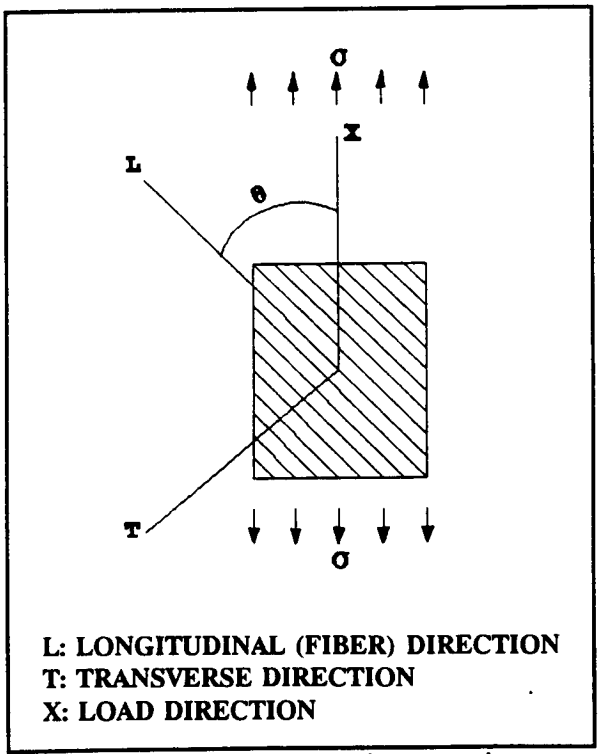

Figure 1. Fiber Orientation.

degrees, the specimen fails by cumulative fiber failure. For larger angles of θ, the failure mode is a crack through the matrix and fiber/matrix interface, parallel to the fibers. This has been observed both for static and fatigue loading by many investigators. The explanation for these phenomena is as follows: when the load is axial (in the fiber direction), it is carried essentially by the fibers. Failure loads then depend on fiber strength, which is of statistical nature, and of matrix and fiber elastic properties. This has been quantitatively shown by Rosen's [8] analysis of static axial strength based on a cumulative damage model. With increased inclination, θ, of the load with respect to fibers, fiber stresses decrease and matrix shear and transverse normal stresses increase. The matrix then fails before the fibers by cracking parallel to the fiber direction.

Consistent with this picture, Mandell *et al.*[2] also listed several possible failure modes: fiber dominated tension or compression; matrix dominated tension, compression, or shear; and interply delamination. The failure of a typical laminate with layers in various directions may be dominated by one of these modes or by a sequence of damage and load redistribution leading to total separation. The fatigue data generated in this research paper are intended to represent the material behavior failing in one of the above modes. These data can then be used with a theoretical model for damage accumulation and load redistribution to predict the failure of

more typical, complex laminates with layers in several directions. The theoretical context for this approach is the "critical element" modeling being pursued by Reifsnider and others [11].

Although a widely accepted composite fatigue theory has not yet been formulated, various theories have been proposed for correlating the fatigue behavior of composites. The available theories can be classified as follows [12]: (1) empirically based fatigue theories, (2) residual strength degradation-based fatigue theories, (3) stiffness change based fatigue theories, and (4) actual damage mechanisms based fatigue theories. Among these theories, empirically based fatigue theories are most commonly used in the fatigue design of wind turbines blades [13]. One of the most often used empirical equations for lifetime is

$$\frac{S}{S_o} = 1 - b(logN) \qquad (1)$$

where N is the cycle to failure, S is the maximum stress on each cycle, S_o is the one-cycle (static) strength, and b is the slope of the normalized S/N curve. To the extent that this equation fits the data, this indicates that the slope of an S-N curve (maximum stress verses log cycles to failure) can often be represented by a straight line. Work by Mandell *et al.* [14] has shown that, for many different matrices and volume percent fiberglass, as well as for fibers alone, the decay constant b is about 0.1. However, a number of cases

which are more severe than this line have also been identified [4], so that the value of 0.1 should not be used for design application directly.

Another useful relationship to fit S/N data is a power law

$$\frac{S}{S_o}=N^{-(\frac{1}{m})} \tag{2}$$

where the constant m has to be evaluated experimentally.

An almost infinite variety of laminates can be used for structural applications. Once it has been decided to use a specific laminate, its fatigue characteristics may be obtained through experiments. It is, of course, not practical to approach the design problem in the inverse way -- that is, to characterize all possible laminates to select the proper one.

Hashin and Rotem [6,15] have studied the fatigue behavior of a graphite-epoxy laminated composite material, and suggested the following correlation between the fatigue strength and the static strength

$$\sigma_f=\sigma_s f(R,N,n,\theta,T) \tag{3}$$

where σ_f and σ_s are fatigue strength and static strength, respectively; f(R, N, n, θ, T) is a function of R, the stress ratio (minimum stress/maximum stress) in fatigue cycling; N, the fatigue life; n, the frequency of load cycling; θ, the fiber orientation for unidirectional composites; and T, the experimental temperature. By decomposing the stress field in the laminate to five primary stresses: intralaminar

longitudinal stress, intralaminar transverse stress, intralaminar shear stress, interlaminar shear, interlaminar normal stress, and evaluating each fatigue function experimentally, the fatigue behavior of multidirectional composite laminates may be predicted using lamination theory and an interactive fatigue failure criterion. Hashin and Rotem's work [15] also shows that the effect of temperature can be introduced by using "shifting factors" for fatigue functions; the experimental results are in good agreement with the theoretical predictions.

Dally and Broutman [16] have shown that the frequency of stress cycling significantly influences the temperature of specimens during fatigue testing. As frequency is increased, the temperature rises and the fatigue life decreases. However, the frequency effects other than from hysteretic heating are small [17]. Research by Creed [3] demonstrated that the results obtained from longitudinal unidirectional tensile fatigue testing with minicoupons at high frequency (30-100 Hz) correlated with data from standard coupons at lower frequencies (1-10 Hz). Surface temperature measurements and finite element analysis verified that no significant hysteretic heating was generated at high frequencies with the very thin specimens.

Longitudinal Reversed Loading Fatigue

Although reversed loading fatigue (tension-compression) is

important in many composite structures, most fatigue testing has been in tension-tension loading (0<R<1), with a smaller number of tests in compression-compression loading (R>1); few tension-compression tests of composites (R<0) have been reported, apparently due to difficulties in this type of testing with thin laminates.

In unidirectional longitudinal composites, the tensile fatigue failure mode involves the opening of matrix cracks and fiber breaks, and the growth of delamination, while the compressive fatigue mode involves buckling of layers after extensive delamination and formation of cracks, and microbuckling or kink bending of fibers [18]. Rotem and Nelson [19] studied the tension-compression fatigue behavior of graphite/epoxy laminates. They showed that both tension and compression failure modes can occur under reversed loading, and that it combined the behavior of both. They also mentioned that the failure was dependent on the specific lay-up (ply orientation arrangement) of the laminate and the difference between the tensile static strength and the absolute value of the compressive static strength. Furthermore, the slope of the S-N curve in reversed loading is steeper than that for tension-tension loading, indicating matrix, rather than fiber dominated behavior with graphite fibers which are fatigue resistant in tension, unlike glass fibers [17].

Rosenfeld and Huang [20] investigated the significance of compressive loading in fatigue of unidirectional

graphite/epoxy laminates. They performed some tests for R=0, -∞, and -1 loading to determine the significance of the compressive loading. These test results indicated a significant life reduction for both R=-∞ and -1 compared with tension-tension loading, with the life reduction for R=-1 being greatest. They concluded that unidirectional specimens under reversed loading fail predominantly in compression for graphite fiber composites.

For laminates containing longitudinal, angle and transverse plies, Reifsnider [21] observed both tension and compression failure modes with a carbon/epoxy composite. At low stress levels, the failure was compressive, while at high stress levels it was tensile failure. This was due to the different ways in which tensile and compressive residual strengths change during fatigue for these particular laminates.

Reversed loading has also been studied by several additional investigators [19,22,23]. The general conclusions reached are that tension-compression fatigue is more severe than pure tension-tension or pure compression-compression fatigue. Several methods have been proposed to predict the fatigue life. Kadi and Ellyin [22] studied unidirectional glass/epoxy composites with different fiber orientations under various stress ratios. They used a fatigue failure criterion for composite laminae based on the input strain energy. The criterion takes into account the effects of both fiber

orientation angle and stress ratio. It is shown that, usually, the tensile and compressive stresses do not contribute equally to the damage. For longitudinal specimens, the slope of the S-N curve under reversed loading is steeper than that under tension loading. The failure mode depended on the magnitude of the applied stress. At high stress levels, the failure mode was an abrupt broom-like tensile failure accompanied by fiber breakage. At lower stress levels, delamination was observed and failure occurred over an extended period. The experiments indicated that the fatigue life of composites for different values of the stress ratio and fiber orientation angle can be correlated though the strain energy theory.

Rotem and Nelson [18,19,23] studied the tension-compression fatigue of a graphite/epoxy laminate. They found that almost all unidirectional specimens failed in compression. The observed mechanism of fatigue failure was the gradual splitting of fiber bundles, which began to buckle from the specimen surface toward the specimen interior until a sudden mid-plane delamination occurred. The result was the buckling of fiber bundles across the entire specimen. Only a few specimens failed in tension. These failures were at relatively low alternating loads. It appears that the fatigue failure process involved a reduction in the constraint against buckling by the development of delamination cracks along the fiber bundles.

Badaliance and Dill [24] observed the fatigue damage

mechanisms in multidirectional graphite/epoxy composites subjected to compression dominated reversed fatigue loading with X-ray radiography. The X-ray radiographs show that the damage progression sequence begins with matrix cracking at the fiber-matrix interface within a ply, followed by delamination in areas that have accumulated extensive matrix cracking. Delamination and intralaminar matrix cracking interact to produce eventual fatigue failure. A damage correlation parameter was developed by summing the strain energy density factors for each ply. This parameter is used with linear fatigue damage and linear residual strength reduction models to predict the spectrum fatigue life of laminates.

The American Society of Testing and Materials (ASTM) standards for fatigue testing of fiber-reinforced composites are only referenced for tension-tension fatigue specimens (ASTM D3039). No standards are presently available for compression-compression or tension-compression fatigue of composite specimens. The standard tension-tension specimen was ruled inadequate since elastic buckling would result under relatively small compressive loads.

In works by Rosenfeld and Huang [20] and by Rotem and Nelson [19], antibuckling devices were used to prevent buckling of the specimen under compressive loading. However, there is no consensus about the validity or usefulness of data obtained in this manner [14]. Often a circular hole is used to initiate failure in the gage section for laminates containing

angle plies [25,26]. This is impractical with unidirectional layups because longitudinal splitting parallel to the fibers at the hole edges would result. Several specimen geometries were investigated in Belinky's study [4] of longitudinal compression-compression fatigue testing, and a suitable specimen geometry was determined. It was established that 0° specimens could be tested without antibuckling devices with very short gage lengths and clamped tabbed ends.

Transverse Fatigue

The performance of unidirectional composites is often limited by transverse cracking in the matrix or interphase. Although few applications exist for unidirectional composite materials, particularly when loaded in the transverse direction where the composite properties are usually governed by the matrix properties, transverse properties are critical in damage development in multidirectional laminates, where typical plies are stressed in all directions. It has also become evident [21,27] that study of the properties in transverse fatigue of unidirectional material can be related to delamination between plies, one of the predominant modes of failure in composite laminates. Therefore, a better understanding of the parameters influencing this type of failure is important for composite design both to prevent delamination and to predict the sequence of damage development in typical multidirectional laminates.

The transverse tensile strength is sensitive to the fiber-matrix interfacial bonding strength, the presence of debonds and defects such as voids in the matrix. These microdefects cause tensile crack propagation and crack coalescence in the matrix and interfaces, and significantly lower the apparent ply transverse strength. As transverse tensile strength is much lower than transverse compressive strength for most polymer-based composites, this property plays a dominant role in initiating ply failures in multidirectional laminates.

The transverse compressive strength is sensitive to factors such as the specimen's thickness, interfacial bonding between fiber and matrix, and so forth [27]. However, for most polymer composites, the transverse compressive strength is several times greater than transverse tensile strength, and the compressive transverse ultimate strain may exceed the longitudinal value. So, its practical role in causing laminate failure is relatively insignificant.

Early work by Bailey and co-workers [28,29] described the increase in transverse ply crack density in a transparent fiberglass [0/90/0] laminate under increasing static tension. They found that cracks initiated in the 90° ply from fibre/matrix debonds at the edge of the coupon and extended across the width of the ply. The 90° ply crack density at the coupon edge appeared to reach a saturation value at failure corresponding to a crack spacing of the order of the transverse ply thickness. A similar pattern of 90° ply cracks

is obtained in crossplied laminates under fatigue loading [30]. This regular crack pattern has been termed the "characteristic damage state" (CDS) by Reifsnider and co-workers [11] who suggest the CDS is characteristic of a particular laminate configuration and is independent of load history and environmental factors. The transverse fatigue properties of the plies is obviously central to this progressive damage development.

Many equations have been proposed to describe the crack growth rate during fatigue, da/dN, as a function of the stress level, crack length, and material properties. The most popular of these equations is one that relates crack growth rates to the fracture mechanics parameters represented by the stress intensity factor. This equation is known as the Paris Law [31]:

$$\frac{da}{dN} = C(\Delta K)^m \qquad (4)$$

where C and m are material constants and ΔK is the stress intensity range K_{max}-K_{min}.

For many polymers, the data show such a linear relationship over a range when plotted on a log-log scale [32]. The same fatigue failure mechanisms that occur in unreinforced polymers also occur in fiber reinforced composites when the failure is dominated by matrix failure [33]. However, this equation can only predict the growth of cracks parallel to the fibers under cyclic loading in the

propagation stage. The fraction of the lifetime spent in the initiation stage is difficult to predict, and depends on flaw characteristics.

A few tensile fatigue results for the transverse properties of unidirectional composites have been reported in the literature [15,34,35]. S-N curves are all represented by straight lines on linear-log plots and show no fatigue limit.

Rotem and Nelson [15] have studied the fatigue behavior of a T300-5208 graphite/epoxy composite at elevated temperatures, relating static strength and fatigue through a fatigue function depending on whether fatigue is dominated by fibers or matrix. They have shown that for graphite/epoxy at R=0.1:

$$S/S_o = 1 - 0.033*\log(N) \quad \text{(fiber dominated)} \quad (5)$$

$$S/S_o = 1 - 0.080*\log(N) \quad \text{(matrix dominated)} \quad (6)$$

where S and S_o are maximum stress and static strength respectively and N is the number of cycles to fail.

Yang *et al.* [36] proposed a stiffness degradation model which they used successfully to predict the residual stiffness for composite laminates under constant amplitude fatigue loadings. They used this model to predict the fatigue life of matrix-dominated composites under tension-tension fatigue loading [37]. It was shown that comparisons between theoretical predictions and experimental results were reasonable.

Little work has been published on the transverse fatigue properties under compressive loading. The reason could be

that, as mentioned before, the transverse compressive strength for most polymer composites is several times greater than tensile strength, so that it is a less critical property.

It should also be mentioned that under reversed cyclic loading the damage modes discussed in tension and compression may interact to produce a "worst case" that is distinct in its severity [23].

Fatigue Life Diagram

The fatigue life of a material is often represented by an S-N diagram, which is a plot of maximum applied stress(S), or stress range, ΔS (the total, or double amplitude S_{max}-S_{min}, Figure 9), against the number of cycles to failure(N), for a particular R value. A log scale is normally used for N. For S, a linear scale is often used, but sometimes a log scale is also used. For composites, as noted earlier, a straight line S-N curve is often observed on either type of plot [38] with a departure from linearity in the low cycle region to the ultimate tensile or compressive stress on the ordinate (N=1). On a log-log scale, the straight line is given by following equation:

$$Y=c*N^{-b} \qquad (7)$$

where Y can be stress(S), normalized stress(S/S_o) or strain, b is the slope of the regression line and c is a constant representing the point of intersection of the regression line with the ordinate (Y-axis).

The S-N curve describes the relationship between maximum cyclic stress or stress amplitude and lifetime usually for a uniaxial applied stress having a specified stress ratio. For a given stress ratio, R, the S-N curve defines the lifetime, N, as a function of the maximum applied stress, S.

Another useful format for presentation of fatigue data is the Goodman Diagram, which represents various combinations of uniaxial mean and alternating stress for failure at a specified lifetime based on S-N curves. Figure 2 illustrates the characteristics of the Goodman Diagram [39]. The cyclic (alternating) stress is the half-amplitude of the waveform

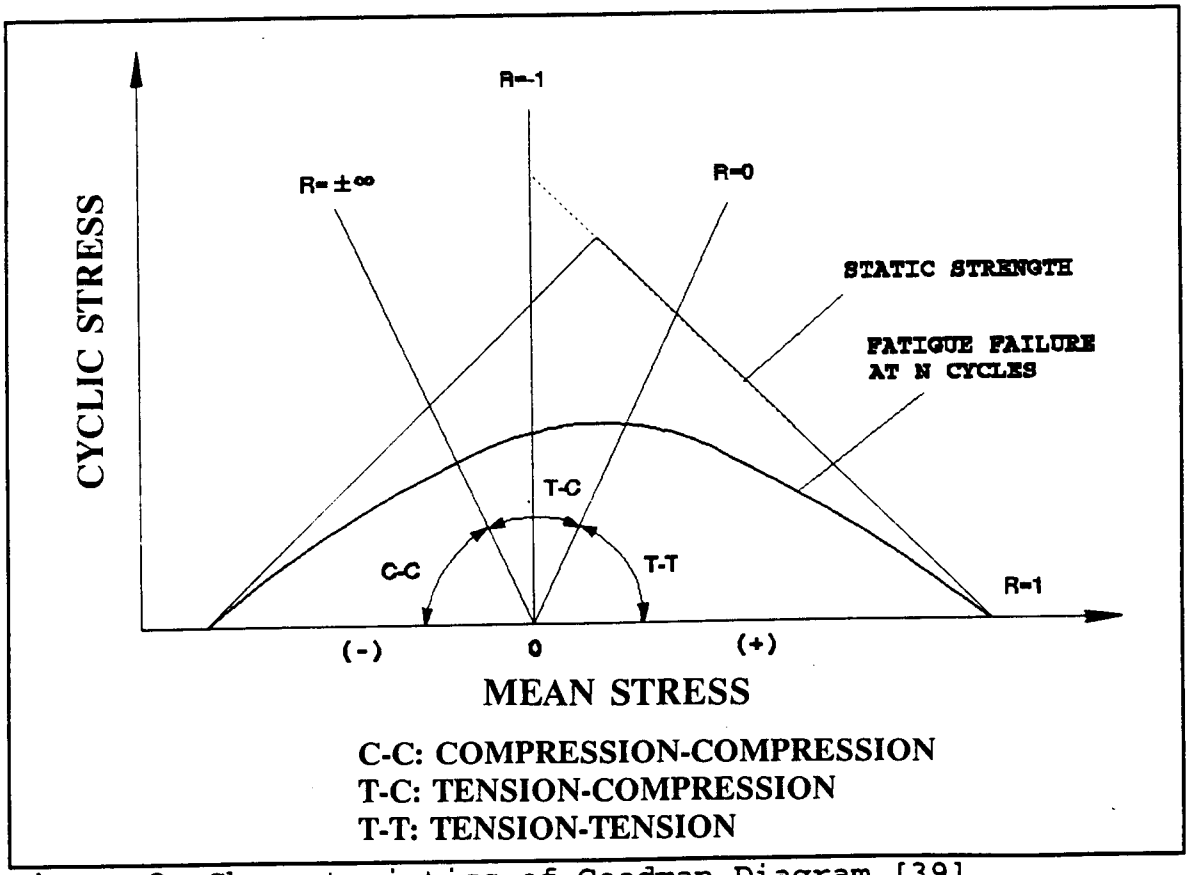

Figure 2. Characteristics of Goodman Diagram [39].

(S_{max}-S_{min})/2; the mean stress is (S_{max}+S_{min})/2 (Figure 9). It is shown that different regimes of fatigue loading can be located. This format is convenient for interpolation for different values of stress ratio. Therefore, it is more useful for design purposes than the S-N curve [13]. The disadvantage is that the construction of the Goodman Diagram requires many data points to cover the whole spectrum of fatigue loading, compressing many S-N curves at different R values.

Several composite fatigue diagrams have been reported in the literature. Among these, Owen *et al.* [40] reported the Goodman Diagram for unidirectional carbon/epoxy composite. Kim [41] constructed the Goodman Diagram for graphite-epoxy with the layup of $[0°/45°/90°/-45°]_{2s}$*. Netherlands Energy Research Foundation [42] established a fatigue database of glass/polyester and glass/epoxy composites for wind turbines with the layups of 0, 45, 0/45 and generated the Goodman Diagrams for those materials. The Goodman Diagrams generated in this research represents the first known published diagram obtained in the cycle range up to 10^8 for composites.

Rotem and Nelson [19] introduced a "fatigue envelope" to describe the fatigue behavior with varying mean loads similar to a Goodman presentation. The abscissa is the mean stress and the ordinate is the maximum loading stress with lines indicating the maximum and the minimum of the fatigue amplitude that will cause failure after a particular number of

**Note: This notation refers to a laminate with eight unidirectional plies arranged symmetrically about the mid-thickness, as [0/45/90/-45/-45/90/45/0] [41].*

cycles. Each envelope is for a given number of cycles. As for the Goodman Diagram, the advantage of this presentation is the ease of identification of the failure mode. The disadvantage is that it requires many data points at different R values. Fatigue data for graphite/epoxy composites with the layups $[0°]_{16}$, $[\pm 45°]_{4s}$, $[0°,90°]_{4s}$, $[0°,\pm 45°,90°]_{2s}$, $[0°,\pm 45°,0°]_{ns}$, $[90°,\pm 45°,90°]_{ns}$ have been developed by Rotem *et al.* [18,19,23] and fatigue envelopes have been generated for those materials.

CHAPTER 3

EXPERIMENTAL TESTING METHODS

The objective of the experimental testing program was to accumulate static strength and dynamic fatigue data for unidirectional longitudinal and transverse E-glass/polyester composites and generate the Goodman Diagrams for lifetime prediction of wind turbine blades. This required the development of test specimens which provide the expected location and mode of failure under the different loading conditions, where the failure modes desired are those representative of standard test specimens and applications.

One of the important requirements of the testing program was to maintain consistency with the previous work by Belinky [4]. Therefore, all of the fatigue data were obtained utilizing the same test equipment and environment. Also, all of the longitudinal specimens had basically the same width and thickness and were obtained from the same manufacturing process.

Specimen Preparation

Longitudinal specimens were fabricated from Knytex D155 unidirectional E-glass cloth and Corezyn 63-AX-051

orthopthalic polyester resin. The cloth is in the form of strands containing several hundred fiber each, stitched together with an organic yarn. Transverse specimens were fabricated from Knytex D100 unidirectional E-glass cloth with the same resin. Densities of the materials were 2.54 g/cc for E-glass and 1.2 g/cc for polyester (information provided by manufacturers). The catalyst for the resin was 2% methyl ethyl ketone peroxide (MEKP) by volume.

Fabrication was carried out through resin transfer molding (RTM) at room temperature. The procedure was developed in the research by Hedley [43] and was also described by Belinky [4]. To summarize the procedure, catalyzed resin is injected into a mold containing reinforcement arranged in desired amount and orientation. The curing composite plate was kept in the mold for approximately two hours at room temperature and then removed from the mold and postcured in an oven at 140°F overnight.

Longitudinal Specimens

Two plies of Knytex D155 E-glass cloth were used to make a 430 mm long by 170 mm wide plate for longitudinal specimens. Specimens 6.35 mm wide were cut from the cured plate using a diamond saw blade. In order for the specimens to fail in the gage section, it was found to be necessary to taper the gage section thickness down from 0.9 mm to 0.5 mm (approximately one ply thickness) in the center, as in Belinky's work [4].

Tapering was accomplished using a Dremel tool, yielding a radius of curvature of the tapered region of 17 mm, and a uniform thickness across the width of the gage section. Tabs were cut from sheets of Plastifab (0°/90°) fiberglass/epoxy mat and were bonded onto the specimens using Hysol EA 9309.2NA epoxy. Tabbed specimens were placed in an oven at 140°F for overnight to ensure complete adhesive curing. Figure 3 illustrates the R=0.5 tensile specimen geometry.

To avoid elastic buckling in compression, a short gage length of 5.2 mm was used for R=-1 reversed loading specimens (see Figure 4). Untapered specimens were used to measure the initial tensile and compressive modulus as it was impossible to strain gage the small, tapered section of the specimen which were not flat.

Transverse Specimens

Four plies of ~~Knytex~~ Hexcel D100 E-glass cloth were used to make a plate for transverse specimens. The fabric was chosen because it is thinner than Knytex D155 E-glass cloth. As four-ply symmetric angle-ply specimen will be used in the future study of shear dominated failure mode, it is critical to make the angle-ply specimen as thin as possible in order to test at high frequency without significant hysteretic heating. The thin fabric was used to make the transverse specimen so that the results can be compared with shear dominated failure. The proper gasket thickness was use to produce a constant specimen

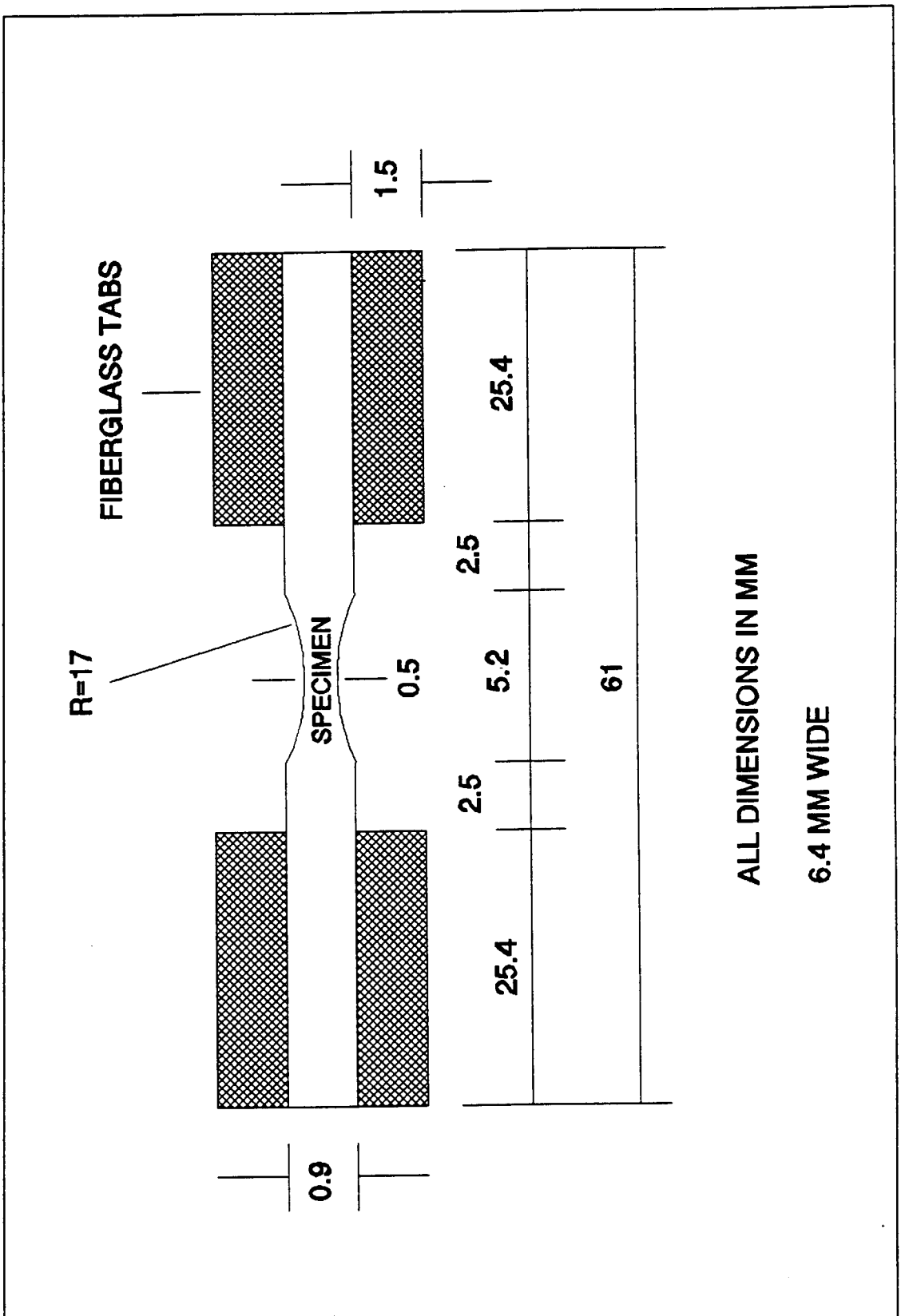

Figure 3. Geometry of Longitudinal R=0.5 Tensile Specimen.

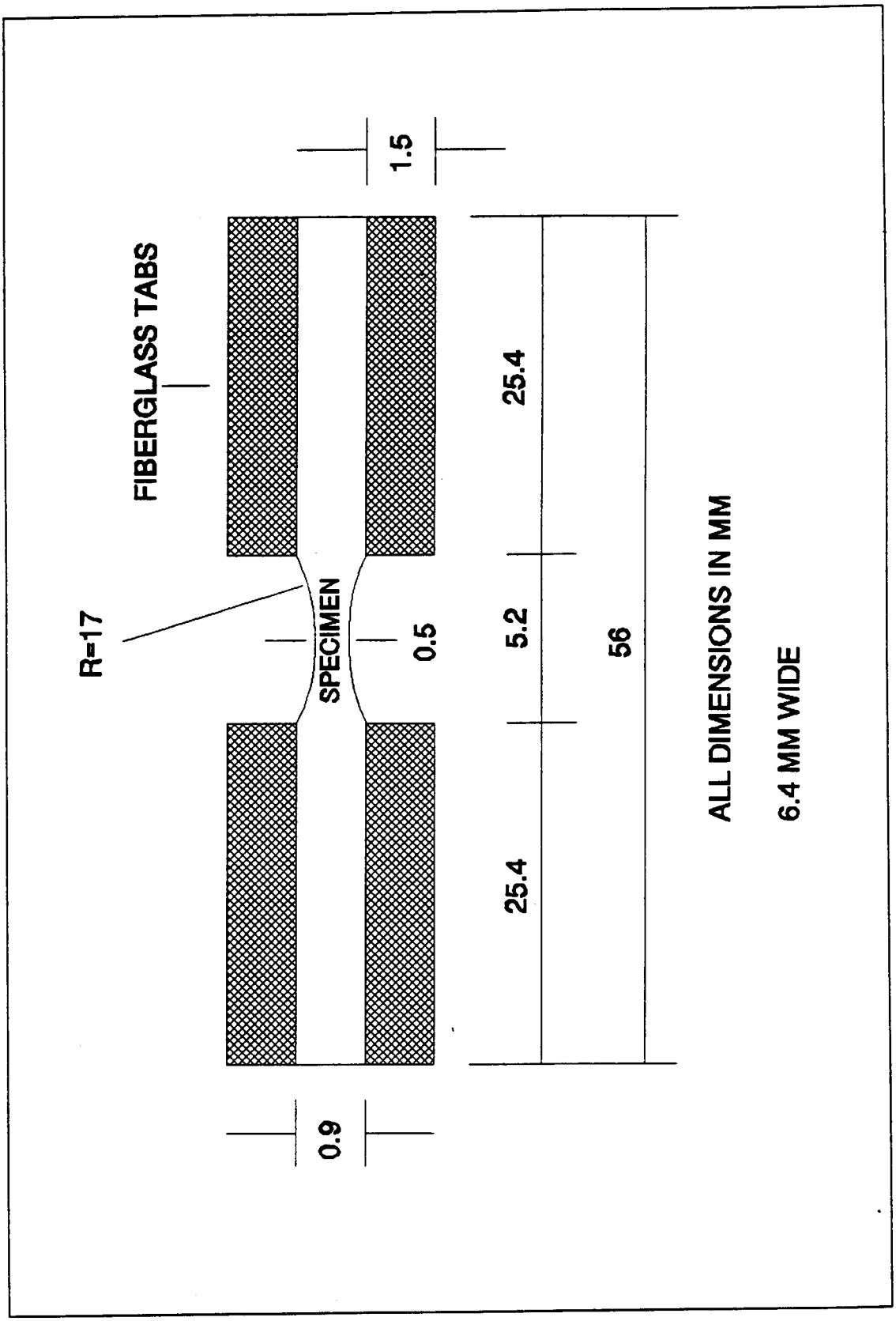

Figure 4. Geometry of Longitudinal Reversed Loading Specimen.

thickness at the desired fiber content. To avoid fiber wash, the unidirectional fiber cloth was laid in a direction parallel to the resin flow. Injection was done slowly to avoid fiber movement and to accomplish total wet-out of the fiber strands. Specimens 19 mm wide were cut in the transverse direction from the cured plate. For R=0.5 and 0.1 tensile specimens, specimen geometry was 19 mm wide by 76.2 mm long by approximately 1.3 mm thick (see Figure 5). To avoid elastic buckling, a short gage length of 5.2 mm was used for R=2 and 10 compressive specimens and R=-1 reversed loading specimens (see Figure 6).

A proper transverse specimen is difficult to make, especially for a tensile or reversed loading specimen. It is found in the testing that tensile strength varied for specimens from different plates and for specimens cut from different positions of a plate. These differences are most likely caused by different porosity and flaw size in the specimens. Further studies show that the tensile strength is higher and more stable for the specimens cut from the first half part of a plate (close to inlet of the mold) than the specimens from the second half part (close to outlet of the mold). Therefore, several plates were made and only the first half parts of the plates, which show similar and stable strength, were used to make the specimens for tensile and reversed loading testings.

Testing Equipment and Procedures

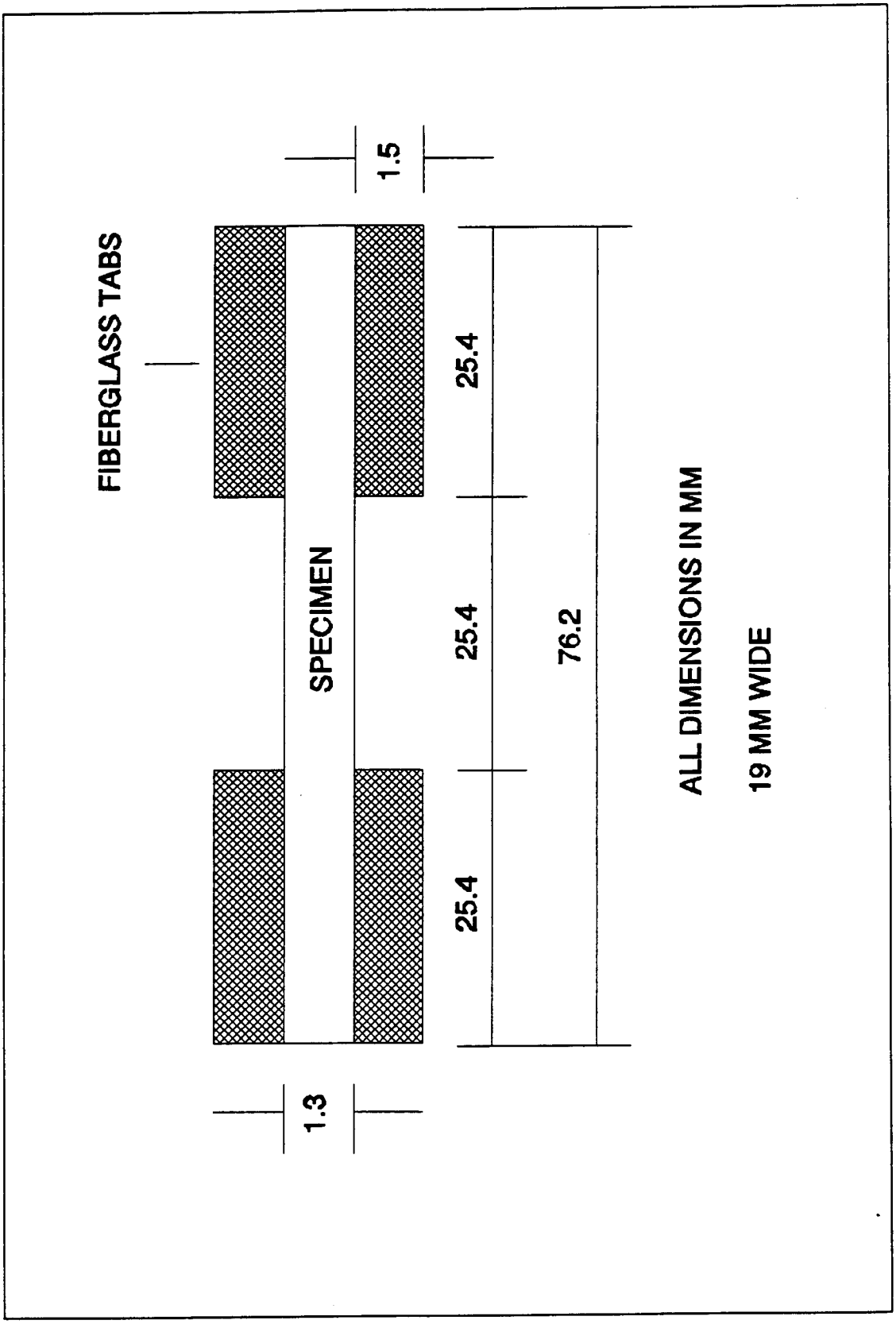

Figure 5. Geometry of Transverse R=0.5 and 0.1 Specimen.

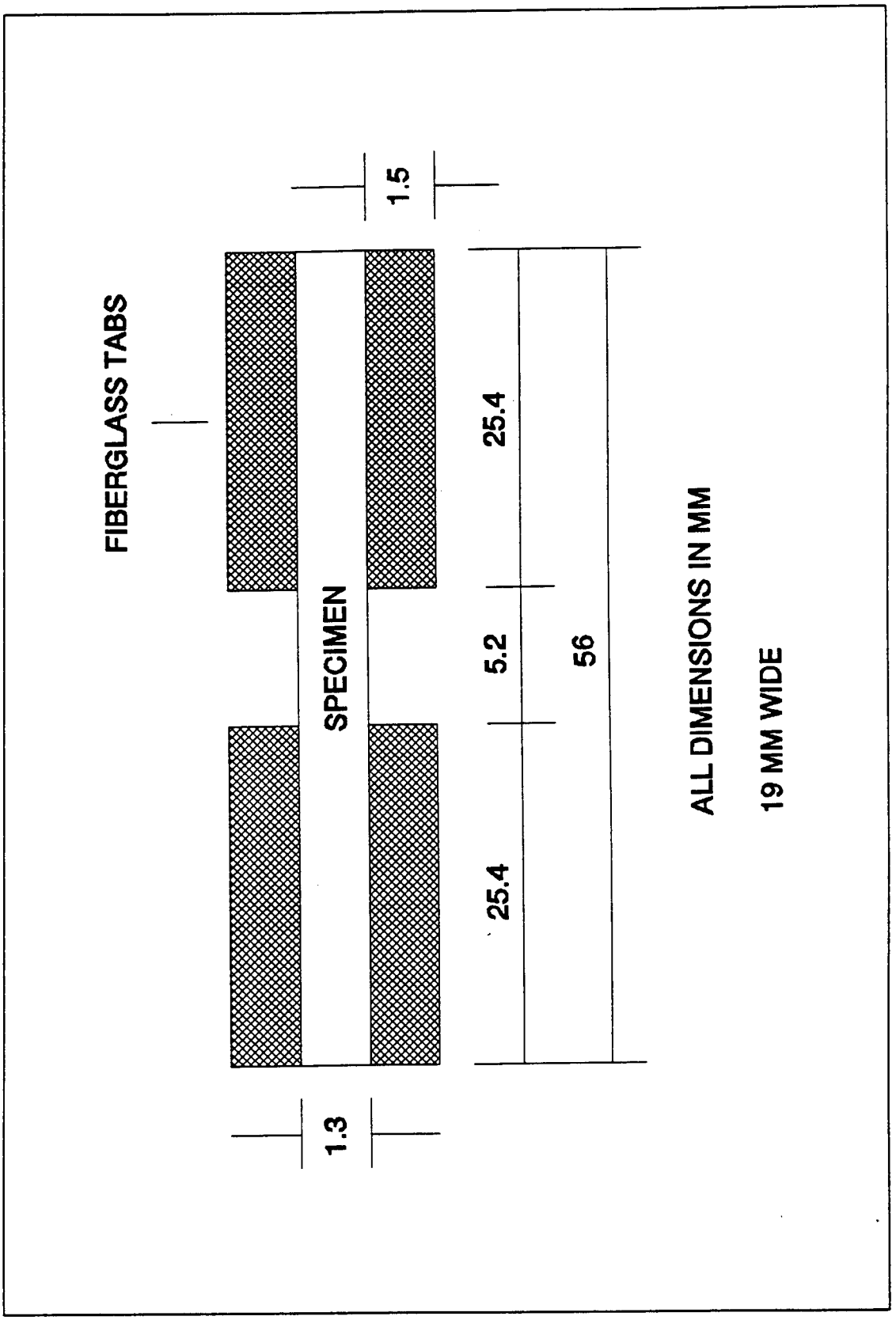

Figure 6. Geometry of Transverse R=2, 10, -1 Specimen.

The fatigue testing equipment used throughout this study is a servohydraulic testing machine (Instron Model 8511) with a load capacity of 10,000 Newton. The machine is controlled by an Instron Model 8500 controller and computer software. This machine is designed for high frequency testing. It has a 45 liter per minute servo valve and operates at 20,700 kPa hydraulic pressure supplied by a 91 liter/min pump. Figure 7 is a photograph of the Instron 8511.

The static tests were conducted under displacement control with a linear ramp waveform (force versus time). Strain for slow static tests was measured using Micro-Measurements EA-06-

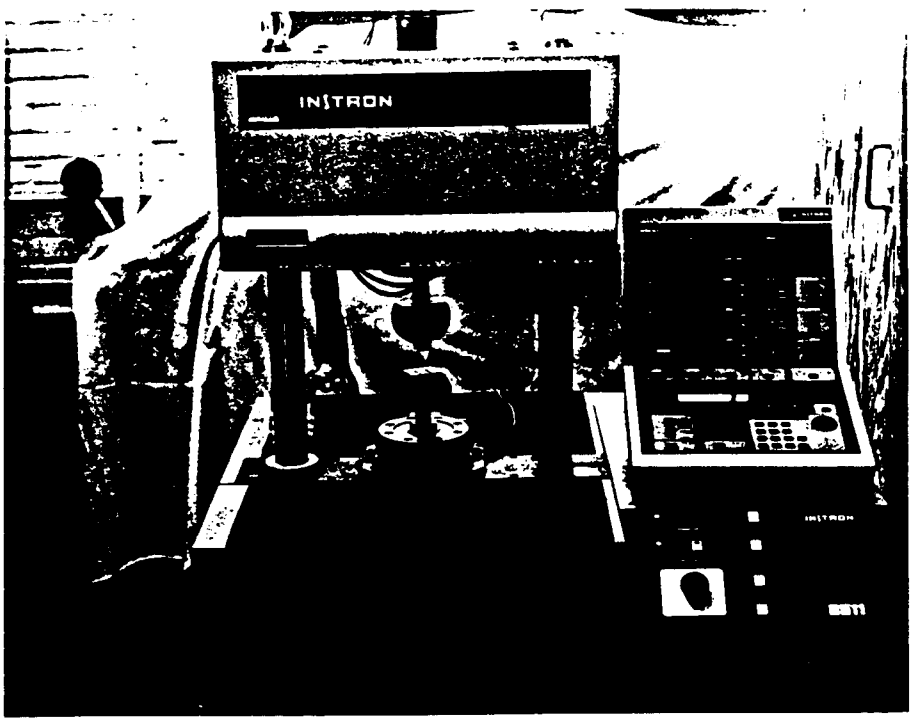

Figure 7. Photograph of Instron 8511.

062AP 350 ohm strain gages and an Instron 2.54 mm displacement extensometer (Model Number 2620-826). Proper displacement rates were chosen for slow tests to break the specimens in about 3 minutes. The displacement rates for single cycle fast tests on the fatigue S-N diagrams were consistent with a fatigue test frequency of 20 Hz, producing failure in about 0.05 seconds.

All fatigue tests were run under load control with a constant force amplitude sine wave input. The amplitude and average load were determined from the R value and maximum (tensile) or minimum (compressive) stress level of each test. The test frequencies were varied with stress level in order to maintain a constant average loading rate, consistent with earlier work [4], with higher frequency at lower stresses. The specimen was initially loaded to the average stress with a ramp speed to load in at about 30 seconds; the cyclic load was then imposed. At the beginning of a test, the cyclic load amplitude was increased gradually to avoid damaging the specimen with a possible overload on the first cycle. The number of cycles to fatigue failure, N, was recorded by the counter on the control panel. If the specimen did not fail prior to 10^8 cycles, the test was terminated without failure, and an arrow is used to mark the result on graphs as a runout. Waveform quality was monitored with an analog oscilloscope. Specimen surface temperatures were measured with Omega Tempilaq liquid crystal paints which melt at specific

temperatures.

The porosity content of specimens was determined by quantitative microscopy methods using a Leitz Wetzlar light microscope connected to a Sony 13 inch monitor by a Panasonic CL110 color video camera. Optical micrographs were taken of polished sections normal to the fibers. A grid was superimposed over the micrograph, and the fraction of grid intersections falling within pores was manually determined. The resulting ratio of grid intersections falling in pores to total grid intersections is the area fraction of pores on that cross section. Fiber volume fraction was determined by burning off matrix from a representative section of the composite plate, following the ASTM Standard D3171.

All tests were conducted in ambient laboratory air with generally low humidity and temperatures ranging from 65° to 80° Fahrenheit.

CHAPTER 4

RESULTS AND DISCUSSION

Longitudinal Test Results

Slow Static Tests

Slow stress-strain tests were used for an accurate modulus determination, using untapered longitudinal specimens. Several tests were conducted, and typical stress-strain curves for tensile and compressive tests are shown in Figure 8. This Figure shows only the initial portions of the stress-strain curves for modulus determination. The moduli from these curves were 39.2 GPa and 41.2 GPa; and these values are used to calculate the strains experienced by specimens during fatigue tests. The fiber volume content of this material sample was 49% and the porosity about 2%.

Fatigue Results

Longitudinal S-N curves were determined for three different R values in Belinky's research [4], R=10, 2, and 0.1. The present study extends this database to R=0.5 and -1. R=0.1 and 0.5 represent tensile fatigue tests with stress ratios of 0.1 and 0.5. R=10 and 2 represent compressive fatigue tests with stress ratios of 10 and 2. R=-1 is reversed

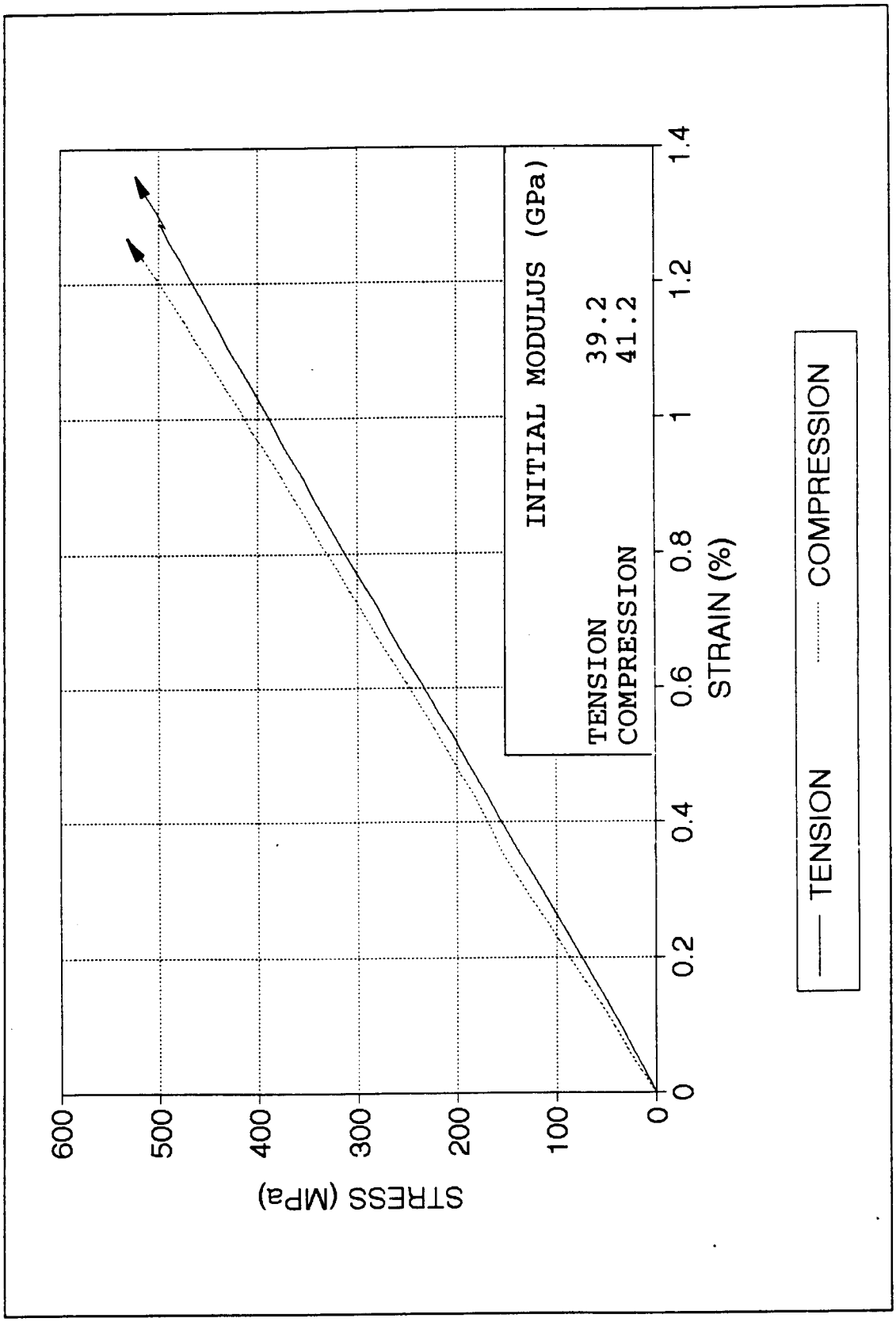

Figure 8. Stress-Strain Curves for Typical Longitudinal Specimen. (Low Strain Portion Only).

loading with equal maximum and minimum stress. The relationships of stress versus time for the sine waves at different R values are illustrated in Figure 9.

Figure 10 shows normalized S-N (stress versus number of cycles to failure) data obtained at the R value of 0.5 compared with 0.1 data. The raw data for the longitudinal tests with different R values are listed in Appendix A. The strength determined from single cycle tests for the R=0.5 material batch is about 9% lower than that of the R=0.1 batch reported by Belinky [4]. This difference is most likely the result of different fiber volume fractions between the two plates (49% versus 67% for untapered specimens); it is difficult to produce two identical plates. The moduli for the R=0.5 and 0.1 batches are 39.2 GPa and 46.2 GPa. Therefore, the calculated average failure strains of single cycle tests are 3.41% and 3.18% respectively, about 6.7% different.

The S-N curve slope for R=0.5 for Figure 10 is considerably flatter than that for R=0.1. This is not unexpected, due to the decreased cyclic amplitude at the same maximum stress value for R=0.5 versus 0.1. Specimens tested with lower amplitudes at the same maximum stress level are expected to last longer than those tested with larger amplitudes at the same maximum stress level. The runout data with arrows represent the specimens running to 10^8 cycles without failure. These tests were run at an initial maximum strain of about 1.02%, calculated through the modulus as

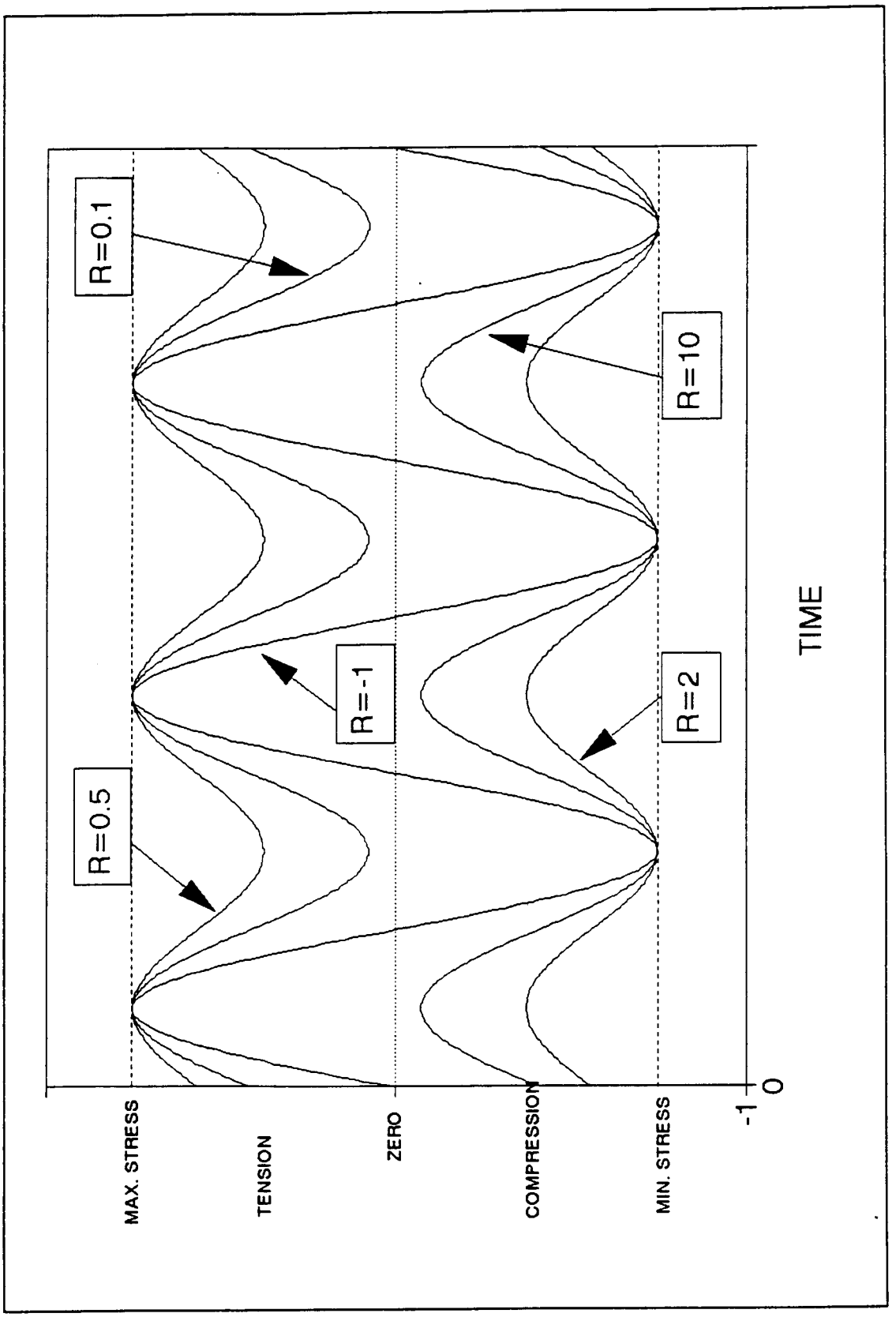

Figure 9. Sine Waveforms for Different R Values.

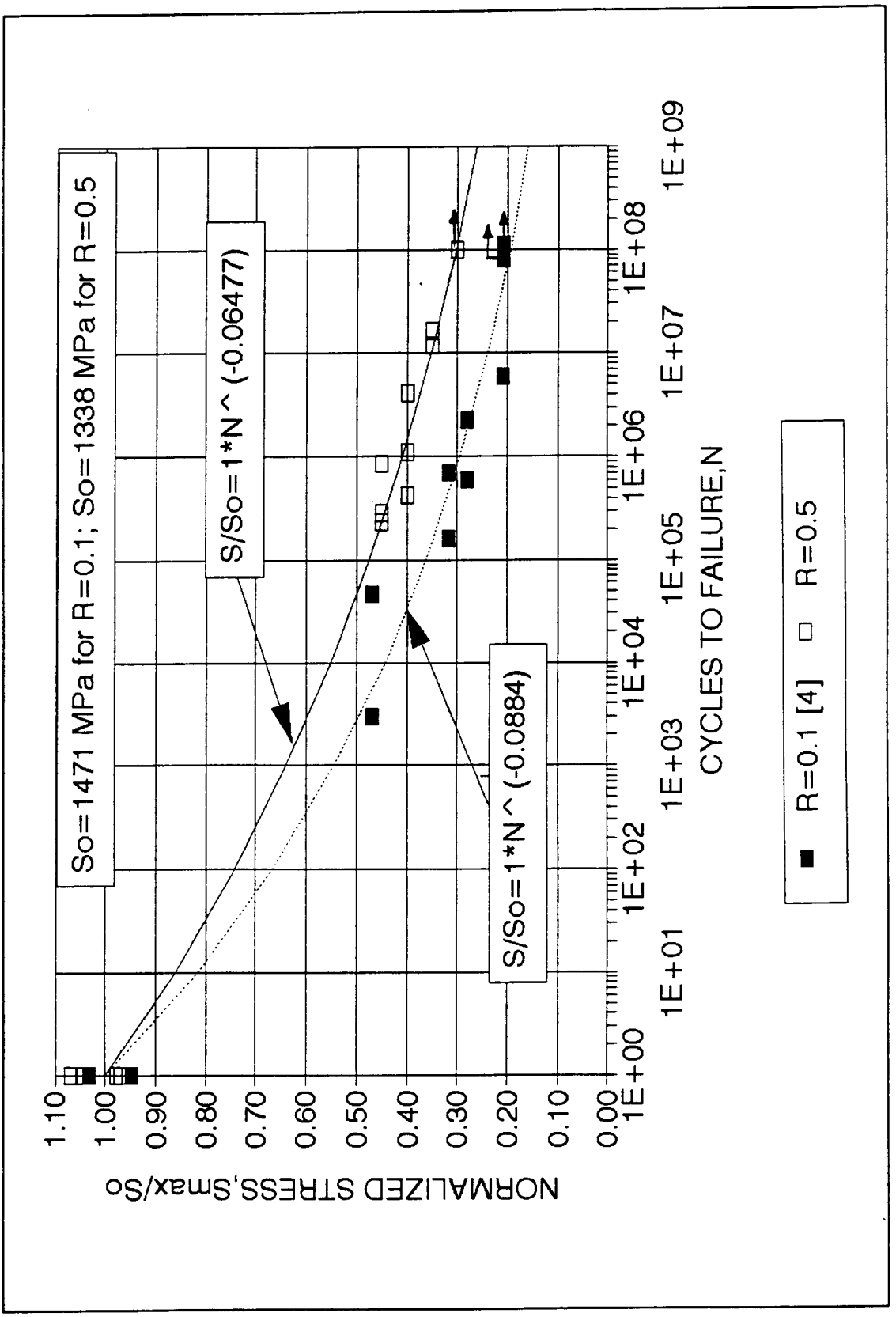

Figure 10. Longitudinal R=0.5 S-N Data Compared with R=0.1 Data from Ref.[4].

stress/modulus using the controlled stress and measured modulus. Testing time for the runout specimens was about 11 days. A least squares power law fit (forced through the single cycle average strength and including runout points) provides the best fit to the data (R^2=0.9157) (compared with Equation 2). A least square power law curve fit is also done for points above 10^5 cycles (including runouts); the goodness of fit is 0.8817 (Figure 11). This curve fit is used in establishing the Goodman Diagram above 10^5 cycles as a better fit to the higher cycle data, following Belinky [4]. Appendix C gives power law fits for fatigue data above 10^3 and above 10^5 cycles used to construct the Goodman Diagrams. The fits to particular cycle ranges are done to provide the best representation of the data in that particular cycle range. (In most cases, forcing the fit through S_o at one cycle does not provide the best representation of the data.)

The raw data for R=-1 reversed loading are listed in Appendix A. It was observed during the tests that hysteretic heating caused temperature rises; the surface temperature was above 175°F at high frequency. This effect is stronger at R=-1 apparently because the amplitude in reversed loading tests is larger compared with that at other R values. Therefore, temperature was measured with Omega Tempilaq paint to keep the surface temperature of specimens below 125°F, and, as a result, test frequencies did not exceed 50 Hz. Testing time for a 10^8 cycle data point was about 23 days.

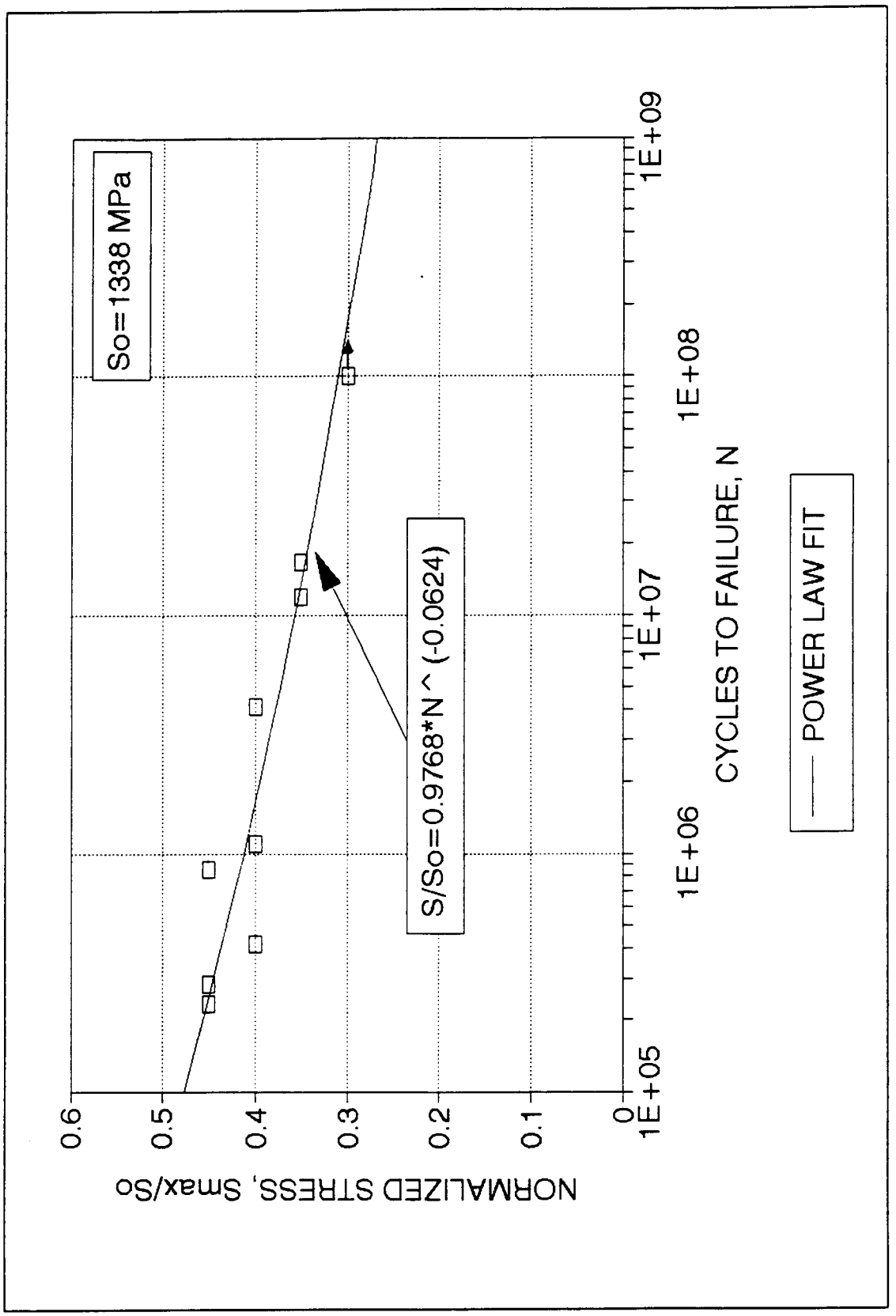

Figure 11. Power Law Fit of S-N Data for R=0.5 Above 10^5 Cycles.

Figures 12 and 13 show the reversed loading fatigue data compared with the R=0.1 tensile and R=10 compressive fatigue curves. The tensile and compressive strengths are lower than for the R=0.1 and 10 batches; this is apparently caused by different fiber contents and fiber arrangement [4]. The R=-1 data fall well below the R=0.1 curve and slightly below the R=10 curve. The data are closer to the R=10 compressive curve than to the R=0.1 tensile curve (tensile strength is approximately twice as high as compressive strength). As noted later, it was observed in reversed loading tests that high stress tests failed in a more compressive mode while lower stress tests failed in a more tensile appearing mode.

As described under specimen fabrication, the geometry of the reversed loading specimen is different from the geometries of tensile and compressive specimens. It is short in gage section compared with tensile specimens to avoid elastic buckling. It differs from the compressive specimens as the gage section is tapered like tensile specimens to prevent the tab debonding. To verify whether the fatigue data are consistent in spite of the difference in specimens geometry, several R=0.1 tensile tests and R=10 compressive tests were done using reversed loading specimen shape. The results are consistent with R=0.1 and R=10 fatigue curves (see Figures 12 and 13). Thus, the different specimens, material batches, and normalizing values produce consistent fatigue trends on the normalized plots. Earlier work [3,4] has shown that the R=0.1

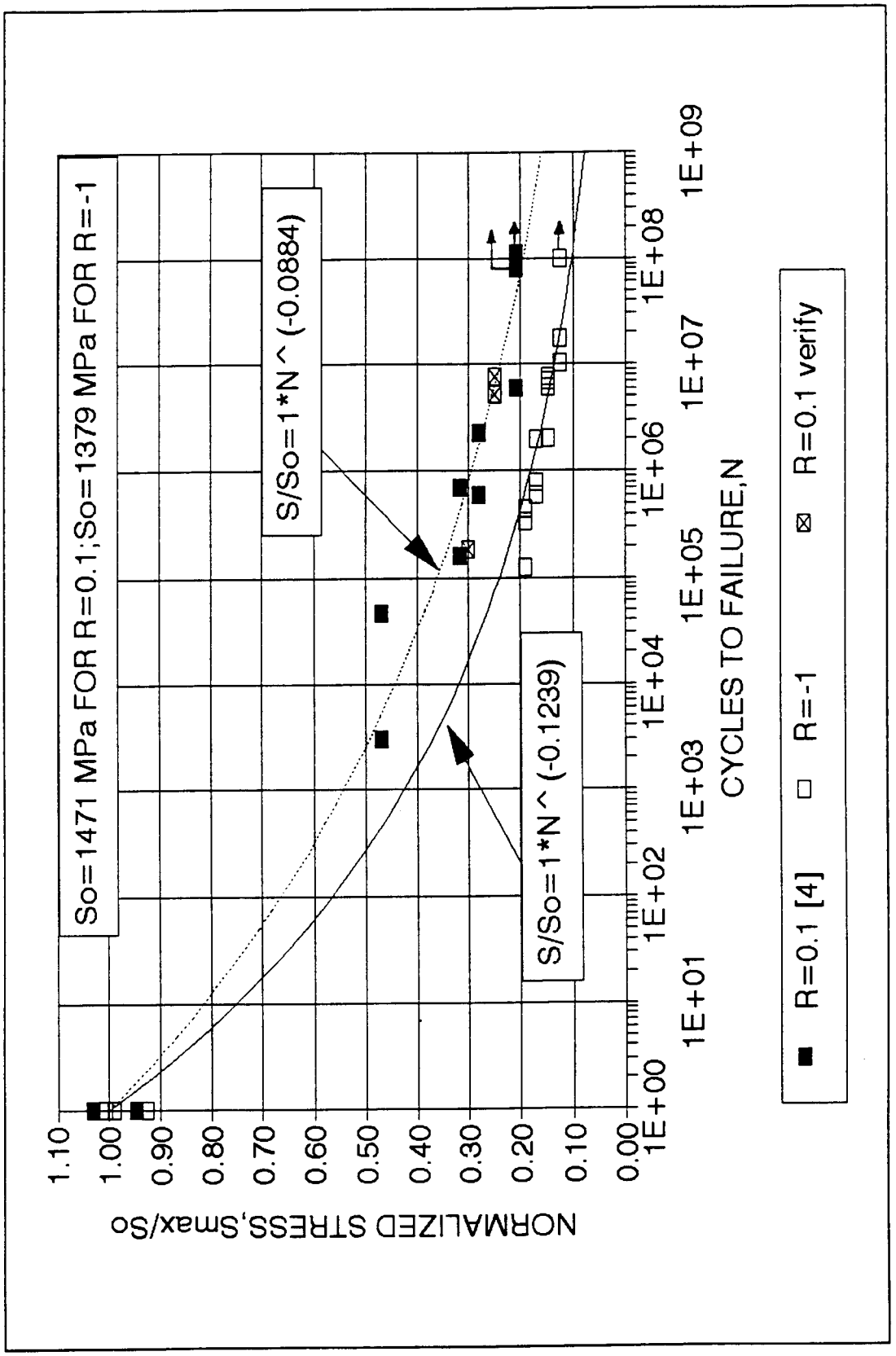

Figure 12. Longitudinal R=-1 S-N Data Normalized by the Tensile Strength Compared With R=0.1 Data from Ref.[4].

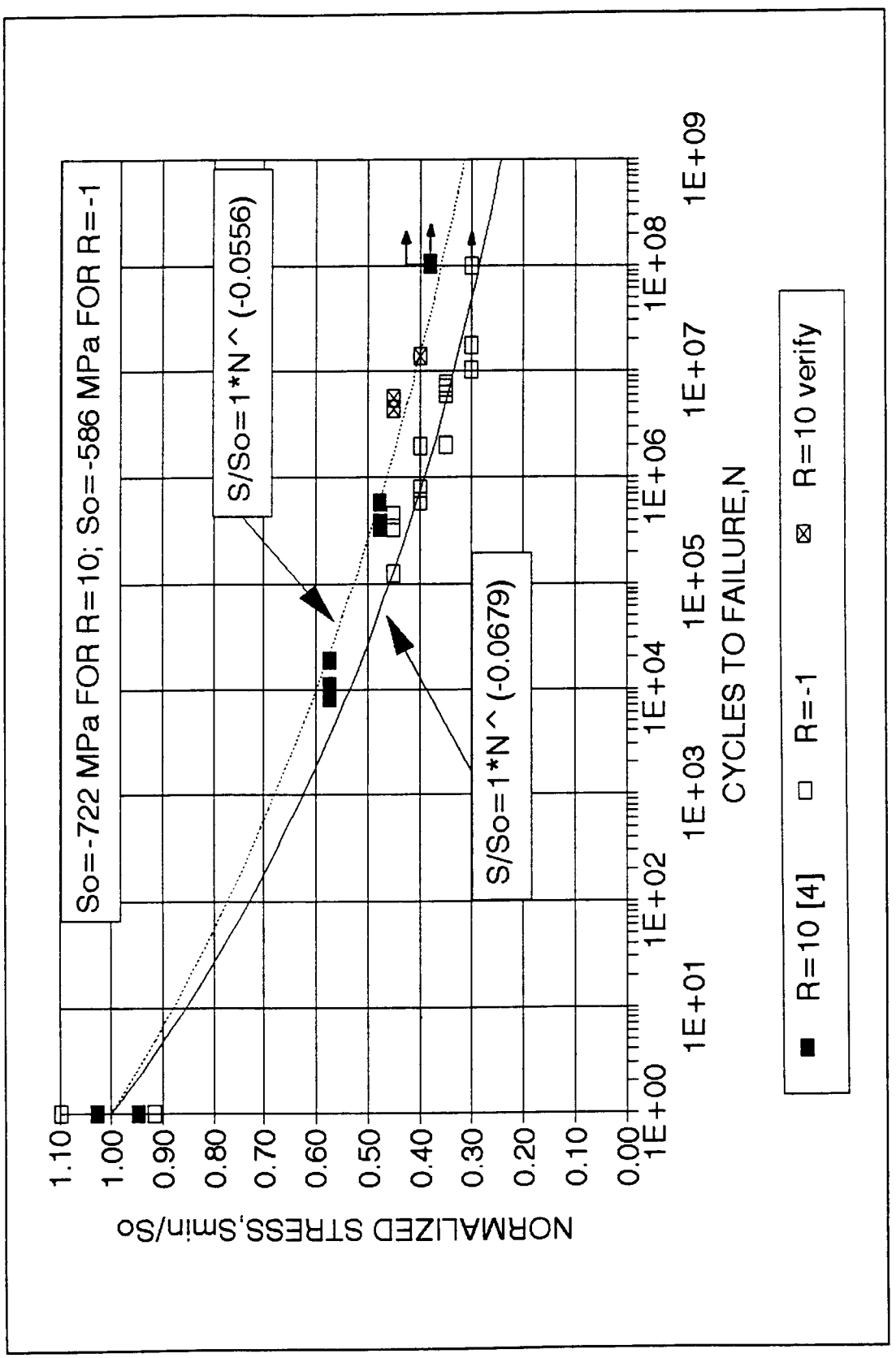

Figure 13. Longitudinal R=-1 S-N Data Normalized by the Compressive Strength Compared With R=10 Data from Ref.[4].

and 10 high frequency data correlate well with those for standard coupons at lower frequency.

A linear regression fit including runout points was done for the points above 10^5 cycles. The slope of regression line, b, is 0.0755. The goodness of the fit is R^2=0.8649. Figure 14 shows the fit plotted on a linear-log scale; this is used to plot Goodman Diagrams above 10^5 cycles.

Few reversed loading tests have been reported in the literature, especially for E-glass composites. The only reference found in longitudinal reversed loading of E-glass/polyester composites is a fatigue database by Bach *et al.* [38] with the data taken from reports of the named laboratories and a Concerted Action Report. The strength of material they selected is different from this study, about 1.8% failure strain in tension and 1.4% failure strain in compression, compared with 3.43% failure strain in tension and 1.46% in compression in this study. The slope of regression line is 0.121, compared with 0.0775 in this study. Therefore, this study shows less fatigue sensitivity of E-glass/polyester than the result in Bath's [38] database. This difference is most likely the result of different materials and test geometries, and the lateral compression restrain used in Bath's database for compression loading. In addition, Bath's database extrapolates the fatigue to 10^8 cycles. The fatigue data up to 10^8 cycles in this study is first measured data of this kind reported.

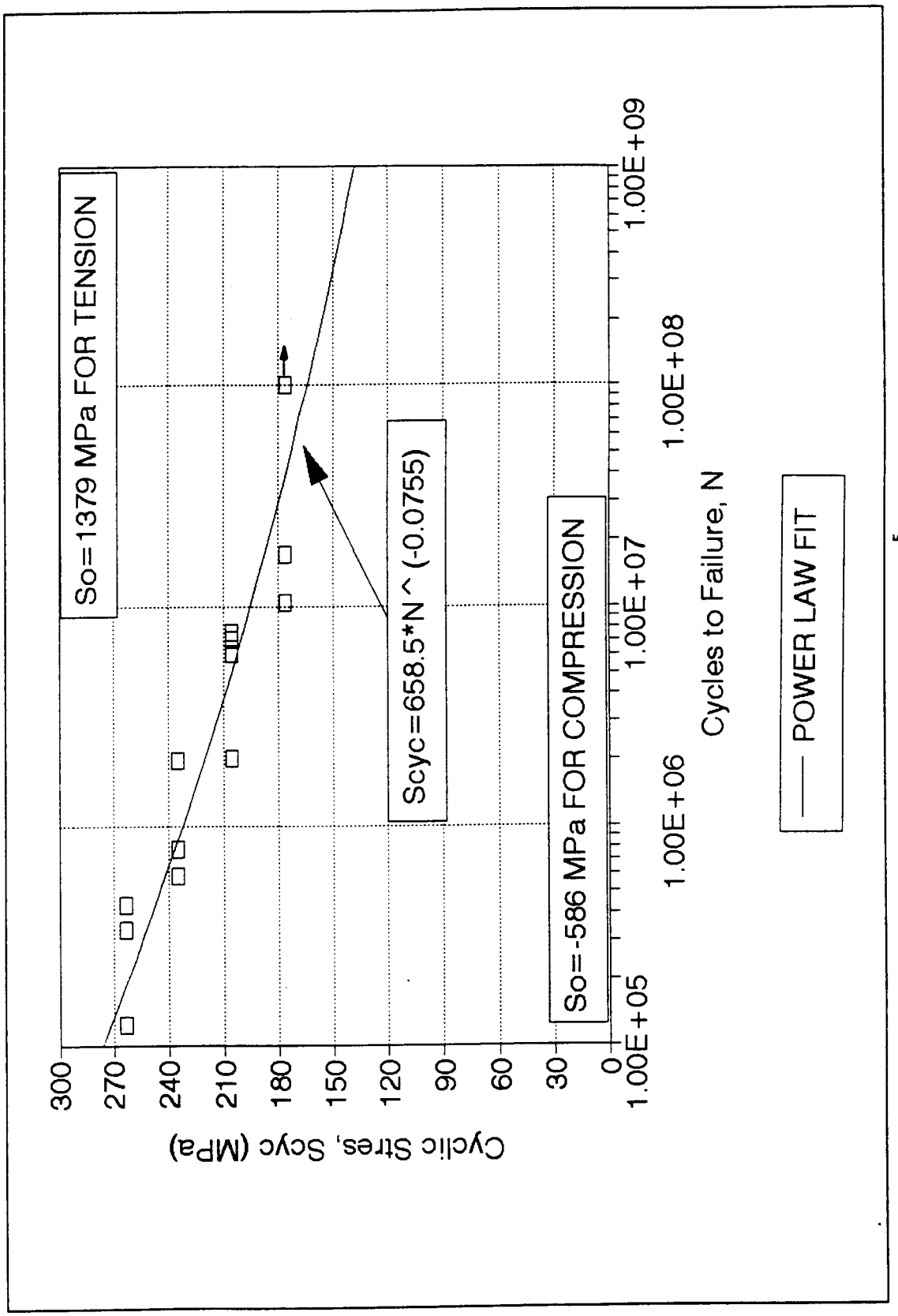

Figure 14. Power Law Fit of R=-1 S-N Data Above 10^5 Cycles.

Tests were also conducted in reversed loading with an R value of -0.5 to extend this database, but only to 10^7 cycles in this case. This reversed loading corresponds to a stress ratio range of interest for wind turbine blades. Figure 15 shows the R=-0.5 curve, with the raw data in Appendix A. The data show little difference from the R=-1 data.

Goodman Diagrams

Goodman Diagrams are commonly used in industry for design purposes and lifetime predictions. They present various combinations of uniaxial mean and cyclic stress or strain for failure at a specified lifetime.

As mentioned in Chapter 2, the Goodman Diagram is generated based on the S-N diagram curve fits. For composites, a straight line is often observed on a log-log scale of the S-N diagram [3] with a departure from linearity in the low cycle region to the ultimate tensile or compressive stress on the ordinate (N=1). Therefore, the linear regression is calculated for data with $N \geq 10^3$ and $N \geq 10^5$. Runouts (data from tests which did not fail before 10^8 cycles) are included in the calculation. In the regression analysis, the number of cycles to failure, N, is taken as the independent variable and the normalized load level S/S_o as the dependent variable. Appendix B gives the actual data and Appendix C gives the curve fits used in generating the Diagrams.

On a log-log scale, the straight line is given by

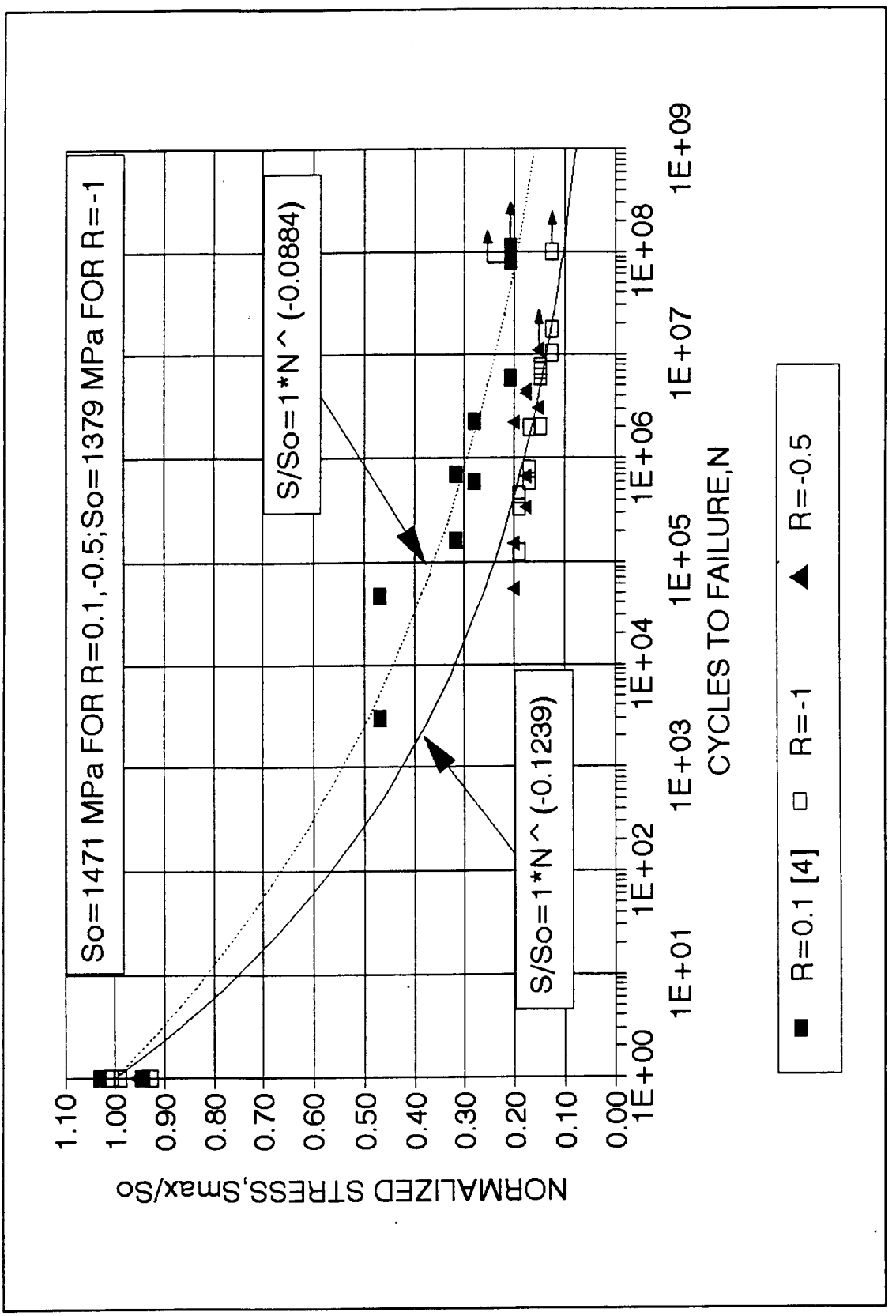

Figure 15. Longitudinal R=-0.5 S-N Data Compared with R=0.1 [4] and R=-1.

following equation:

$$\frac{S}{S_o} = c * N^{-b} \qquad (8)$$

where S/S_o is the normalized maximum stress, b is the slope of the regression line and c is a constant representing the point of intersection of the regression line with the ordinate (Y-axis). The curve usually does not pass through the one-cycle data if only fatigue data are included. As shown in Appendix B, no data between 1 and 10^3 cycles were collected in the tests. This could be of particular importance in reversed loading, where a failure mode change may affect the S-N curve slope.

Linear regressions were conducted by Belinky [3] for E-glass/polyester longitudinal tests at R=0.1, 10 and 2. R=-1 and 0.5 data fits were done in this study. The constants c and b are listed in Table 1 for the data fits for $N \geq 10^3$ and Table 2 for $N \geq 10^5$ cycles. R^2 in the tables represents standard deviation of the linear regression fits.

Table 1: Linear Regression for Longitudinal $N \geq 10^3$ Data.

R	c	b	R^2
0.1	0.969	0.0862	0.8748
0.5	0.977	0.0623	0.8817
-1*	0.477	0.0755	0.8649
-1#	1.124	0.0755	0.8649
10	0.862	0.0445	0.9895
2	0.869	0.0209	0.5131

Note: (a) * signifies the normalization performed with tensile strength

(b) # signifies the normalization performed with compressive strength

Table 2: Linear Regression for Longitudinal $N \geq 10^5$ Data.

R	c	b	R^2
0.1	0.740	0.0699	0.8987
0.5	0.977	0.0623	0.8817
-1*	0.477	0.0755	0.8649
-1#	1.124	0.0755	0.8649
10	0.802	0.0402	0.9976
2	0.802	0.0162	0.8490

Note: (a) * signifies the normalization performed with tensile strength

(b) # signifies the normalization performed with compressive strength

The linear regression fits represent the average fatigue life of specimens at a particular R value and maximum stress, over the cycle range given. The corresponding uniaxial mean and cyclic stress for failure at a specified lifetime are calculated and plotted on Goodman Diagrams. While it has been found that these data can be used to predict the behavior of typical industry materials in certain fiber dominated cases [3,4,5], many industry materials such as those using triax reinforcement, show more severe fatigue sensitivity [2].

Figure 16 is a stress-based Goodman Diagram for the failure cycles from 10^5 to 10^8. As R=0.5 tensile specimens for this research and R=0.1 tensile specimens for the previous research by Belinky [2] were made from different composite plates, their strengths were different. Therefore, the tensile strength of specimens in the Goodman Diagram has been

normalized by the average strength. Figure 17 is a normalized Goodman Diagram with R=2, 10 and -1 data normalized by the compressive strength, and R=0.1 and 0.5 normalized by tensile strength.

To generate the strain-based Goodman Diagrams, the mean strain and cyclic strain of each R value test were calculated by dividing by the initial modulus. Strains for the R=-1 data were divided by its average tensile and compressive initial modulus. The strength and modulus of each R value test are listed in Table 3.

Table 3: Strength and Modulus.

Stress Ratio (R)	Tensile Strength (MPa)	Compressive Strength (MPa)	Initial Modulus (GPa)
0.1	1471		46.20
0.5	1338		39.23
-1	1379		39.23
-1		586	41.16
10		722	35.65
2		722	35.44

Figure 18 shows the strain-based Goodman Diagram from 10^5 to 10^8 cycles. Figure 19 is the strain-based Goodman Diagram from 10^3 to 10^8 cycles. Figures 18 and 19 are different in the cycle ranges of 10^5 to 10^8 because data before the 10^5 cycles were accounted for in Figure 19 and not accounted in Figure 18. The strain-based Goodman Diagram is different in shape from stress-based Goodman Diagram mainly because the modulus for the R=0.1 material batch was higher than the others.

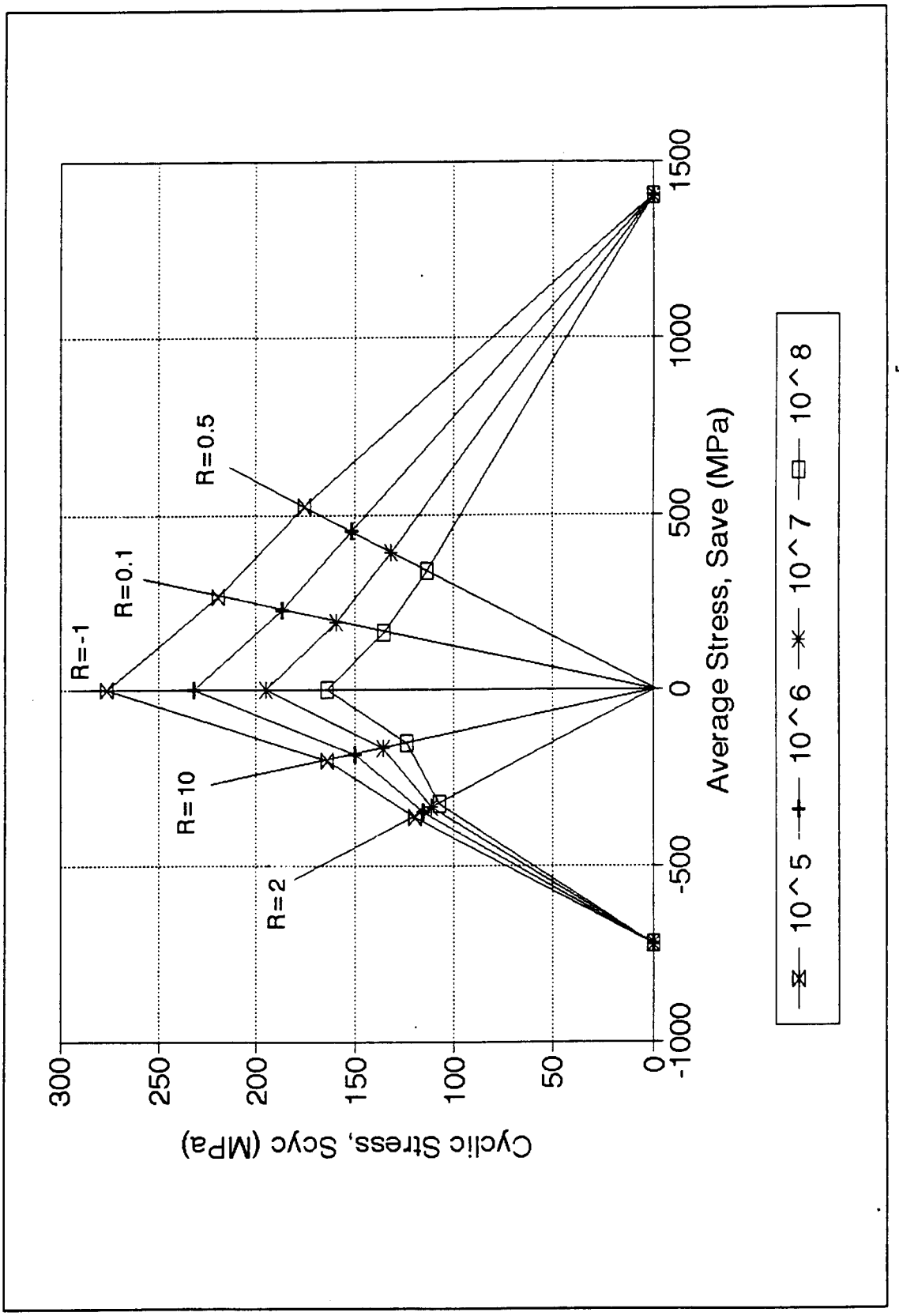

Figure 16. Longitudinal Stress-based Goodman Diagram Above 10^5 Cycles.

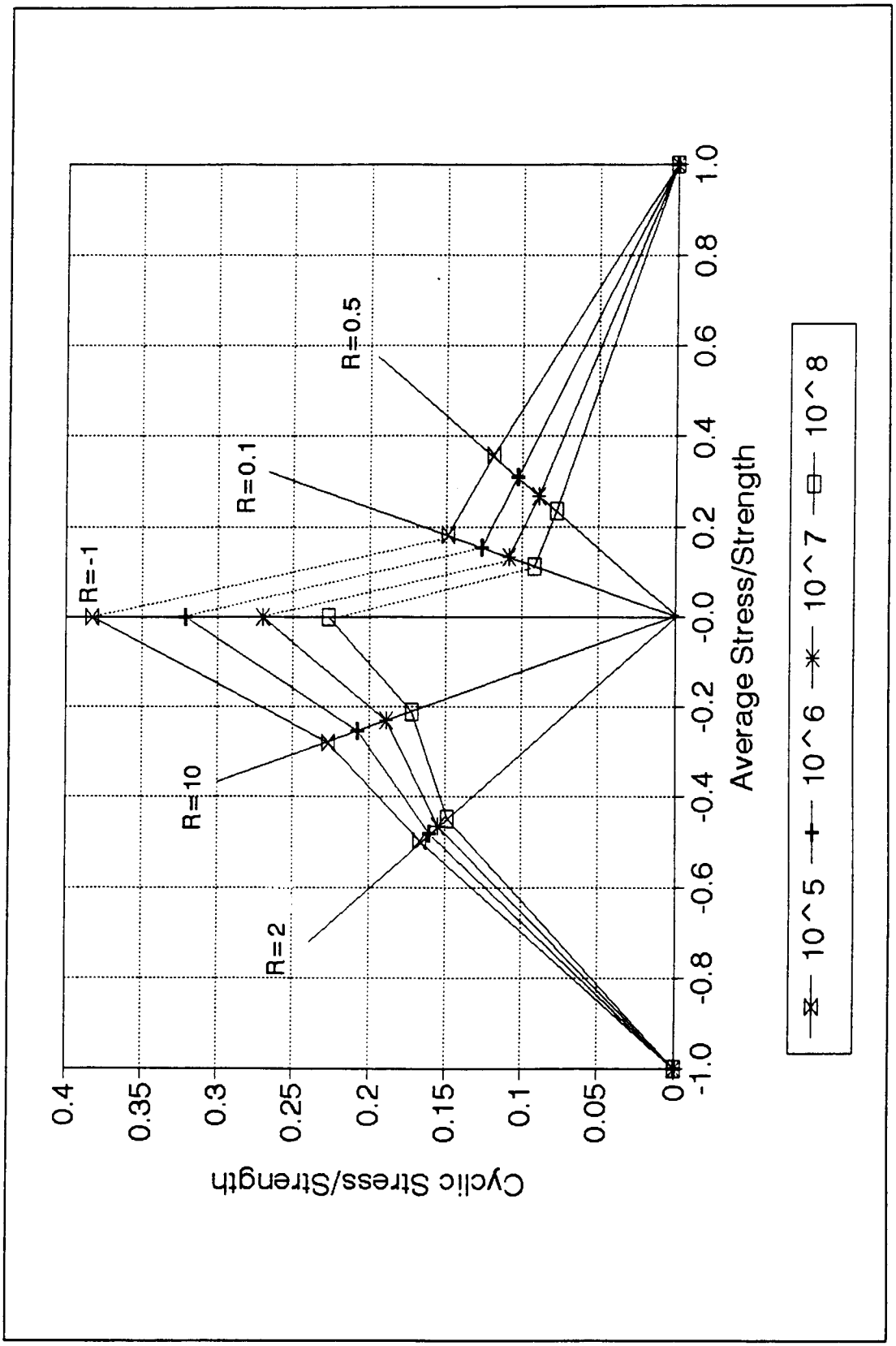

Figure 17. Longitudinal Normalized Goodman Diagram (R=2, 10, -1 Normalized by Compressive Strength; R=0.1, 0.5 Normalized by Tensile Strength).

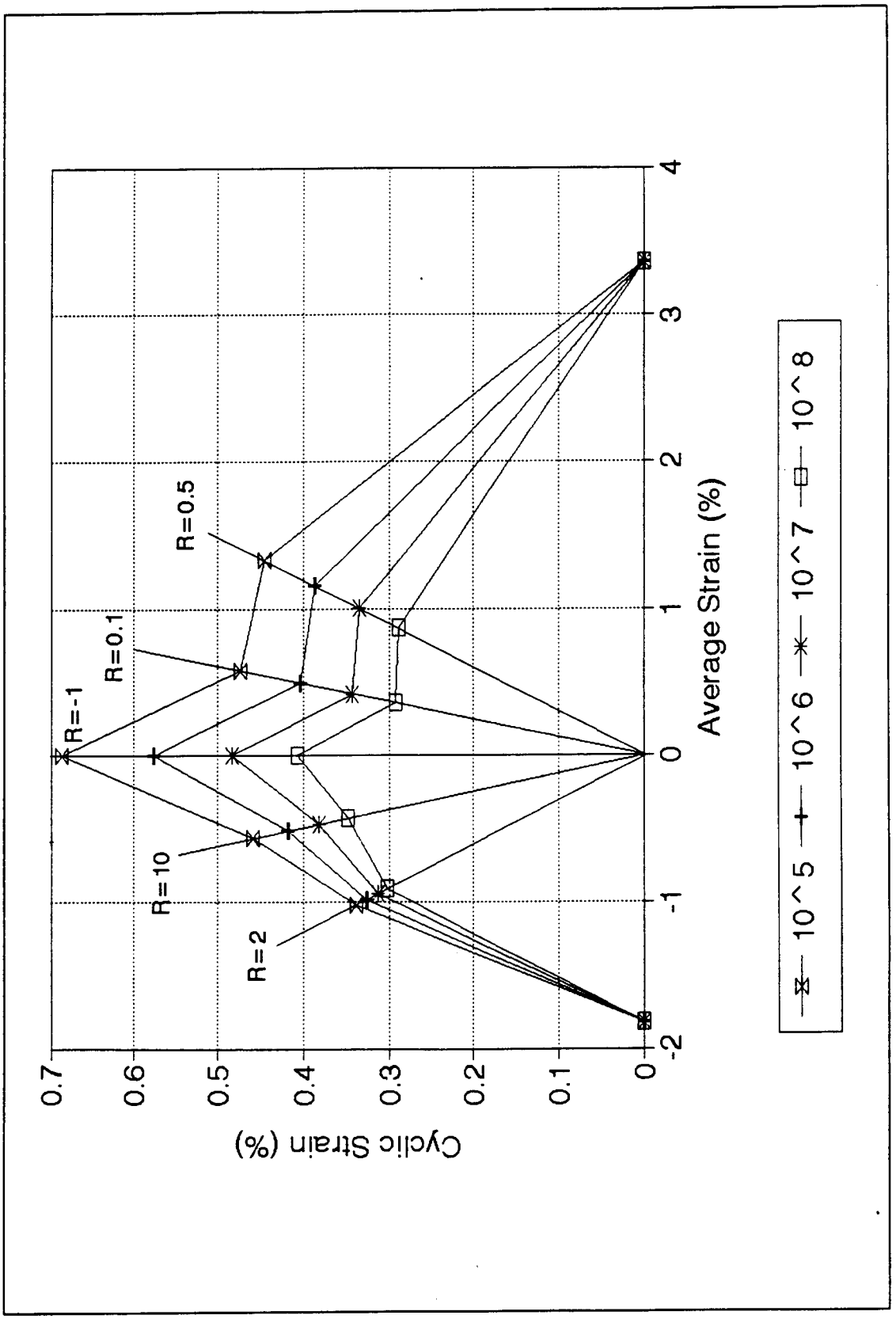

Figure 18. Longitudinal Strain-based Goodman Diagram Above 10^5 Cycles.

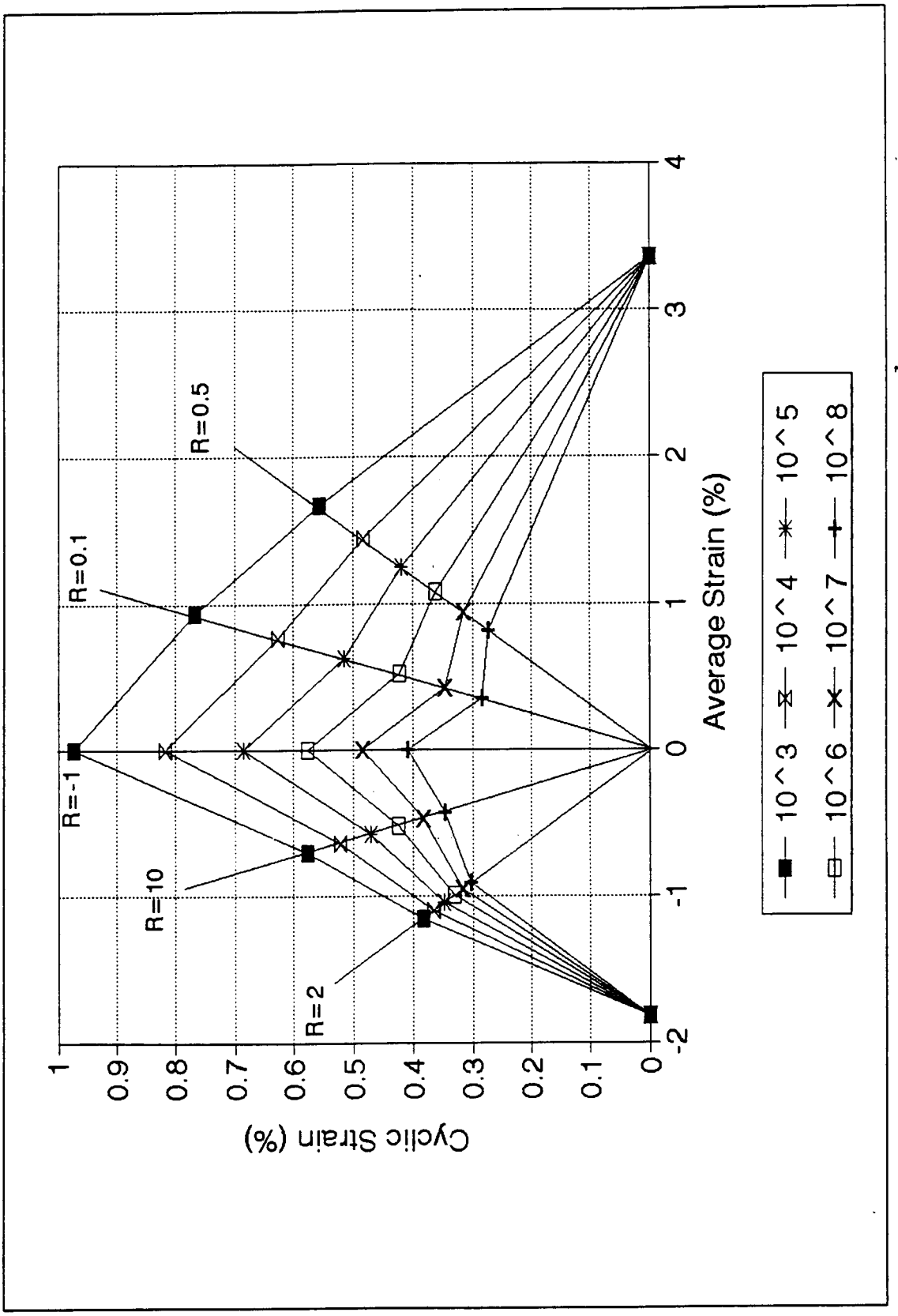

Figure 19. Longitudinal Strain-based Goodman Diagram Above 10^3 Cycles.

The Goodman Diagram from one cycle to 10^3 cycles is important for the low cycle fatigue applications. The reason this kind of Goodman Diagram was not generated in this research is that the tensile strength and compressive strength of reversed loading tests were different. Therefore, it is difficult to interpret the one cycle cyclic stress of R=-1 tests. Furthermore, no data between 1 and 10^3 cycles were collected in the tests, and the curve fits in this range may not represent the behavior well.

A Goodman Diagram of unidirectional E-glass/polyester composite was also generated by Bath *et al.* [38] with selected data of five R values, R=0.1, 10, -1, 0.4, -2.5, and extrapolated to 10^8 cycles. The R=0.4 and -2.5 data for their Goodman Diagram is chosen from the tests of 0/45 specimens, R=10 data from 0/45 and 0/10 specimens, and R=0.1 data from 0, 0/c (c means that the laminate contains layers with choppered fibers), 0/45, 0/10 and 0/30 materials, R=-1 data from 0,0/c/90, 0/90, 0/c and 0/45 laminates. The average failure strain is relatively low in their Goodman Diagram, about 1.8% in tension and 1.4% in compression, compared with 3.3% and 1.8% in this study. This study show less fatigue sensitivity than Bath's database [38], the slope of regression line for R=0.1, 10 and -1 S-N data are 0.0699, 0.0402, 0.0755, respectively, for $N \geq 10^3$ data, compared with 0.123, 0.074 and 0.121 in their database. Again, the difference is most likely the difference of materials used as well as buckling constrain

effects.

Failure Modes

Representative reversed loading specimens broken under static tension and static compression are shown in Figure 20. Specimens failed under low and high cycles are shown in Figure 21. All specimen failures occurred catastrophically in the gage section, without any noticeable warning such as preliminary cracking. A little delamination along the tapered gage section edges was observed in two high cycle specimens before failure. However, it is believed this minor delamination did not cause premature failure of the specimens.

Figure 22 presents the specimens failed under R=0.5 pure tension fatigue in this research. The characteristic of pure tension failure is fibers broken and pulled out after the axial cracking of the matrix. Typical specimens failed under compressive fatigue mode observed by Belinky [4] are shown in Figure 23 for comparison.

Reversed loading fatigue failure is somewhat different than pure the tension-tension failure mode (Figure 22) and pure compression-compression failure mode (Figure 23). It differs from the tensile failure mode as fiber pull out and brush-like failure surfaces are not observed in reversed loading failure. In compression, the failures appear to be matrix dominated and the failure surface is flatted at an angle to the specimen; while in reversed loading, more fiber

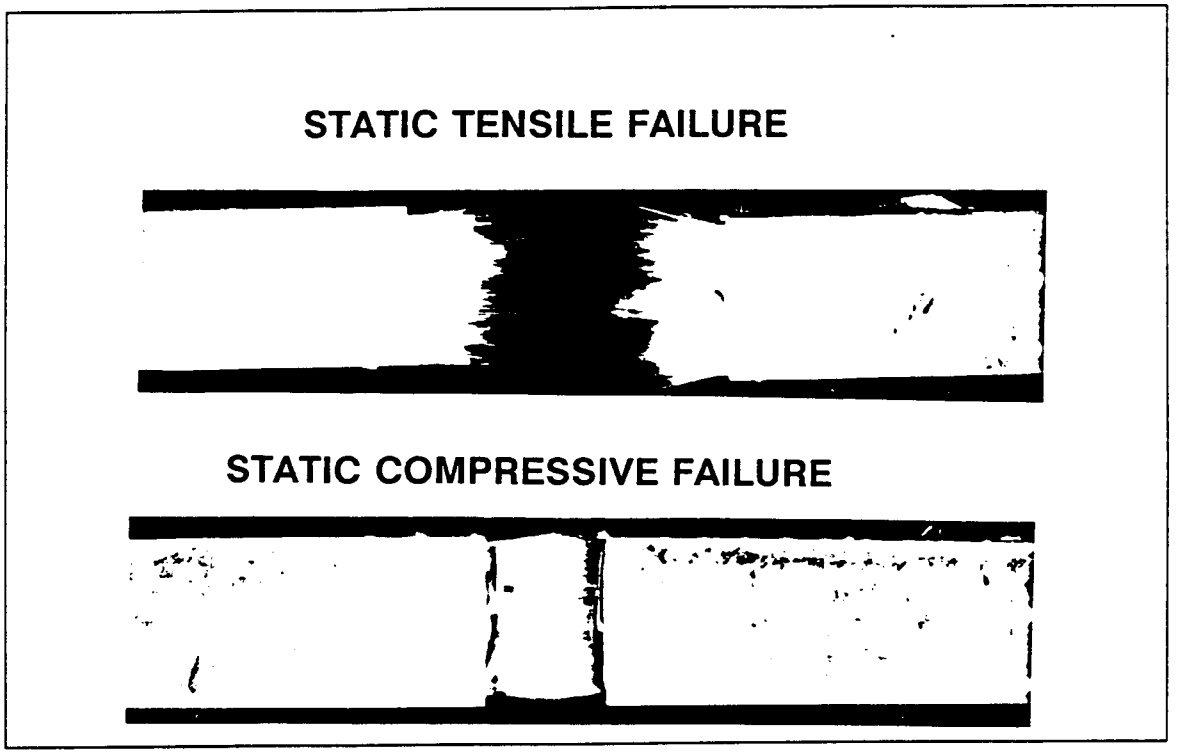

Figure 20. Static Failure of Reversed Loading Specimens

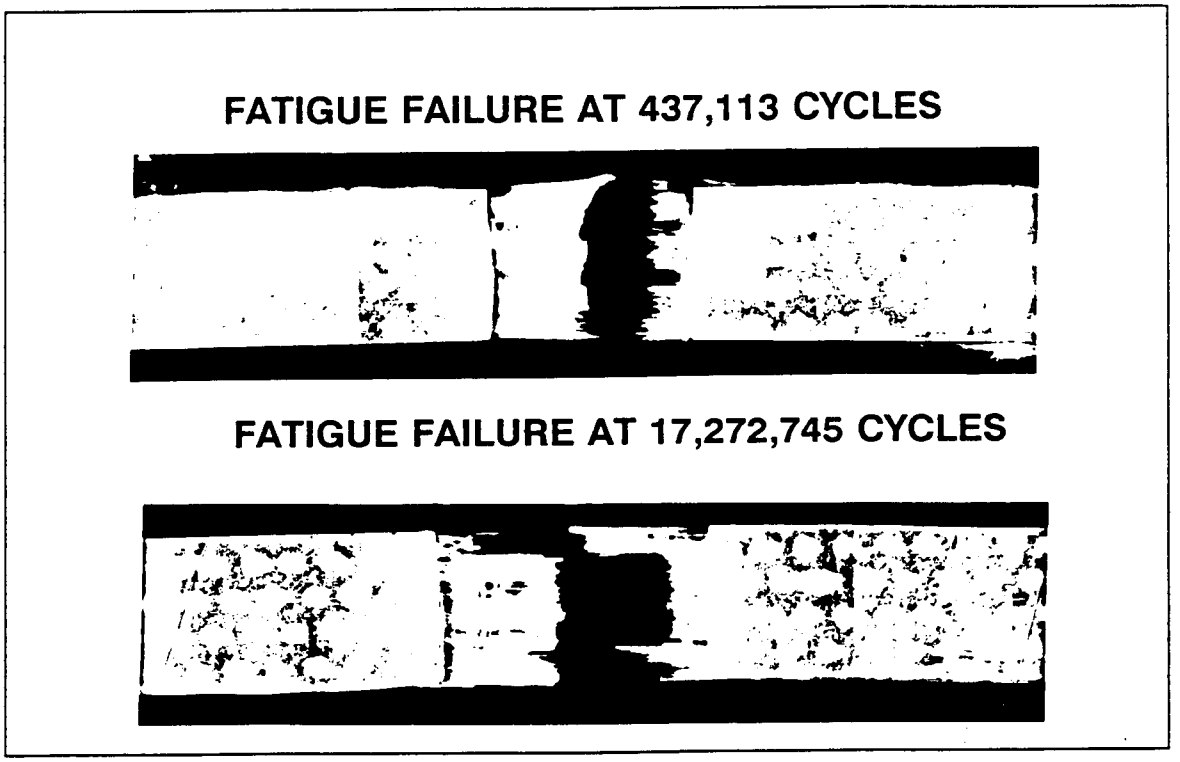

Figure 21. Fatigue Failure of Reversed Loading Specimens.

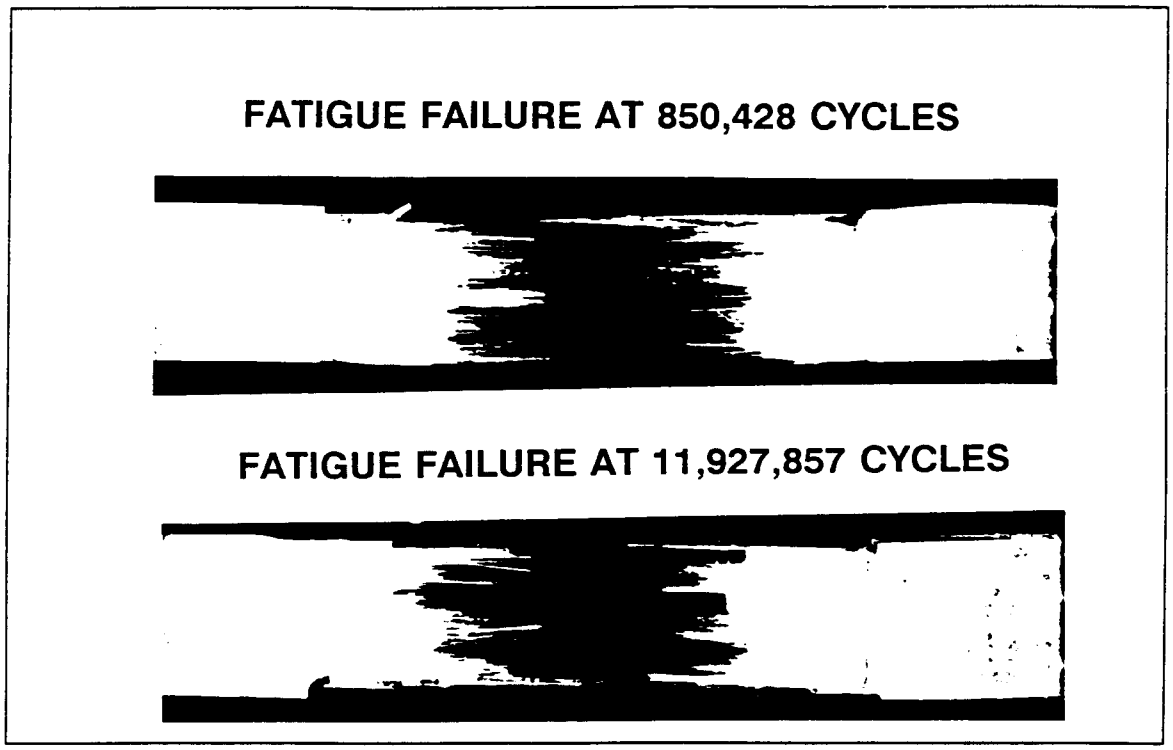

Figure 22. Fatigue Failure of R=0.5 Tensile Specimens.

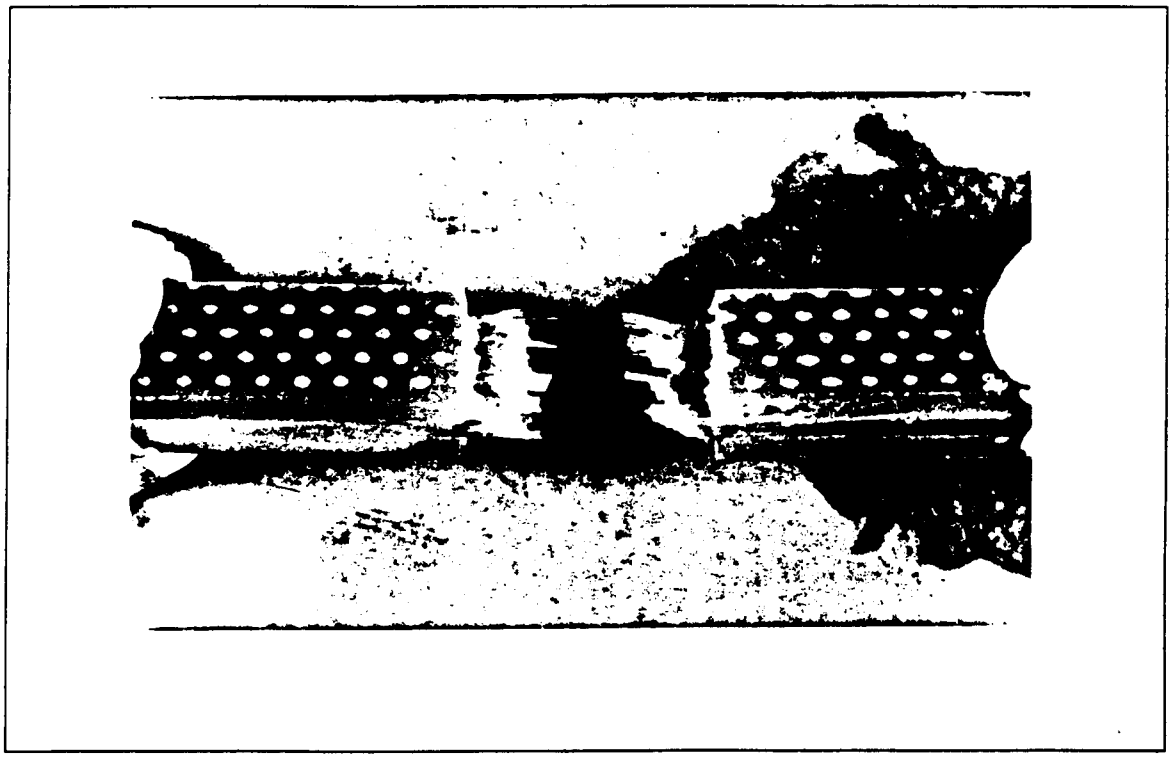

Figure 23. Fatigue Failure of R=10 Compressive Specimen [4].

breakage was found and no sign of buckling is observed. The reversed loading failure mode seems to be a combination of pure tension and pure compression failure modes. It was observed in reversed loading tests that high stress tests failed in a more compressive mode while lower stress tests failed in a more tensile appearing mode. The specimens under higher maximum stress are all broken in thinnest part of gage section, while some specimens under lower maximum stress did not fail in thinnest part of gage section because fiber pull out and delamination are involved.

Transverse Test Results

Fatigue Results

Results from transverse fatigue tests are useful in predicting the onset of initial damage in multidirectional laminates. Total failure then can be predicted by modelling of load redistribution onto the longitudinal plies. Slow static tests were conducted to measure the tensile and compressive modulus of transverse specimens.

The average initial modulus for the tensile tests was 8.62 GPa and the average initial compressive modulus was 8.96 GPa. As tensile and compressive moduli were very close, an average modulus of 8.79 GPa was used to generate the strain-based Goodman Diagrams. The fiber volume fraction of the specimens was 39% and the porosity about 2.6%. The single cycle strength values for tension and compression are 21.5 and 117 MPa,

respectively. This major difference is typical of brittle materials containing flaws, as is the case here.

Five different stress ratio (R) values for transverse tests were studied in this research, R=0.1 and 0.5 tensile fatigue, R=10 and 2 compressive fatigue, and R=-1 reversed loading. Figure 24 shows the normalized S-N data obtained at R values of 0.1 and 0.5. The slope of the R=0.5 S-N curve is considerably flatter than that of R=0.1 curve, consistent with the longitudinal results. To be more complete, 10^8 cycle data are needed in future studies. Therefore, the R=0.5 data in the transverse Goodman Diagrams are subject to change.

Figure 25 gives the normalized S-N data for R=10 and 2 compressive tests. The slope of S-N curve for R=2 is again much flatter than that for R=10. The compressive single-cycle strength is more than five times higher than the tensile single-cycle strength, so the significance of transverse failures in laminates under tensile and compressive loading is markedly different.

The S-N data for R=-1 (reversed loading) are shown in Figure 26 compared with the R=0.1 data. As the specimens were made from different plates, the single-cycle tensile strength for R=-1 specimens was about 16% less than the strength of R=0.1 specimens. In transverse Goodman Diagram generation, the stress level of R=-1 specimens were normalized to a strength of 21.5 MPa, the strength of R=0.1 and 0.5 specimens. The R=-1 S-N data fall below the R=0.1 data amplitude. This indicates

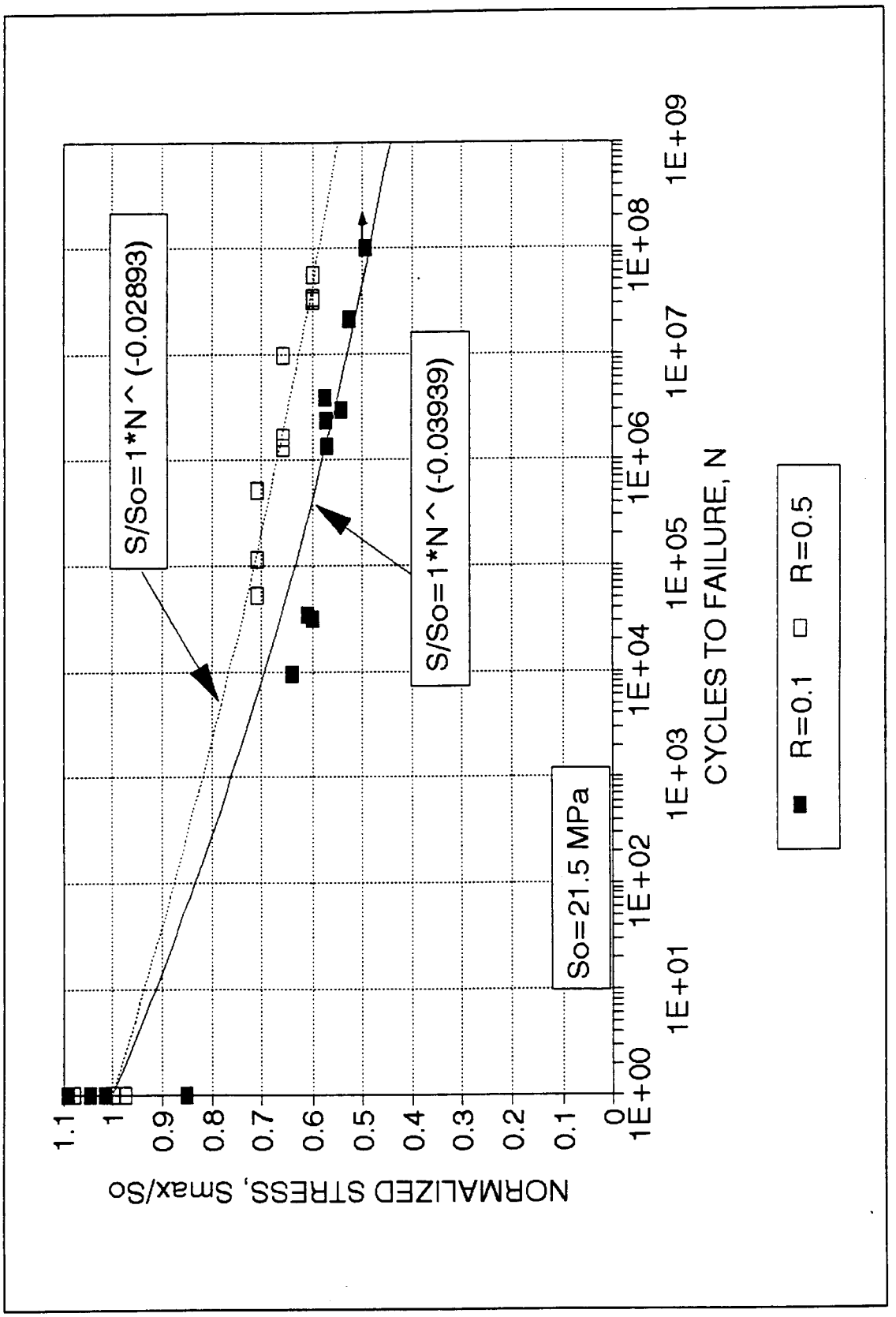

Figure 24. Transverse R=0.1 and R=0.5 S-N Data.

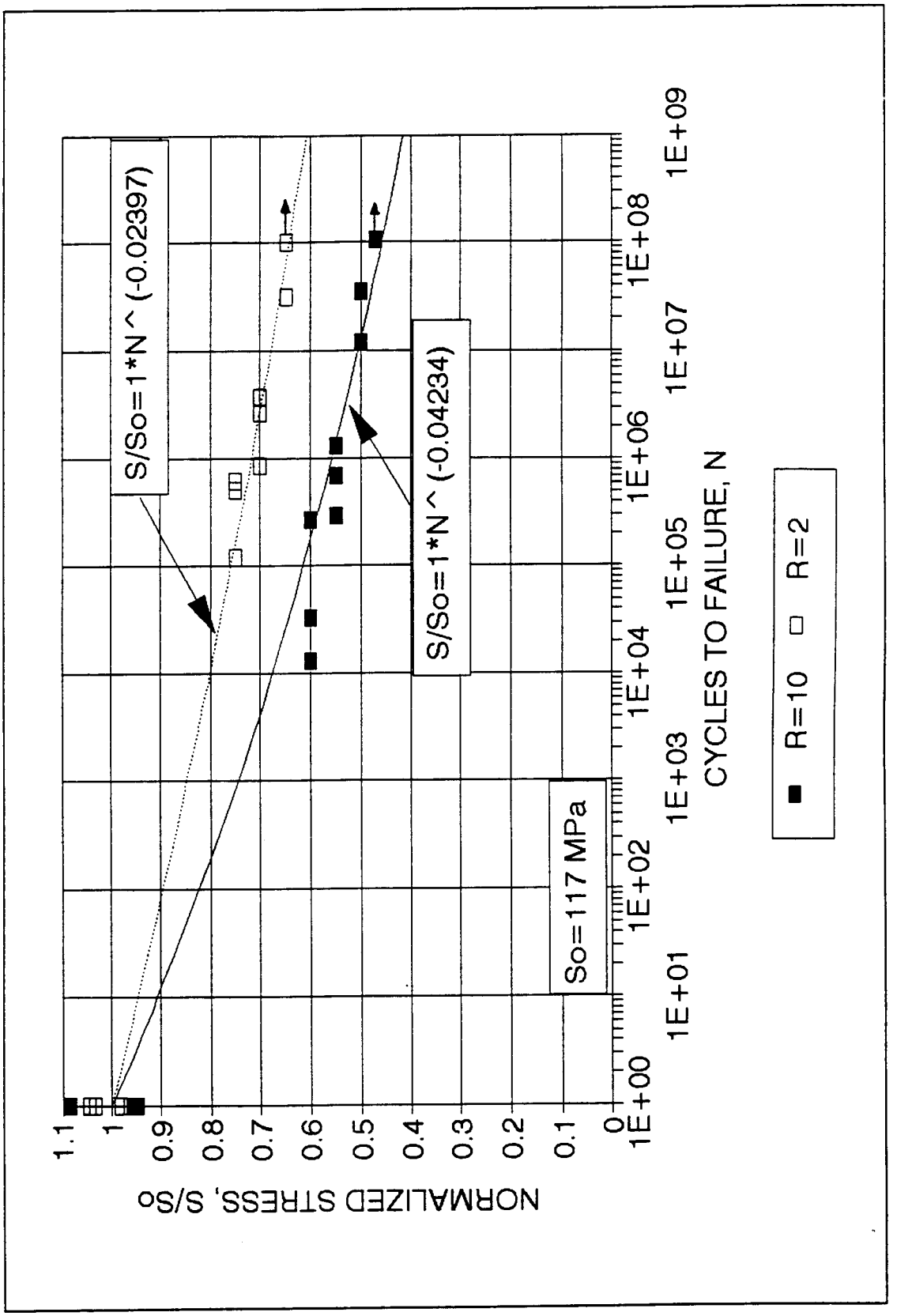

Figure 25. Transverse R=10 and R=2 S-N Data.

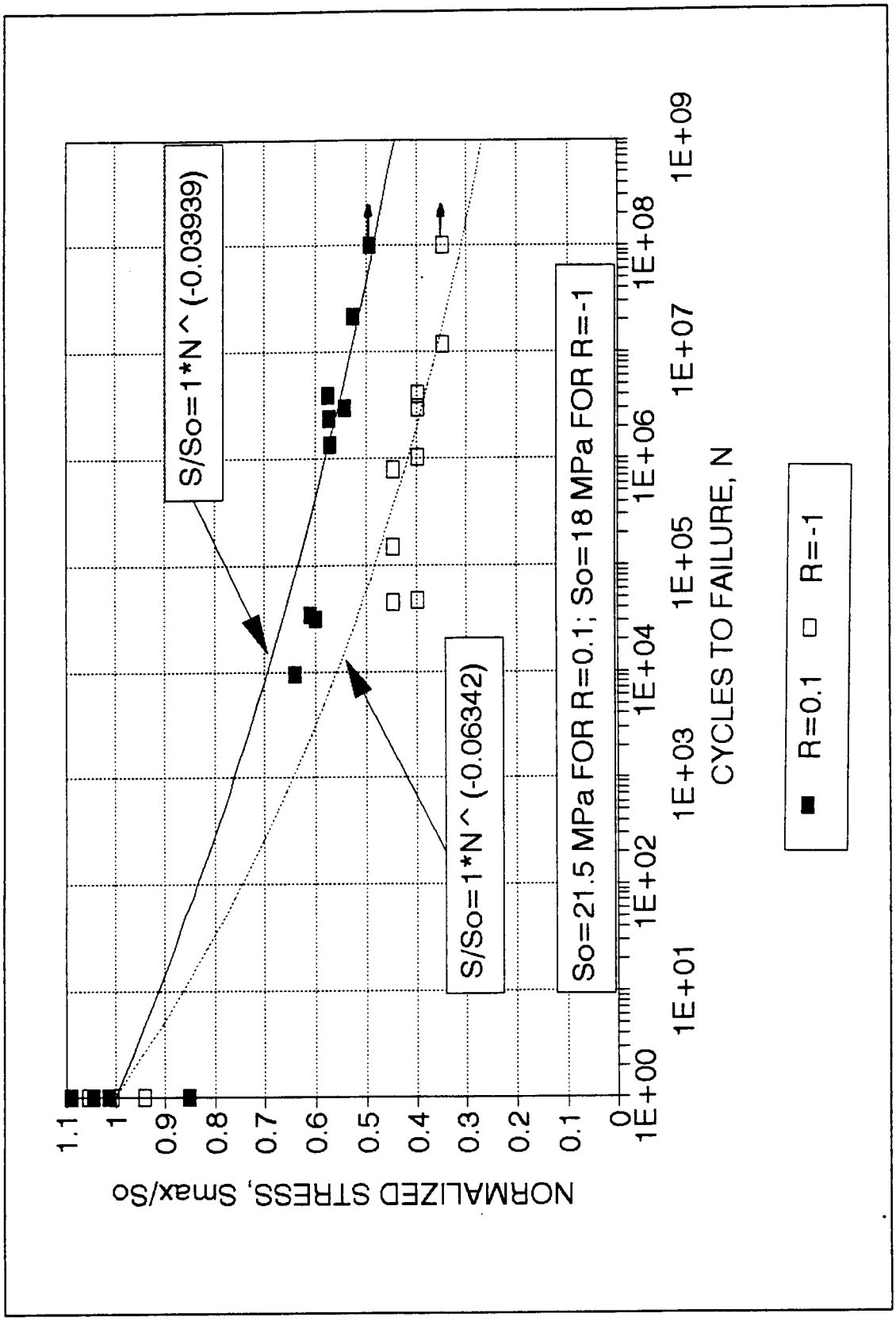

Figure 26. Transverse R=-1 S-N Data Compared with R=0.1 Data.

that reversed loading produces a worst case in this application. All the specimens in the R=-1 tests failed in a tensile appearing mode.

As mentioned in Chapter 2, a few tensile fatigue results for the transverse properties of unidirectional composites have been reported in the literature [15,17,34,35]. R=0.1 S-N curves are all represented by straight lines on linear-log plots with the slopes from 0.07 to 0.1, and show no fatigue limit. The result in this study is consistent with literature, roughly following a 7% decay line. The tensile strength of neat polyester in Mandell's work [17] is 37 MPa, compared with 21.5 MPa in this study. This difference is reasonable as the tensile strength of brittle materials depends on the flaws, and debonds for transverse composites. Acton [34] studied neat epoxy and represented the data by a power fit (including single cycle points), the exponent of the fit is about 22 (see Equation 2), compared with 25 in this study. The difference is insignificant. No report has been found on the transverse fatigue properties under other R conditions.

To generate the transverse Goodman Diagrams, linear regressions for five R value S-N curves were calculated and the results are listed in Tables 4 and 5.

Table 4: Linear Regression for Transverse $N \geq 10^3$ Data

R	c	b	R^2
0.1	0.7924	0.02408	0.8918
0.5	0.9768	0.02709	0.8891

-1*	0.6067	0.02980	0.6123
10	0.8036	0.02805	0.9100
2	1.0170	0.02498	0.8166

Note: * signifies the normalization performed with tensile strength

Table 5: Linear Regression for Transverse N ≥ 10^5 Data

R	c	b	R^2
0.1	0.9512	0.03540	0.8534
0.5	1.0230	0.02995	0.8917
-1*	0.7658	0.04455	0.8166
10	0.8576	0.03215	0.8905
2	1.0170	0.02498	0.8166

Note: * signifies the normalization performed with tensile strength

Based on the linear regression analysis, three transverse Goodman Diagrams were constructed. Figure 27 shows a stress-based Goodman Diagram for the failure cycles from 10^5 to 10^8. Figure 28 is a strain-based Goodman Diagram for the failure cycles from 10^5 to 10^8. Both diagrams used the fatigue data above 10^5 cycles. The strain-based Goodman Diagram from 10^3 to 10^8 cycles is presented in Figure 29. In this diagram, all fatigue data were used except the single-cycle strength data.

Comparing the transverse strain-based Goodman Diagram with the longitudinal case (Figures 19 and 29), the shape is different. The static tensile failure strain for the longitudinal specimen is about 13 times higher than that for transverse specimen, while the static compressive strength is of the same order. This dominates the shape difference. If normalized by their static failure strain, both diagrams are

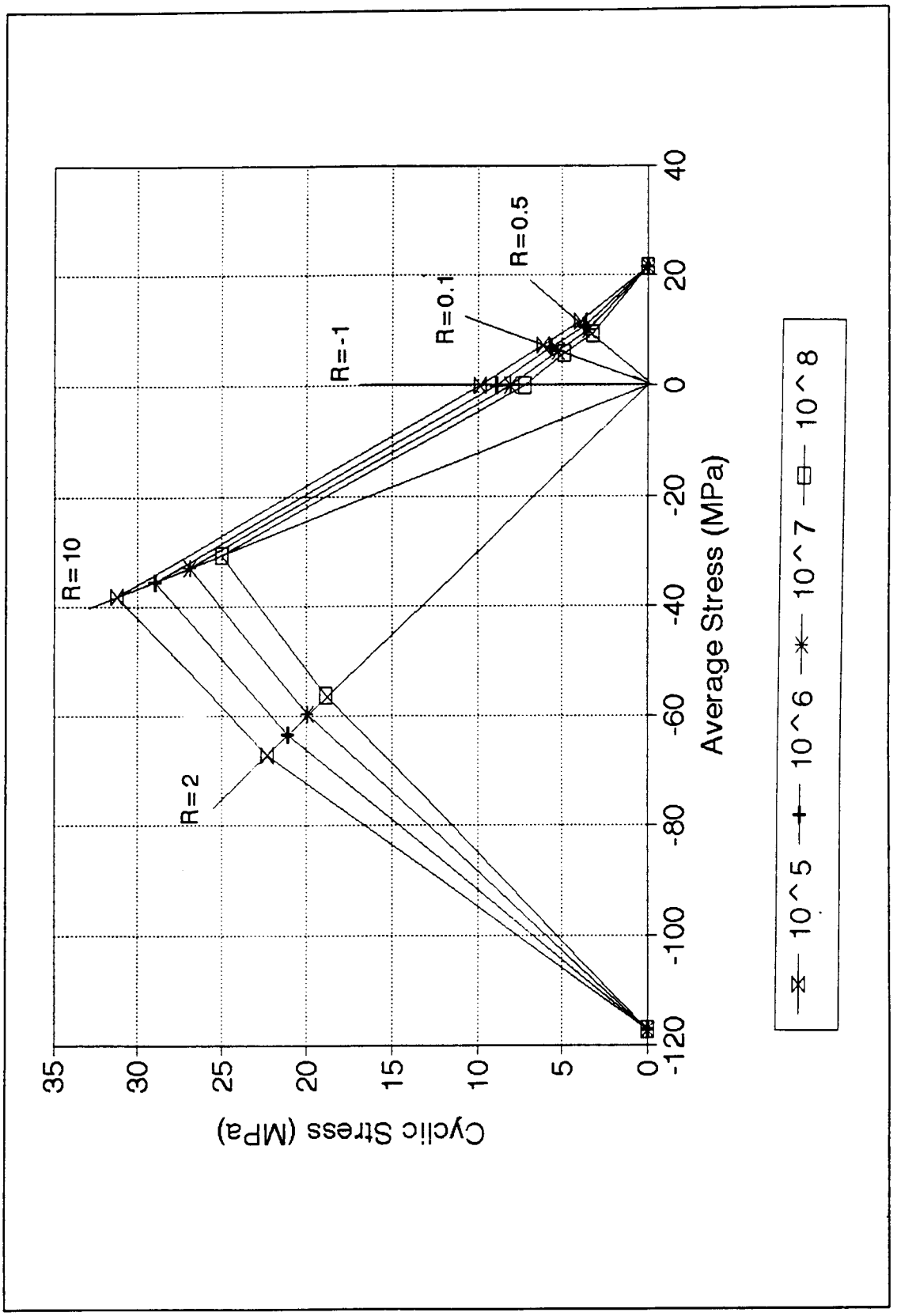

Figure 27. Transverse Stress-based Goodman Diagram Above 10^5 Cycles.

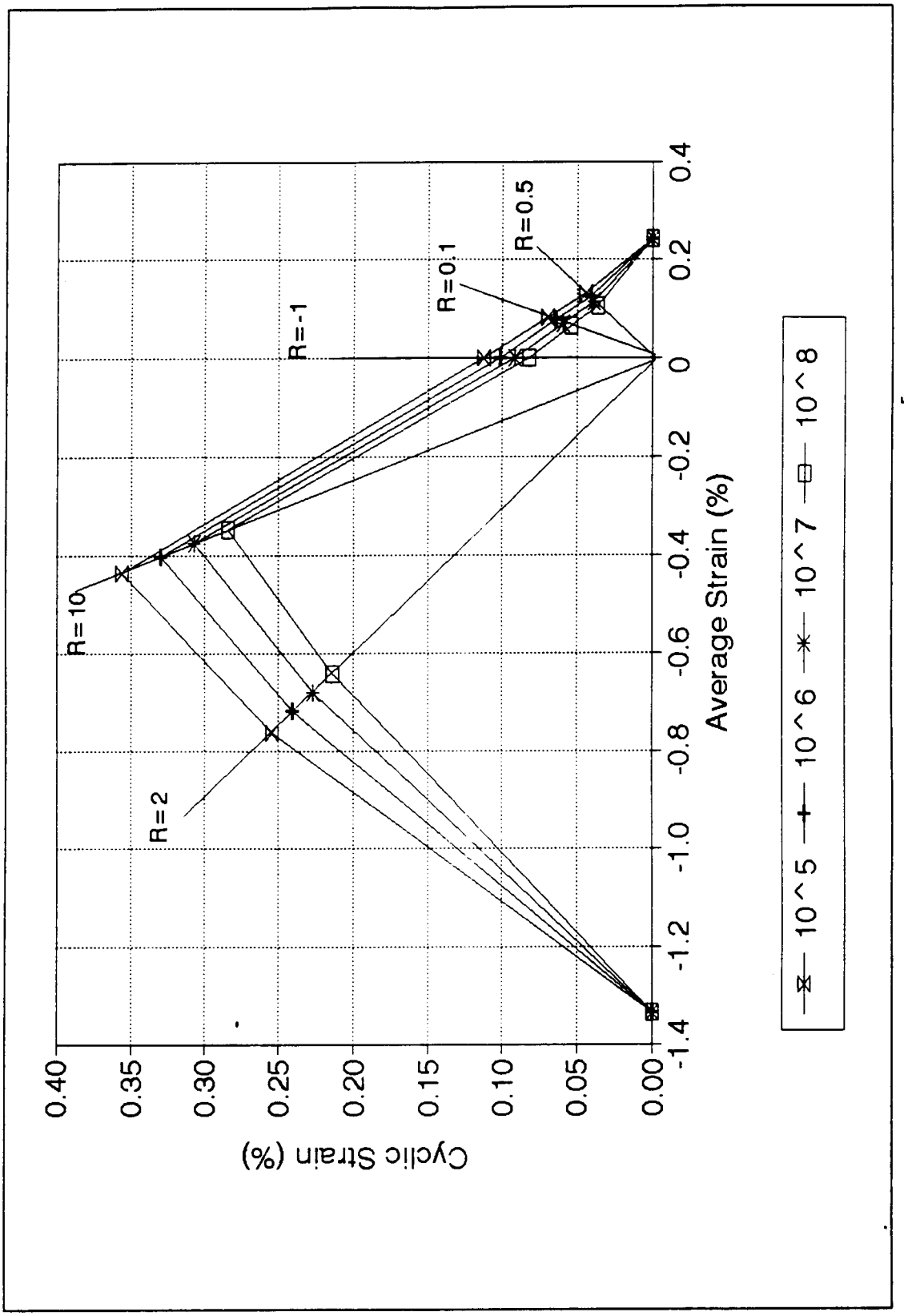

Figure 28. Transverse Strain-based Goodman Diagram Above 10^5 Cycles.

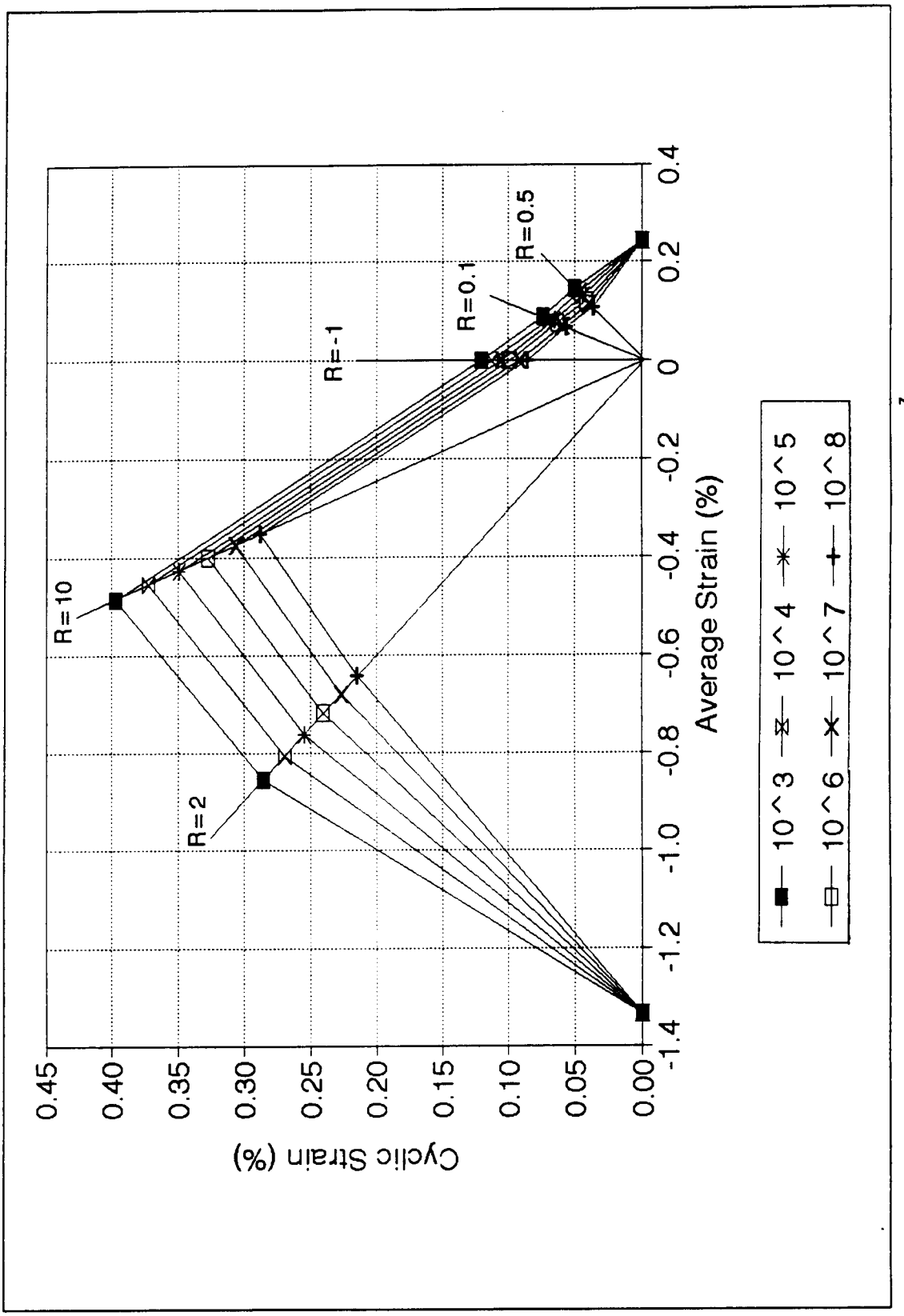

Figure 29. Transverse Strain-based Goodman Diagram Above 10^3 Cycles.

similar in the range from R=-∞ to 10 (pure compression), as they are all matrix dominated failures.

Transverse Failure Modes

Representative transverse specimens broken under pure tensile fatigue are shown in Figure 30. Although the failure is clearly dominated by crack growth in the transverse direction, no stable crack growth was observed run to failure in the tests. All specimen failures occurred suddenly in the gage section. No fiber bridging or breakage along the cracks are observed in the failed specimens. In fact, the failure mode appears to be matrix dominated, and the fatigue sensitivity is similar to that reported for neat matrix materials [17].

The compressive failure mode for transverse specimens is different from the tensile mode (see Figure 31). No failure were found inside the fiber bundles, with all failure zones between the fiber bundles and the matrix. Therefore, compressive failure appears to be matrix-interface dominated.

Although the transverse tests under reversed loading are more fatigue sensitive than are pure tension tests, both failure modes appear to be the same (see Figure 32). The reversed loading failure is in the tensile dominated mode, which is expected from the much lower tensile strength as compared with the compressive strength.

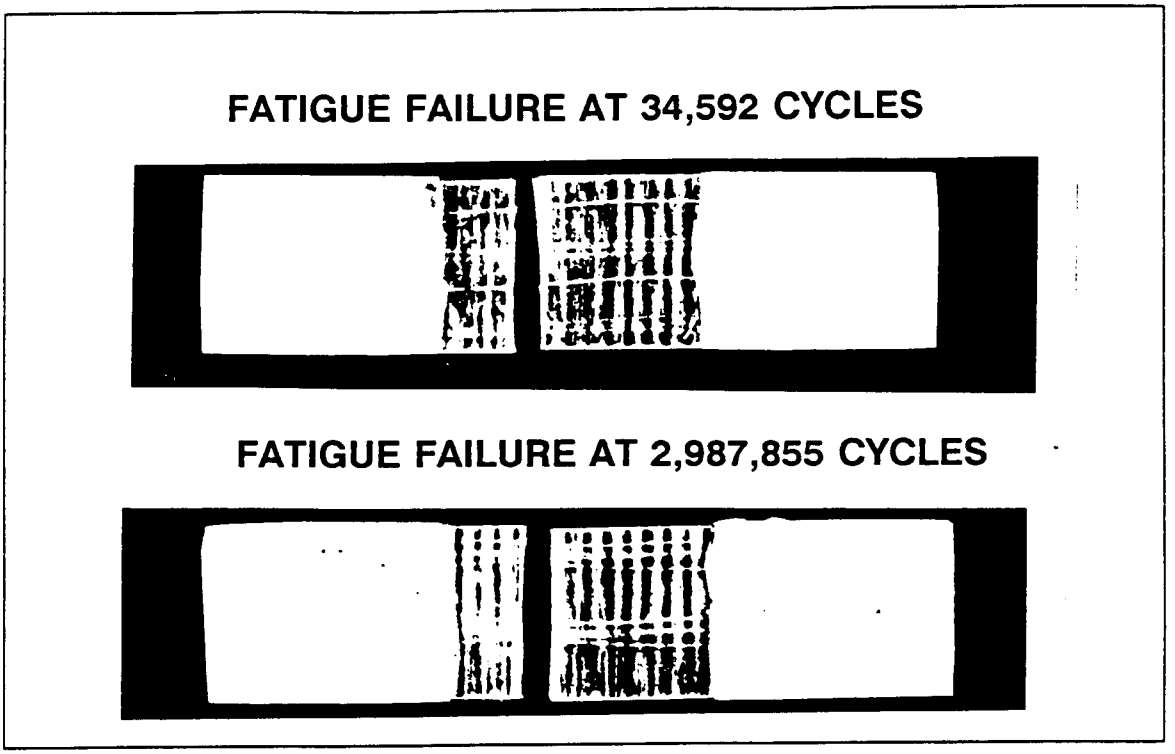

Figure 30. Fatigue Failure of R=0.1 Tensile Specimens.

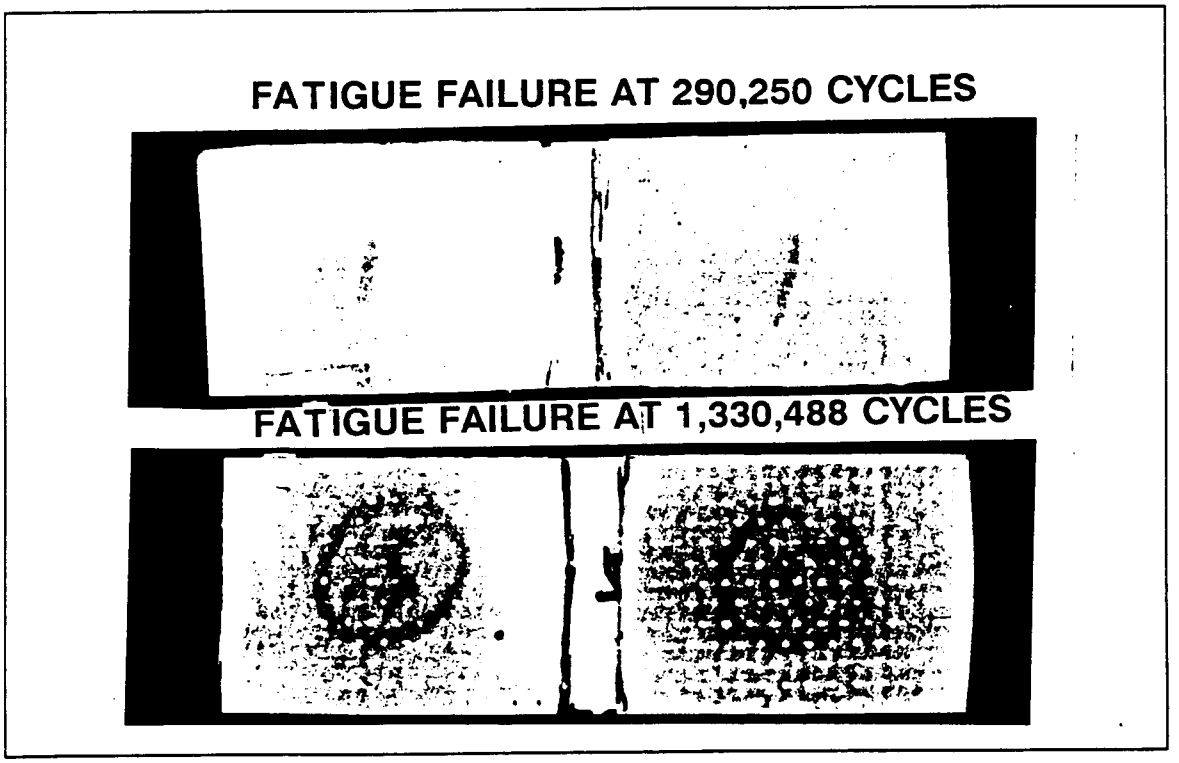

Figure 31. Fatigue Failure of R=10 Compressive Specimens.

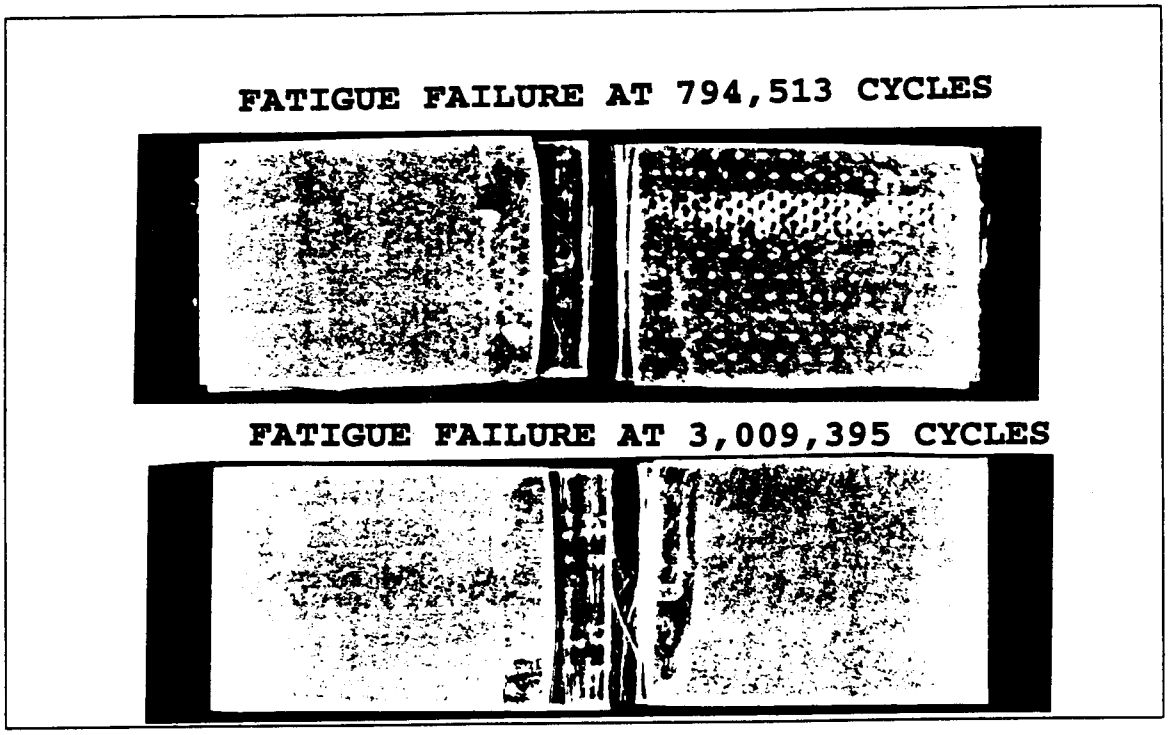

Figure 32. Fatigue Failure of R=-1 Reversed Loading Specimens.

CHAPTER 5

CONCLUSIONS AND RECOMMENDATIONS

Conclusions

The objectives of this research were to develop test methods suitable for high frequency longitudinal reversed loading fatigue tests and transverse fatigue tests at various R values, to obtain S-N fatigue data to high cycles, and to generate longitudinal and transverse fatigue Goodman Diagrams combining the fatigue data generated in previous research by Belinky [4] and this research. These objectives were successfully achieved by the development of suitable specimen geometries and selecting proper test conditions (frequencies) to avoid hysteretic heating failures. The first known 10^8 cycle database for composite materials has been completed and presented as Goodman Diagrams for stress and strain.

Reversed loading is a difficult type of testing, because problems associated with both tensile and compressive testing are involved. Therefore, it is critical to select a suitable specimen geometry. The specimen geometry used in this study was selected after experiments with several other geometries. It is short in gage section to avoid elastic buckling, and thickness tapered in gage section to provide a thin specimen

for heat transfer and to avoid tab debonding. The hysteretic heating effect is stronger in the reversed loading test because the amplitude is larger compared with that at other R values. Therefore, the frequency was lower than for other R values and temperature was measured for each test to avoid overheating. The data obtained were reasonably consistent with R=0.1, 10 data by Belinky [4] and the data out to 10^8 cycles are the first known data in this type of testing for composites.

Transverse fatigue properties are critical in the damage development of typical multidirectional laminates; however few studies of this orientation have been reported in literature. A transverse fatigue database has been well developed in this study through tests conducted at R=0.1, 0.5, 10, 2, and -1. It is the first known database of this type to 10^8 cycles.

Based on the fatigue S-N data and linear regression analysis, longitudinal and transverse Goodman Diagrams have been constructed which can be used in turbine blade lifetime prediction codes [5]. The Goodman Diagrams generated in this study are the first known diagrams to 10^8 cycles without extrapolation for composite materials.

These data should be used with caution. While certain industry laminates correlate with these trends (if the data are normalized by the static strength) when failure is fiber dominated [5], other materials, such as those which are triax based, show more severe fatigue sensitivity. Furthermore, no

fatigue data are available in the 1 to 10^3 cycle range, so curve fits in this range are not experimentally based.

Recommendations

The fatigue behavior of composite materials can be characterized by four failure modes: longitudinal, transverse, shear and delamination. Longitudinal and transverse dominated failure modes in tension, compression, and reversed loading have been studied in previous research by Belinky [4] and in this study. Shear dominated failure and delamination failure modes are important subjects which require further study. Using the results from each of these failure modes, the fatigue behavior of full-size coupons with typical ply configurations could be predicted and the sequence of specimen damage development analyzed.

Loading conditions in wind turbine blades change continuously as the wind characteristics vary. Therefore, another area of importance is to develop a cumulative damage model which treats time varying stress conditions and demonstrate predictions of specimen lifetime under spectral loadings based on the constant amplitude database. In conjunction with this study, it is essential to establish actual blade data, such as load conditions of blades under operation. Those data would then be applied to determine suitable loading conditions for materials under study.

The fatigue behavior of composites with other matrix and

fiber constituents at high cycles is an another important concern that should be addressed. For wind turbine blade materials, E-glass fiber combined with epoxy matrix is often used. A high cycle database should be established and compared with E-glass/polyester materials to determine the overall cost effectiveness.

Finally, the high frequency database should be validated with standard size coupons conducted at lower frequency. These tests should be conducted to as many cycles as possible, and should include both unidirectional and multidirectional laminates typical of wind turbines.

REFERENCES

REFERENCES

1. Committee on Assessment of Research Needs for Wind Turbine Rotor Materials Technology, "*Assessment of Research Needs for Wind Turbine Rotor Materials Technology*", National Academy Press, Washington, D.C., 1991.

2. Mandell, J.F., Creed, R.F., Pan, Q., Combs, D.W., Shrinivas, M., "Fatigue of Fiberglass Generic Materials and Substructures" in SED-Vol 15, Wind Energy 94, ASME, New York, p.p. 207-210 (1994).

3. Creed, R.F., "High Cycle Tensile Fatigue of Unidirectional Fiberglass Composite Tested at High Frequency", Montana State University Masters Thesis, Chemical Engineering Department, 1993.

4. Belinky, A.J., "High Cycle Compressive Fatigue of Unidirectional Glass/Polyester Performed at High Frequency", Montana State University Masters Thesis, Chemical Engineering Department, 1994.

5. Mandell, J.F., "Fatigue of Generic Composite Materials", Department of Energy Wind Program Subcontract Review Meeting, Denver, 1994

6. Hashin, Z. and Rotem, A., "A Fatigue Failure Criterion for Fiber Reinforced Materials", *Journal of Composite Materials,* Vol 17, 1973, p.p. 448-464.

7. Friedrich, K., *Application of Fracture Mechanics to Composites Materials,* Elsevier Science Publishers B.V., Chapter 3-5, 1989.

8. Rosen, B.W. and Dow, N.F., "Mechanics of Failure of Fibrous Composites", in *Fracture,* Vol VII, Liebowitz, H. Ed., Academic Press, (1972).

9. Tai, S.W. and Wu, E.M., "A General Theory of Strength for Anisotropic Materials", *Journal of Composite Materials,* Vol 5 (1971), p.p. 58.

10. Hashin, Z., "Theory of Fiber Reinforced Materials", NASA CR-1974, (1972).

11. Reifsnider, K.L. et. al. "Life prediction Methodologies for Composite Materials", Report of Committee on Life Prediction Methodologies for Composite Materials,

National Research Council, National Academy Press, Washington, D.C. (1991).

12. Sendeckyj, G.P., "Life Prediction for Resin-Matrix Composite Materials", in Fatigue of Composite Materials, Reifsnider, K.L. Ed., Elsevier Science Publishers B.V., p.p. 431-483, 1991.

13. Spera, D.A., "Dynamic Loads in Horizontal-Axis Wind Turbines - Part III: Design Trend Charts", *Proceedings, Wind Energy - 1994 Symposium*, SED-Vol. 15, W.D. Musial *et al.*, eds., New York: American Society of Mechanical Engineers.

14. Mandell, J.F., "Fatigue Behavior of Fibre-Resin composites" in Developments in Reinforced Plastics-2, Properties of Laminates, Pritchard, F. Ed., Applied Science Publishers, London, p.p. 67-107, 1982.

15. Rotem, Assa and Nelson, H.G., "Fatigue Behavior of Graphite-Epoxy Laminated at Elevated Temperature", *Fatigue of Fibrous Composite Materials, ASTM STP 723*, American Society for Testing and Materials, 1981, p.p. 152-173.

16. Dally, J.W. and Broutman, L.J., "Frequency Effects on the Fatigue of Glass Reinforced Plastics", *Journal of Composite Materials*, Vol 1, p.p 424-442, 1967.

17. Mandell, J.F., "Fatigue Behavior of Short Fiber Composite Materials" in Fatigue of Composite Materials, Reifsnider, K.L. Ed., Elsevier Science Publishers, New York, p.p. 232-333, 1991.

18. Rotem, Assa, "Tensile and Compressive Failure Modes of Laminated Composites Loaded by Fatigue with Different Mean Stress", *Journal of Composites Technology and Research*, JCTRER, Vol. 12, No. 4, Winter 1990, p.p. 201-208.

19. Rotem, Assa and Nelson, H.G., "Failure of a Laminated Composite Under Tension-Compression Fatigue Loading", *Composites Science and Technology*, Vol. 36, p.p. 45-62, 1989.

20. Rosenfeld, M.S. and Huang, S.L., "Fatigue Characteristics of Graphite/Epoxy Laminates under Compressive Loading", *Journal of Aircraft*, Vol. 15, p.p. 264-268, 1978.

21. Reifsnider, K.L., *Fatigue of Composite Materials*, Elsevier Science Publishers B.V., Chapters 2-4, 1990.

22. Kadi, H.EL. and Ellyin, F., "Effect of Stress Ratio on the Fatigue of Unidirectional Glass Fibre/Epoxy Composite Laminae", *Composites*, Vol. 25, No. 10, p.p. 917-924, 1991.

23. Rotem, Assa,"The Fatigue Behavior of Orthotopic Laminates under Tension-Compression Loading", *International Journal of Fatigue*, Vol. 13, No. 3, p.p. 209-215, 1991.

24. Badaliance, R. and Dill, H.D., "Damage Mechanism and Life Prediction of Graphite/Epoxy Composite", *Damage in Composite Materials, ASTM STP 775*, K.L. Reifsnider, Ed., American Society for Testing and Materials, p.p. 229-242, 1982.

25. Berg, J.S. and Adams, D.F., "An Evaluation of Composite Material Compression Test Methods", *Journal of Composites Technology & Research*, Vol. 11, 1989, p.p. 41-46.

26. Bakis, C.E., Yih, H.R., Stinchcomb, W.W., and Reifsnider, K.L., "Damage Initiation and Growth in Notched Laminates Under Reversed Cyclic Loading", *Composite Materials: Fatigue and Fracture, Second Volume, ASTM STP 1012*, Paul A. Lagace, ED., American Society for Testing and Materials, Philadelphia, 1989, p.p. 66-83.

27. Wang, A.S.D., "Strength, Failure, and Fatigue Analysis of Laminates", *Engineering Materials Handbook: Volume 1 Composite*, ASM International, 1987, p.p. 236-251.

28. Garrett, K.W. and Bailey, J.E., "Multiple Transverse Fracture in 90° Cross-Ply Laminates of a Glass Fibre-Reinforced Polyester", *Journal of Materials Science*, Vol. 12, 1977, p.p. 157-168.

29. Bailey, J.E. and Parvizi, A., "On Fibre Debonding Effects and the Mechanism of Transverse Ply Failure in Cross-Ply Laminates of Glass-Fibre/Thermoset Composites", *Journal of Materials Science*, Vol. 16, 1981, p.p. 649-659.

30. Reifsnider, K.L. and Jamison, R., "Fracture of Fatigue-Loaded Composite Laminates", *International Journal of Fatigue*, Vol. 4, 1982, p.p. 187-197.

31. Paris, P.C. and Erdogan, F., "A Critical Analysis of Crack Propagation Laws", *Transition ASME, Journal of Basic Engineering*, Vol. 85, 1963, p.p. 528-534.

32. Manson, J.A., Hertzberg, R.W. and Beardmore, P., CRC Critial Review in Macromolular Science VI, Issue 4, 1973, p.p. 433.

33. Boniface, L. and Ogin, S.L., "Application of the Paris Equation to the Fatigue Growth of Transverse Ply Cracks", *Journal of Composite Materials,* Vol. 23, 1989, p.p. 735-754.

34. Acton, A.E., "The Fatigue of Graphite Fiber Reinforced Thermoset and Thermoplastic Matrices", Massachusetts Institute of Technology Ph.D thesis, Department of Materials Science and Engineering, 1986.

35. Hahn, H.T. in *Composite Materials: Testing and Design, 5th Conference, STP 674,* Tsai, S.W. ed., ASTM, 1979, p.p. 762.

36. Yang, J.N., Jones, D.L., Yang, S.H. and Meskini, A., "A Stiffness Degradation Model for Graphite/Epoxy Laminates", *Journal of Composite Materials,* Vol 24, 1990, p.p. 753-769.

37. Lee, L.J., Yang, J.N., and Sheu, D.Y., "Prediction of Fatigue Life for Matrix-Dominated Composite Laminates", *Composite Science and Technology,* Vol 46, 1993, p.p. 21-28.

38. Bach, P.W., "Fatigue Properties of Glass- and Glass/Carbon-Polyester", *Composites for Wind Turbines,* Energieonderzoek Centrum Nederland, ECN-C-90-012, 1990.

39. Rosen, B.W., "Analysis of Material Properties", *Engineering Materials Handbook: Volume 1 Composites,* ASM International, 1987, p.p. 185-205.

40. Owen,M.J, "Fatigue of Carbon-Fiber-Reinforced Plastics", in Composite Materials Vol 5: Fracture and Fatigue, Broutman, L.J. ed., Academic Press, Inc., 1974, p.p. 342-369.

41. Kim, R.Y., University of Dayton Research Institute, unpublished research, 1986. From *Engineering Materials Handbook Vol 1: Composite,* ASM International, 1987, p.p. 438-441.

42. Desmet, B.J. and Bath, P.W., "Database Fact: Fatigue of Composites for Wind Turbines", Energieonderzoek Centrum Nederland, ECN-C-94-045, 1994.

43. Hedley, C., "Mold Filling Parameters of Resin Transfer Molding of Composites", Montana State University

Masters Thesis, Chemical Engineering Department, 1994.

44. ASTM Committee, *ASTM Standards and Literature References for Composite Materials*, American Society for Testing and Materials, 1987, p.p. 35-39.

APPENDIX A

INITIAL MODULUS FOR EACH BATCH OF SPECIMENS

INITIAL MODULUS FOR EACH BATCH OF SPECIMENS

Initial modulus of each batch of specimens was measured or calculated from the slow static tests and the results were shown in the following Table A1:

Table A1. Initial Modulus for Each Batch of Specimens (GPa).

Batch	Loading	Test 1	Test 2	Test 3	Test 4	Average Modulus
Longitudinal R=-1 and 0.5 Batch	Tension	42.4	38.3	37.1		39.2
	Compression	39.5	41.9	42.3		41.2
Transverse R=0.1 Batch	Tension	8.21	8.83	8.34	9.10	8.62
Transverse R=0.5 Batch	Tension	8.08	8.84	9.17		8.69
Transverse R=10,2 Batch	Compression	8.21	9.08	9.58		8.96

Note: (1) as an extension to database, modulus for R=-0.5 batch was not measured, average modulus for longitudinal R=-1 and 0.5 batch was used
(2) average transverse modulus for R=0.1 batch and R=10 and 2 batch was used as the initial modulus of transverse R=-1 batch

APPENDIX B

SUMMARY OF FIBERGLASS FATIGUE RESULTS

LONGITUDINAL RESULTS

TEST & SAMPLE ID #	MAX OR MIN STRESS MPa	R	FREQ. Hz	INITIAL E** GPa	MAX OR MIN STRAIN (%)	CYCLES TO FAIL
#001 CT4	1627.22		20	46.2	3.53	1
#002 AT2	1516.90		20	46.2	3.28	1
#003 AT26	1392.79		20	46.2	3.01	1
#004 CT3	1344.52		20	46.2	2.91	1
#005 AT27	689.50	0.1	20	46.2	1.49	2,982
#006 CT1	689.50	0.1	20	46.2	1.49	45,845
#007 AT19	468.86	0.1	60	46.2	1.01	157,502
#008 AT18	468.86	0.1	60	46.2	1.01	702,844
#009 AT23	413.70	0.1	80	46.2	0.896	602,984
#010 AT20	413.70	0.1	80	46.2	0.896	2,269,945
#011 CT5	310.28	0.1	100	46.2	0.672	5,902,329
#012 CT6	310.26	0.1	100	46.2	0.672	78,810,903
#013 CT2	310.28	0.1	100	46.2	0.672	*110,539,817
014 TF513	1296.26		20	39.2	3.31	1
015 TF512	1425.89		20	39.2	3.64	1
016 TF515	1396.24		20	39.2	3.56	1
017 TF516	1310.05		20	39.2	3.34	1
018 TF525	601.93	0.5	60	39.2	1.54	235,881
019 TF526	601.93	0.5	60	39.2	1.54	284,150
020 TF527	601.93	0.5	60	39.2	1.54	850,428
021 TF521	535.05	0.5	80	39.2	1.36	417,082
022 TF528	535.05	0.5	80	39.2	1.36	1,095,381
023 TF522	535.05	0.5	80	39.2	1.36	4,112,276
024 TF529	468.17	0.5	100	39.2	1.19	11,927,857
025 TF520	468.17	0.5	100	39.2	1.19	16,711,593
026 TF519	401.29	0.5	100	39.2	1.02	*100,000,000
#027 AC14	-741.90		20	35.6	-2.09	1
#028 AC17	-741.21		20	35.6	-2.09	1
#029 AC13	-883.29		20	35.6	-1.93	1
#030 AC11	-413.70	10	40	35.6	-1.17	8,226
#031 AC12	-413.70	10	40	35.6	-1.17	10,886
#032 AC8	-413.70	10	40	35.6	-1.17	19,210
#033 AC15	-344.75	10	60	35.6	-0.97	337,992
#034 AC16	-344.75	10	60	35.6	-0.97	375,478
#035 AC7	-344.75	10	60	35.6	-0.97	587,407
#036 AC30	-275.80	10	100	35.6	-0.78	*103,112,335
#037 AC10	-275.80	10	100	35.6	-0.78	*103,573,682
#038 AC19	-551.60	2	60	35.4	-1.56	9,255
#039 AC26	-551.60	2	60	35.4	-1.56	12,319
#040 AC29	-551.60	2	60	35.4	-1.56	22,071
#041 AC20	-551.60	2	60	35.4	-1.56	46,085
#042 AC21	-482.65	2	80	35.4	-1.36	11,347
#043 AC24	-482.65	2	80	35.4	-1.36	38,158
#044 AC31	-482.65	2	80	35.4	-1.36	45,312

TEST & SAMPLE ID #		MAX OR MIN STRESS MPa	R	FREQ. Hz	INITIAL E** GPa	MAX OR MIN STRAIN (%)	CYCLES TO FAIL
#045	AC22	-482.65	2	80	35.4	-1.36	103,970
#046	AC32	-448.18	2	100	35.4	-1.26	17,937
#047	AC35	-448.18	2	100	35.4	-1.26	3,891,657
#048	AC25	-448.18	2	100	35.4	-1.26	*100,081,219
#049	AC23	-413.70	2	100	35.4	-1.17	*107,413,026
050	TCT1	1367.28		20	39.2	3.49	1
051	TCT2	1387.27		20	39.2	3.54	1
052	TCT3	1279.02		20	39.2	3.26	1
053	TCT4	1527.24		20	39.2	3.89	1
054	TCC1	-646.06		20	41.2	-1.57	1
055	TCC2	-463.34		20	41.2	-1.13	1
056	TCC3	-689.50		20	41.2	-1.68	1
057	TCC4	-537.12		20	41.2	-1.30	1
058	TC15	264.09	-1	30	40.2	0.657	124,952
059	TC16	264.09	-1	30	40.2	0.657	337,226
060	TC13	264.09	-1	30	40.2	0.657	437,113
061	TC11	234.43	-1	30	40.2	0.583	591,914
062	TC7	234.43	-1	30	40.2	0.583	781,045
063	TC9	234.43	-1	30	40.2	0.583	1,981,821
064	TC22	205.47	-1	40	40.2	0.511	2,037,672
065	TC18	205.47	-1	40	40.2	0.511	6,141,627
066	TC6	205.37	-1	40	40.2	0.511	7,080,727
067	TC10	205.47	-1	40	40.2	0.511	7,605,707
068	TC21	175.82	-1	50	40.2	0.437	10,382,631
069	TC19	175.82	-1	50	40.2	0.437	17,272,745
070	TC20	175.82	-1	50	40.2	0.437	*100,000,000
071	TC601	1617.83		20	40.2	4.024	1
072	TC602	1381.70		20	40.2	3.437	1
073	TC603	1409.57		20	40.2	3.506	1
074	TC604	-745.71		20	40.2	1.855	1
075	TC605	-715.86		20	40.2	1.781	1
076	TC606	-687.09		20	40.2	1.709	1
077	TC608	293.73	-0.5	20	40.2	0.731	54,401
078	TC609	293.73	-0.5	20	40.2	0.731	151,631
079	TC613	293.73	-0.5	20	40.2	0.731	2,215,625
080	TC610	257.01	-0.5	20	40.2	0.639	338,635
081	TC611	257.01	-0.5	20	40.2	0.639	677,151
082	TC616	257.01	-0.5	20	40.2	0.639	4,237,939
083	TC614	257.01	-0.5	20	40.2	0.639	4,554,382
084	TC612	220.30	-0.5	20	40.2	0.548	3,089,148
085	TC615	220.30	-0.5	20	40.2	0.548	*11,113,718
			TRANSVERSE RESULTS				
086	90CF6	-126.94		20	8.96		1
087	90CF5	-112.18		20	8.96		1
088	90CF7	-110.87		20	8.96		1

TEST & SAMPLE ID #		MAX OR MIN STRESS MPa	R	FREQ. Hz	INITIAL E** GPa	MAX OR MIN STRAIN (%)	CYCLES TO FAIL
089	90CF10	-70.33	10	50	8.96	-0.79	13,122
090	90CF17	-70.33	10	50	8.96	-0.79	33,632
091	90CF15	-70.33	10	50	8.96	-1.79	268,262
092	90CF12	-64.47	10	70	8.96	-0.72	290,250
093	90CF11	-64.47	10	70	8.96	-0.72	697,512
094	90CF18	-64.47	10	70	8.96	-0.72	1,330,488
095	90CF21	-58.61	10	100	8.96	-0.65	12,000,998
096	90CF9	-58.61	10	100	8.96	-0.65	34,986,168
097	90CF20	-55.16	10	100	8.96	-0.62	*107,839,549
098	CF501	-112.93		20	8.96		1
099	CF502	-112.59		20	8.96		1
100	CF503	-120.92		20	8.96		1
101	CF504	-114.94		20	8.96		1
102	CF518	-87.91	2	40	8.96	-0.98	121,730
103	CF514	-87.91	2	40	8.96	-0.98	511,744
104	CF517	-87.91	2	40	8.96	-0.98	621,878
105	CF513	-82.05	2	60	8.96	-0.92	853,552
106	CF512	-82.05	2	60	8.96	-0.92	2,675,404
107	CF507	-82.05	2	60	8.96	-0.92	3,705,190
108	CF511	-76.19	2	80	8.96	-0.85	31,971,669
109	CF523	-76.19	2	80	8.96	-0.85	*100,682,804
110	90FT5	21.86		20	8.62	0.254	1
111	90FT6	18.32		20	8.62	0.212	1
112	90FT7	23.46		20	8.62	0.272	1
113	90FT1	22.51		20	8.62	0.361	1
114	90FT1	13.78	0.1	60	8.62	0.160	9,383
115	90FT19	13.15	0.1	60	8.62	0.153	34,592
116	90FT3	12.93	0.1	60	8.62	0.150	31,952
117	90FT16	12.41	0.1	80	8.62	0.144	3,895,837
118	90FT17	12.33	0.1	80	8.62	0.143	2,372,150
119	90FT15	12.30	0.1	80	8.62	0.143	1,351,172
120	90FT8	11.67	0.1	100	8.62	0.135	2,987,855
121	90FT4	11.31	0.1	100	8.62	0.131	21,111,725
122	90FT11	10.60	0.1	100	8.62	0.123	*102,350,298
123	TI501	20.94		20	8.69	0.241	1
124	TI502	21.44		20	8.69	0.247	1
125	TI503	23.19		20	8.69	0.267	1
126	TI509	15.30	0.5	60	8.69	0.176	53,275
127	TI507	15.30	0.5	60	8.69	0.176	114,090
128	TI505	15.30	0.5	60	8.69	0.176	523,634
129	TI508	14.21	0.5	80	8.69	0.164	1,308,671
130	TI504	14.21	0.5	80	8.69	0.164	1,665,220
131	TI506	14.21	0.5	80	8.69	0.164	9,806,694
132	TI514	13.11	0.5	80	8.69	0.151	31,443,023
132	TI515	13.11	0.5	80	8.69	0.151	34,693,646
133	TI513	13.11	0.5	80	8.69	0.151	50,666,199

TEST & SAMPLE ID #	MAX OR MIN STRESS MPa	R	FREQ. Hz	INITIAL E** GPa	MAX OR MIN STRAIN (%)	CYCLES TO FAIL
134 TCH1	18.20		20	8.79	0.207	1
135 TCH2	19.06		20	8.79	0.191	1
136 TCH3	17.02		20	8.79	0.194	1
137 TCH12	8.07	-1	20	8.79	0.092	45,172
138 TCH12	8.07	-1	30	8.79	0.092	151,463
139 TCH10	8.07	-1	30	8.79	0.092	794,513
140 TCH14	7.17	-1	60	8.79	0.082	47,385
141 TCH13	7.17	-1	60	8.79	0.082	1,043,369
142 TCH16	7.17	-1	60	8.79	0.082	3,009,395
143 TCH7	7.17	-1	60	8.79	0.082	3,973,407
144 TCH15	6.27	-1	80	8.79	0.071	11,733,016
145 TCH19	6.27	-1	100	8.79	0.071	*100,153,319

Note: (1) # signifies the data from Belinky [4]
(2) * signifies run-outs (no failure)
(3) ** average value of elastic modulus in the load direction measured for that batch of material

APPENDIX C

POWER LAW FITS FOR FATIGUE DATA

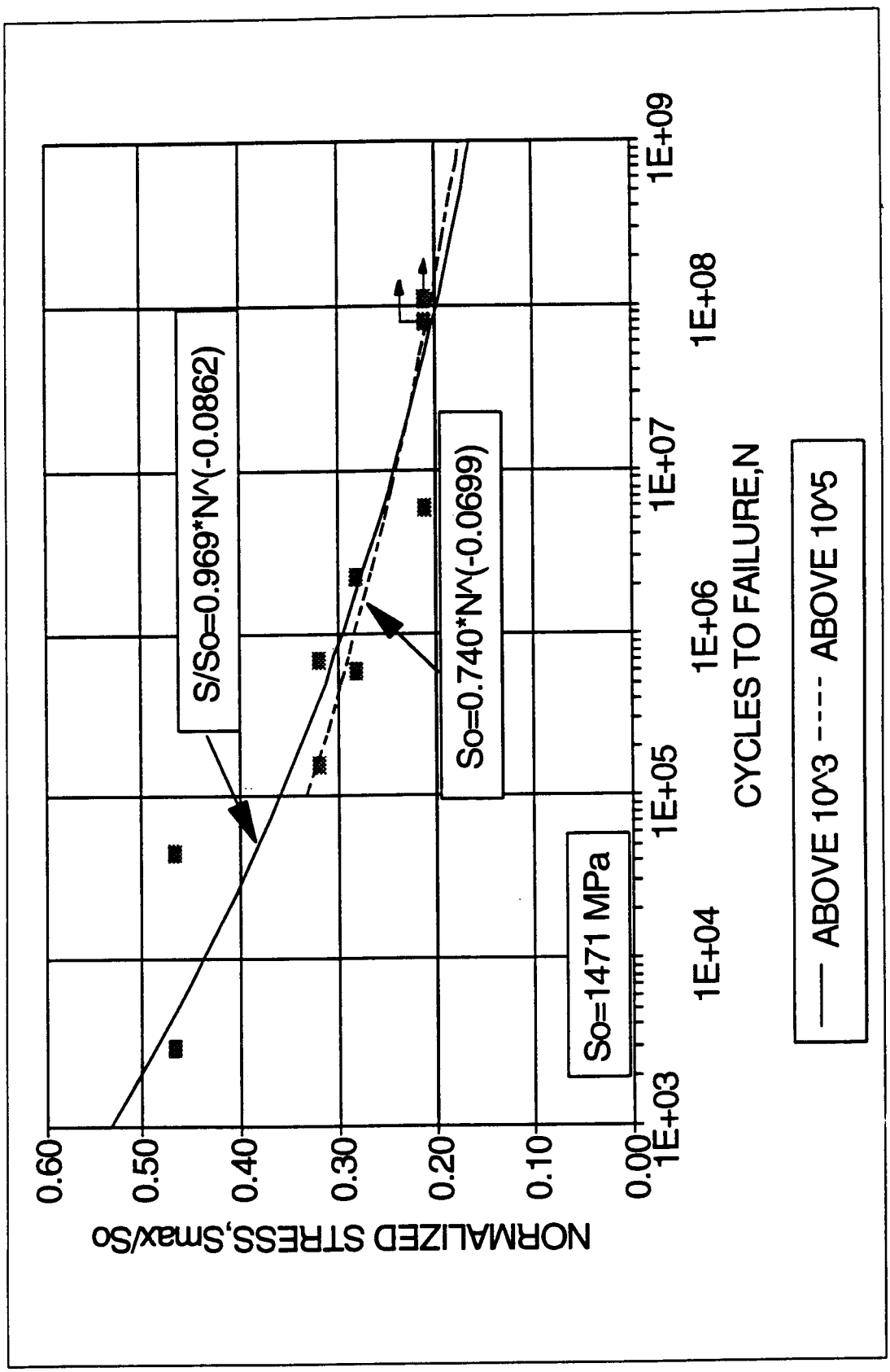

Figure C1. Power Law Fits of S-N Data for Longitudinal R=0.1 [4] Above 10^3 and Above 10^5 Cycles.

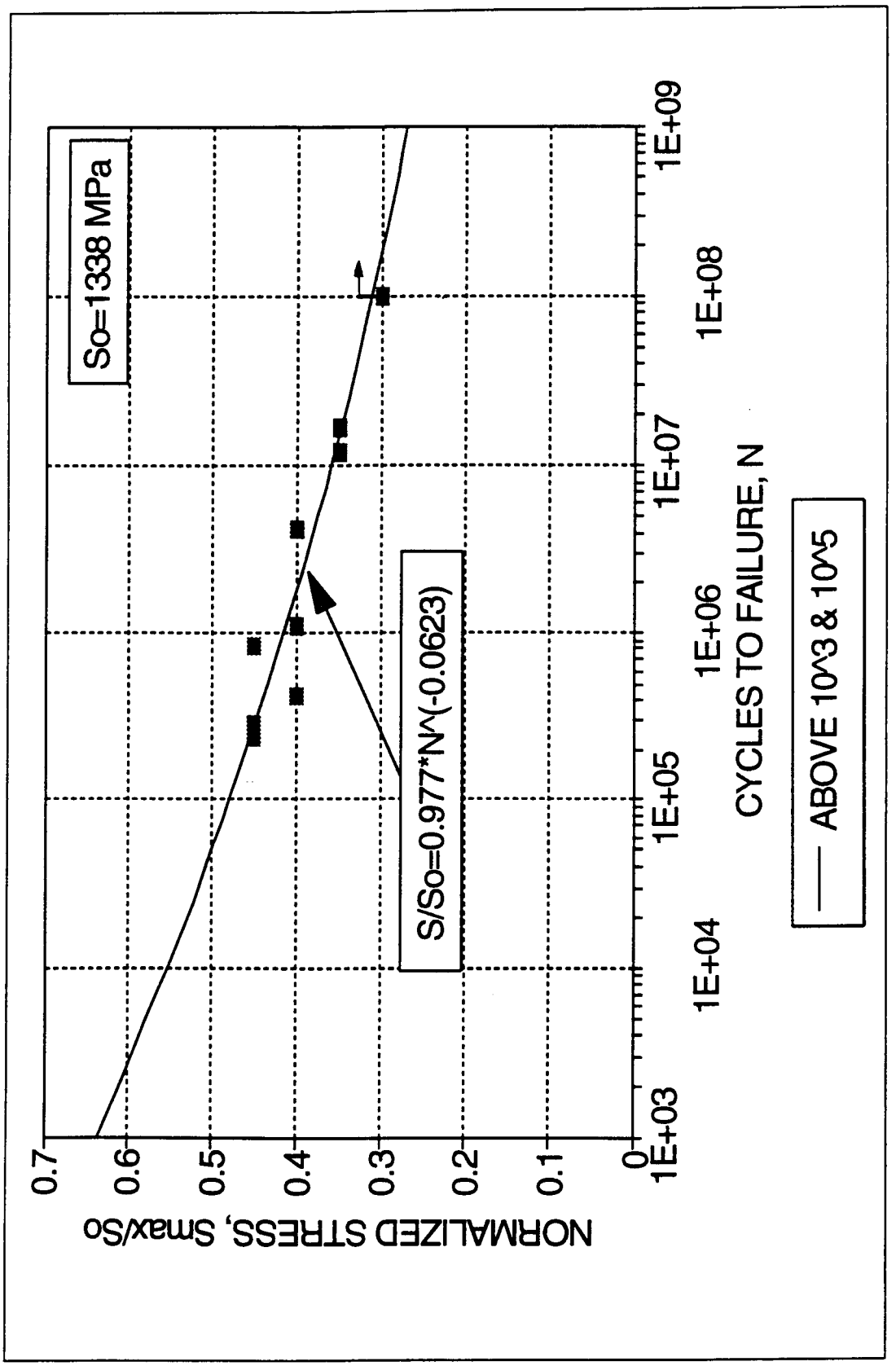

Figure C2. Power Law Fits of S-N Data for Longitudinal R=0.5 Above 10^3 and Above 10^5 Cycles.

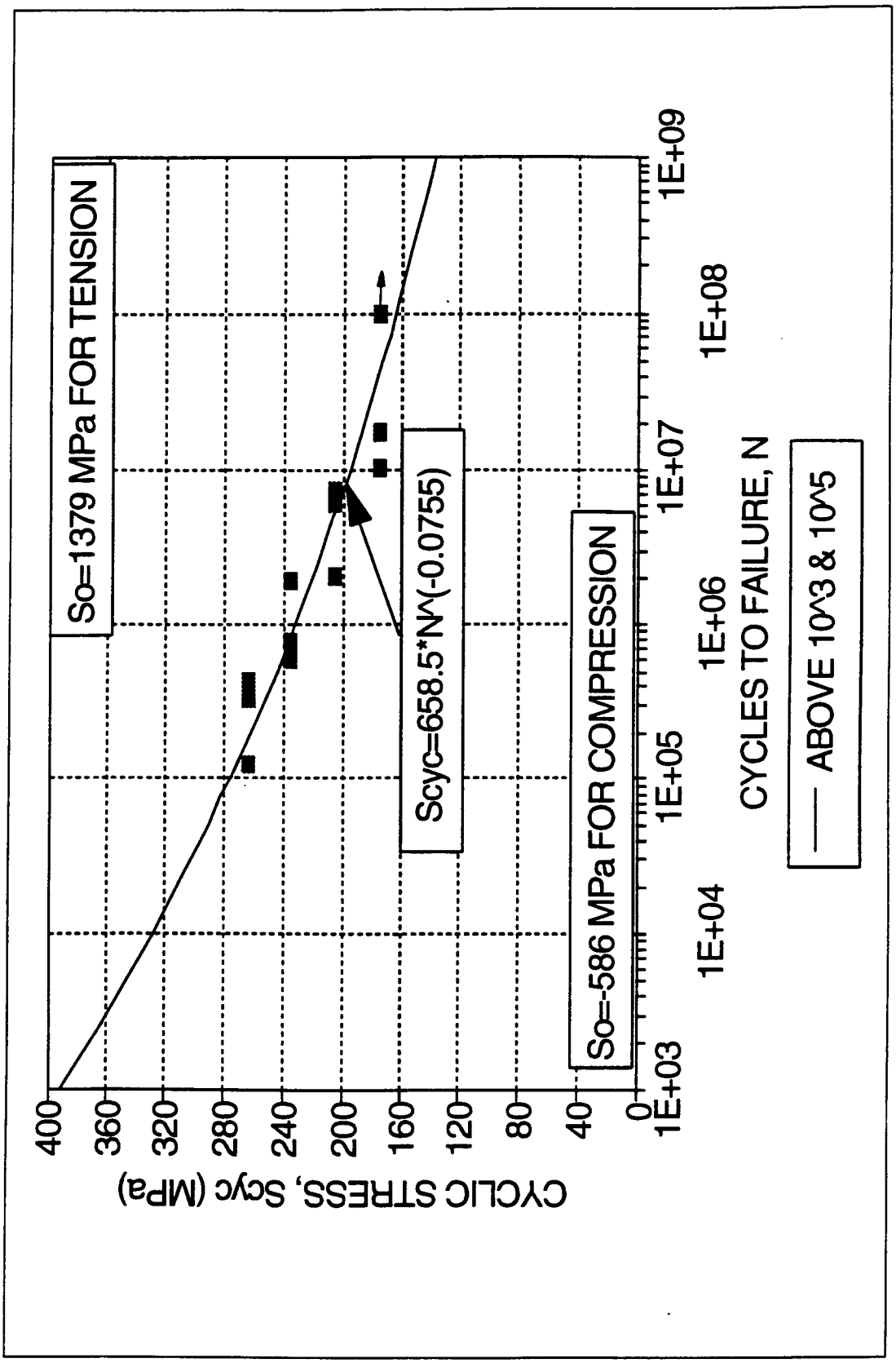

Figure C3. Power Law Fits of S-N Data for Longitudinal R=-1 Above 10^3 and Above 10^5 Cycles.

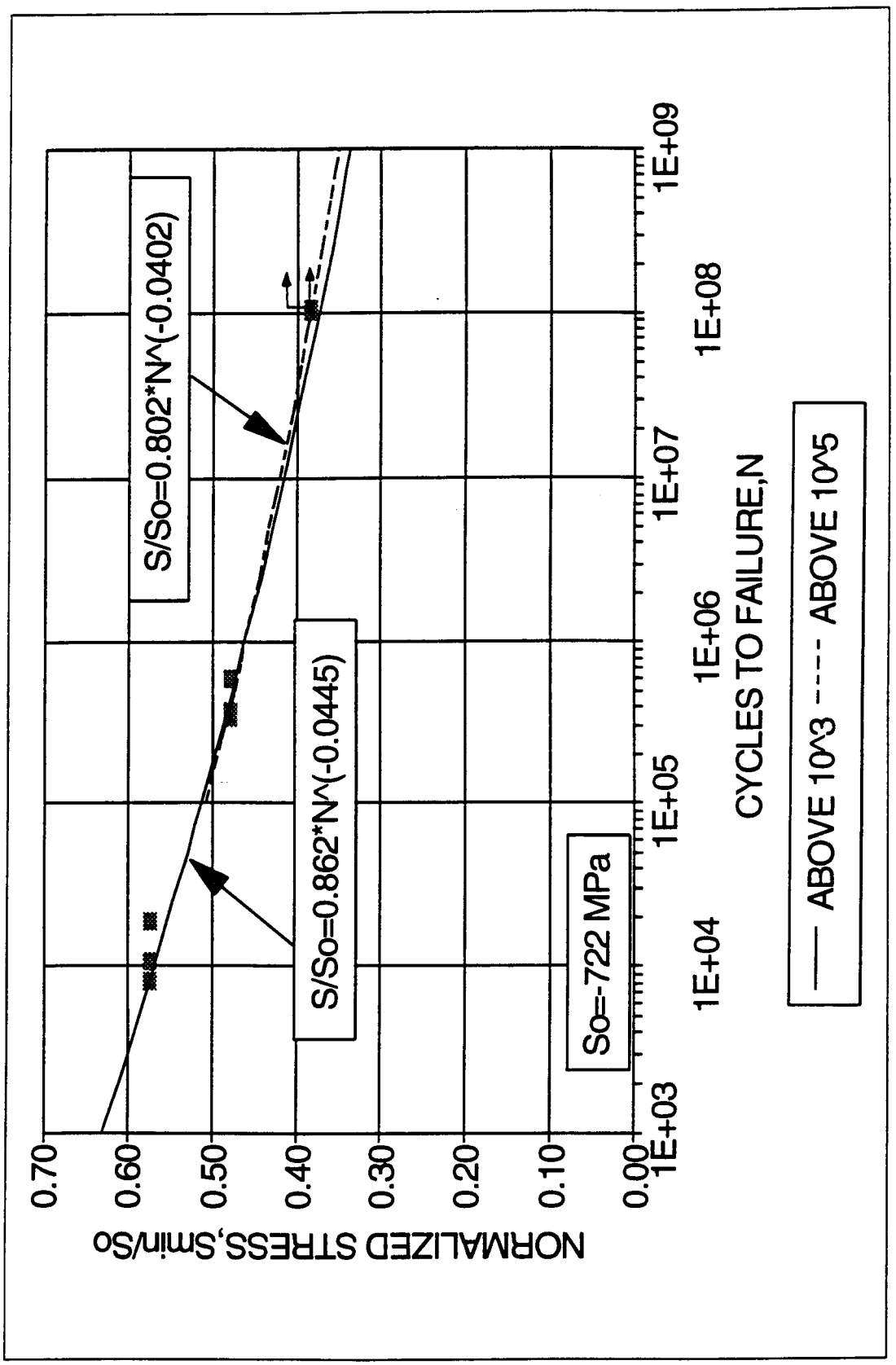

Figure C4. Power Law Fits of S-N Data for Longitudinal R=10 [4] Above 10^3 and Above 10^5 Cycles.

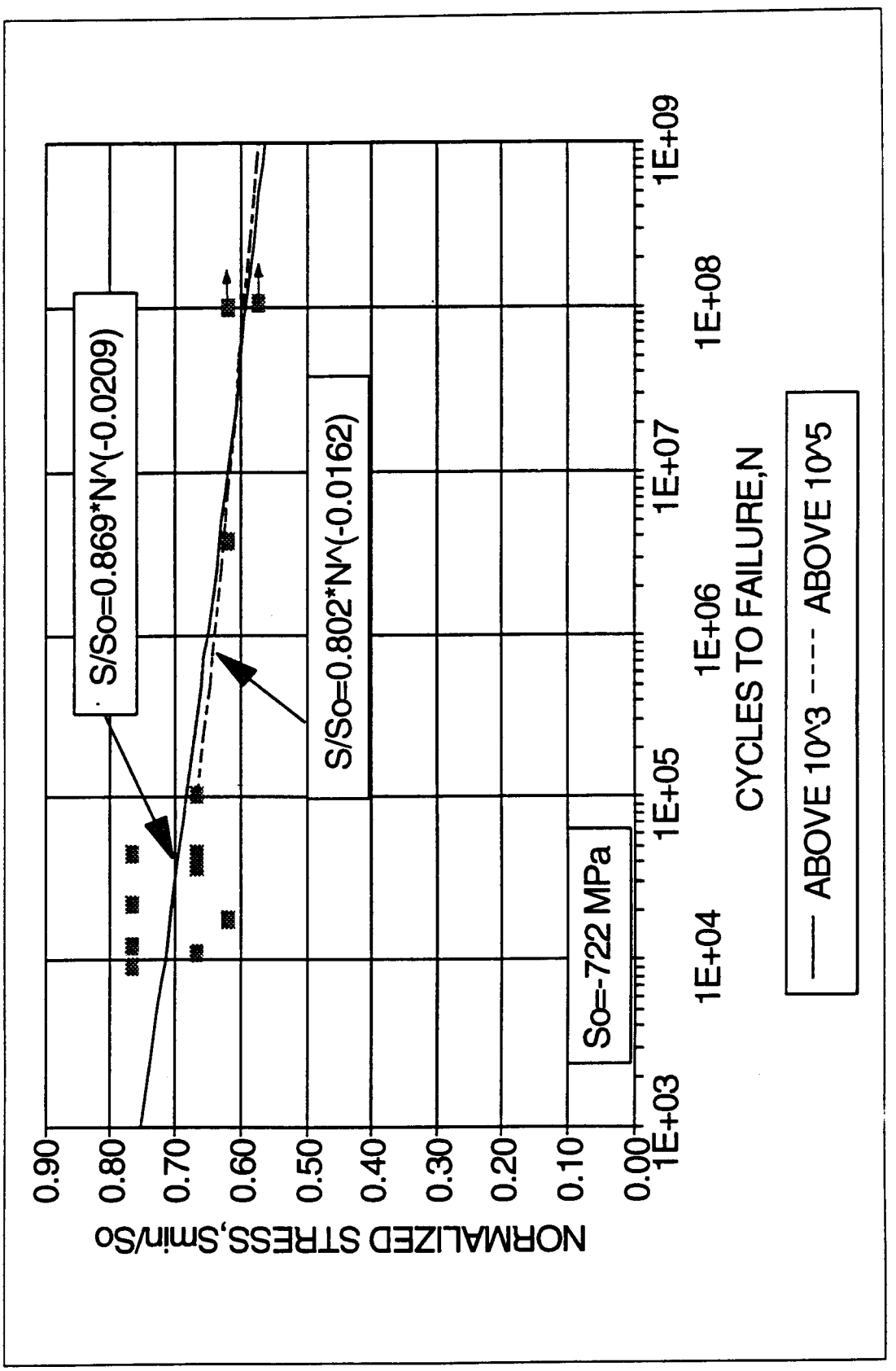

Figure C5. Power Law Fits of S-N Data for Longitudinal R=2 [4] Above 10^3 and Above 10^5 Cycles.

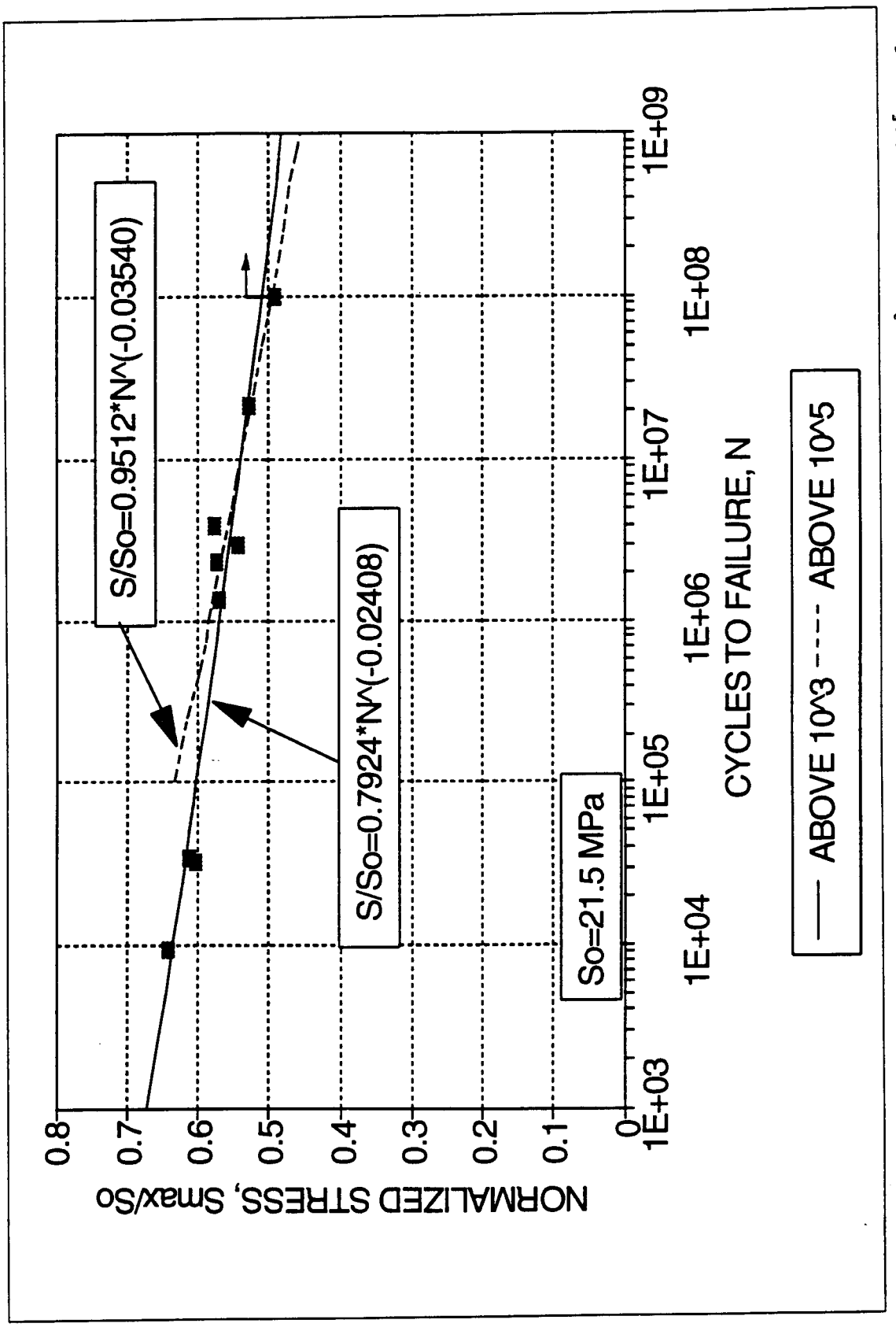

Figure C6. Power Law Fits of S-N Data for Transverse R=0.1 Above 10^3 and Above 10^5 Cycles.

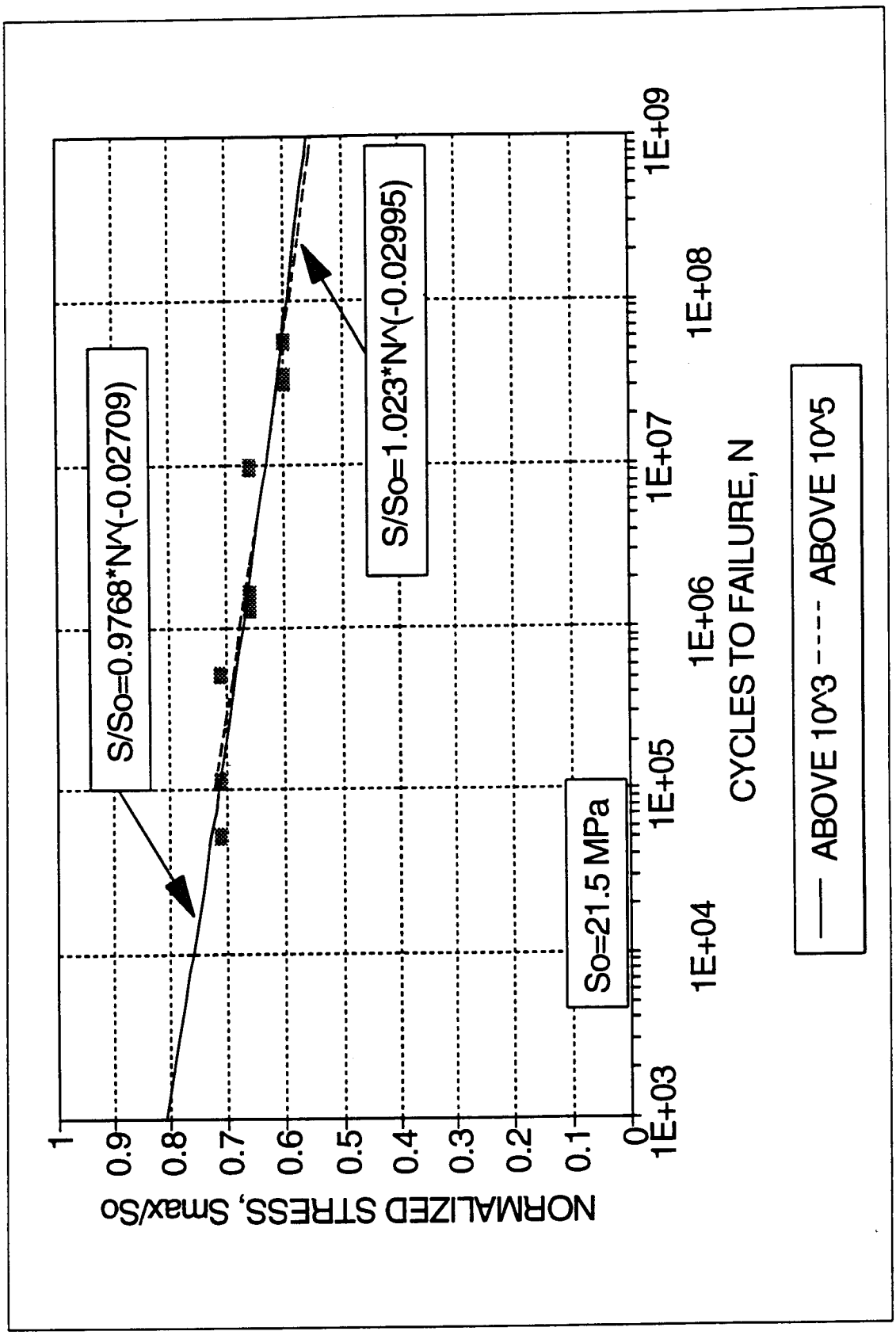

Figure C7. Power Law Fits of S-N Data for Transverse R=0.5 Above 10^3 and Above 10^5 Cycles.

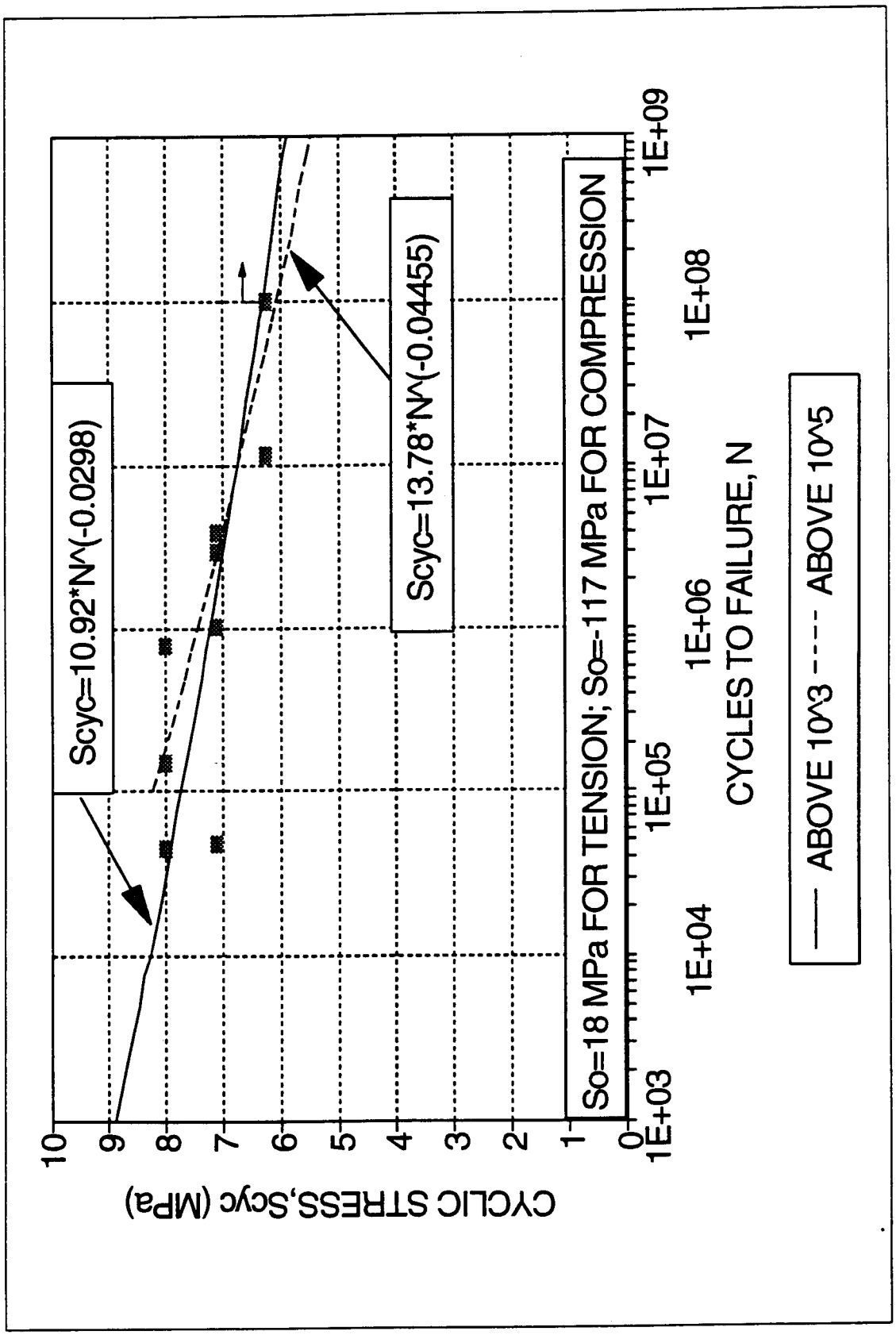

Figure C8. Power Law Fits of S-N Data for Transverse R=-1 Above 10^3 and Above 10^5 Cycles.

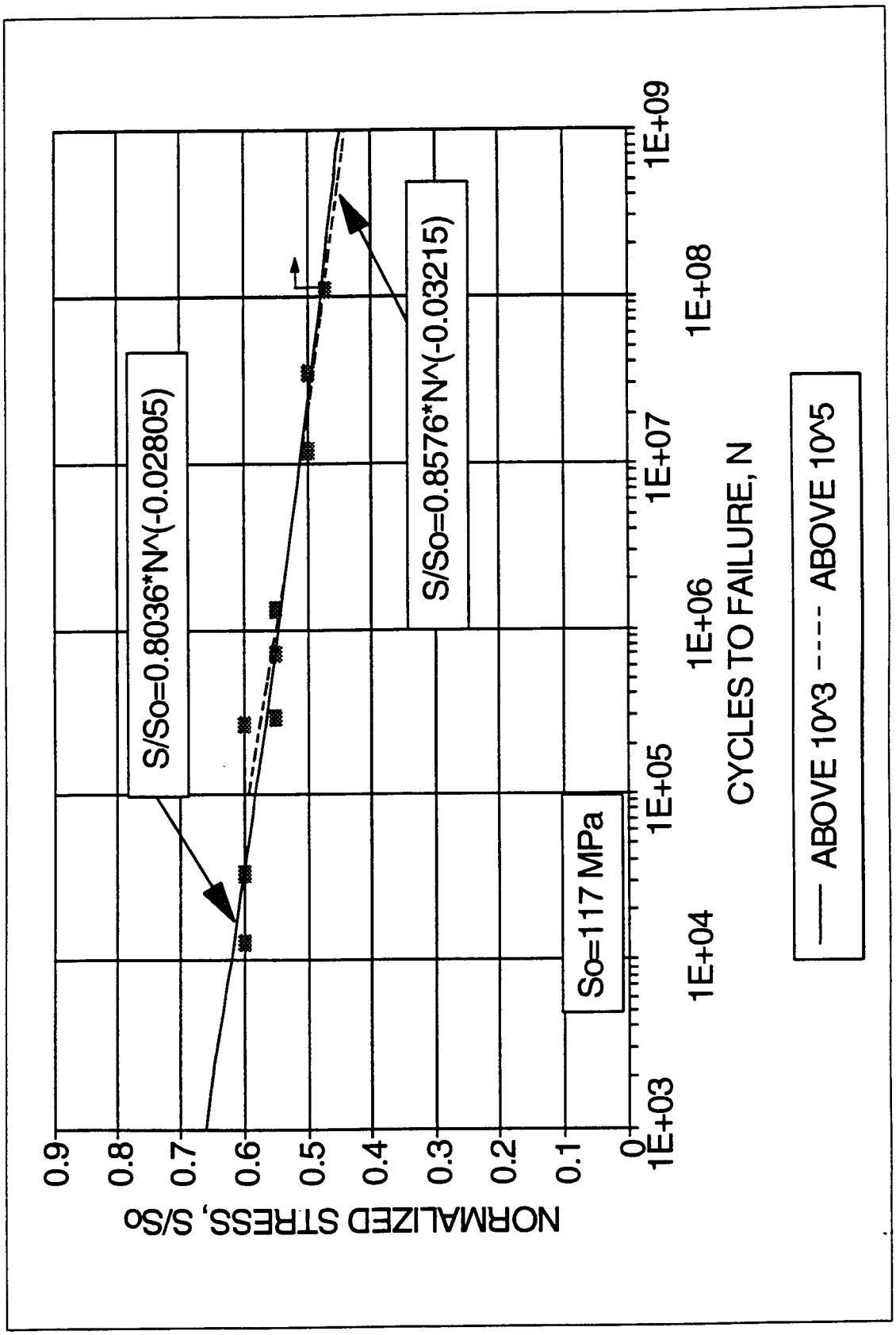

Figure C9. Power Law Fits of S-N Data for Transverse R=10 Above 10^3 and Above 10^5 Cycles.

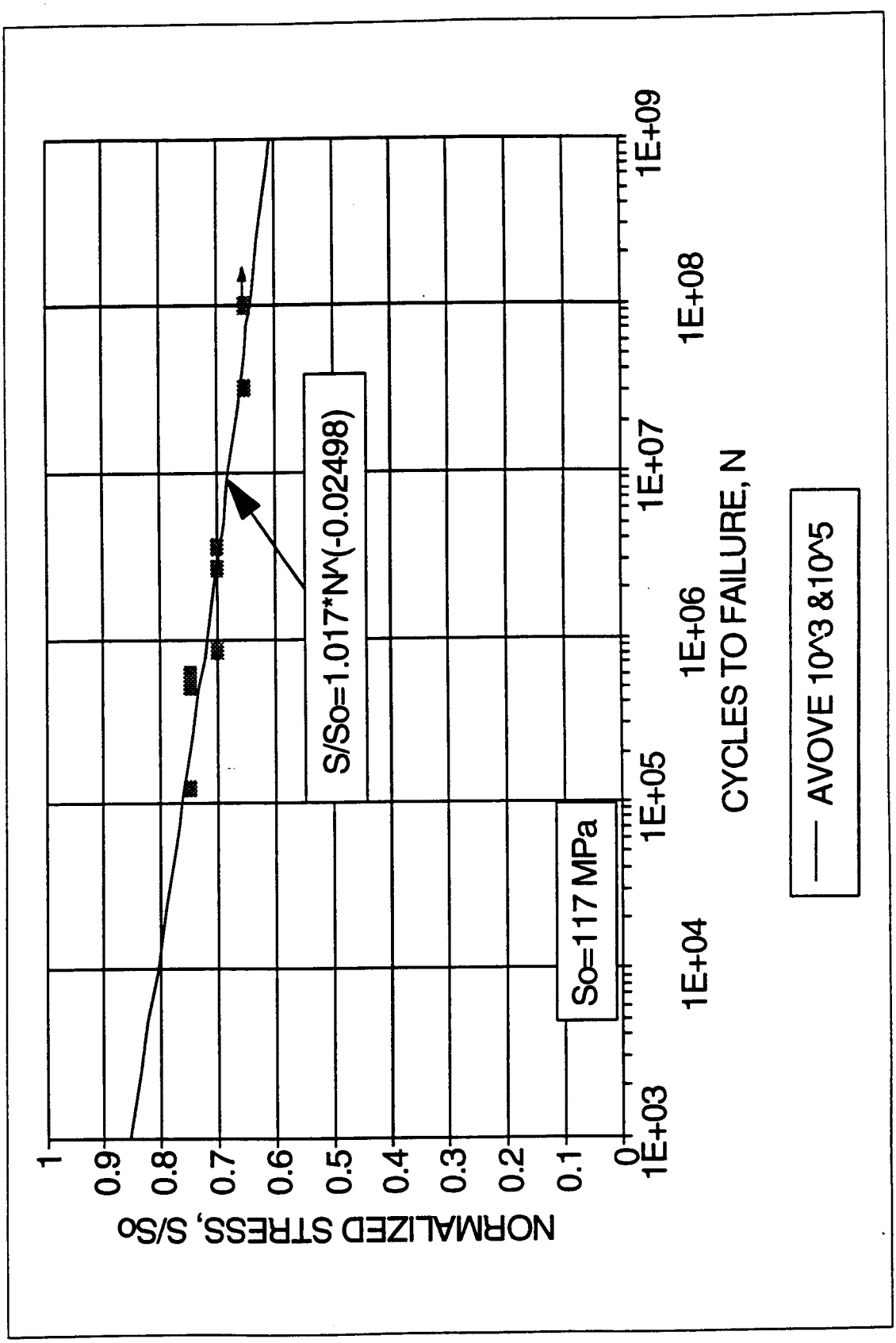

Figure C10. Power Law Fits of S-N Data for Transverse R=2 Above 10^3 and Above 10^5 Cycles.